Investigation of Sf-9 Cell Metabolism Before and After Baculovirus Infection Using Biovolume: a Case for the Improvement of Adeno-Associated Viral Vector Production

by

Yu-Lei Cheng

A thesis

presented to the University of Waterloo

in fulfillment of the

thesis requirement for the degree of

Master of Applied Science

in

Chemical Engineering

Waterloo, Ontario, Canada, 2009

Author’s Declaration

I hereby declare that I am the sole author of this thesis. This is a true copy of the thesis, including any required final revisions, as accepted by my examiners.

I understand that my thesis may be made electronically available to the public.

Abstract

Adeno-associated viral (AAV) vectors have been shown to be potential vectors for the treatment of diseases, including protocols using RNA interference (RNAi). AAV vector production in insect cells using the baculovirus vector expression system has been a major advance in furthering their use. A major limitation of AAV vector production at high cell densities is a reduction in cell specific yield, which is thought to be caused by nutrient limitations. Nutrient consumption profiles after infection, however, have still not been fully characterized, probably due to the difficulty of characterizing consumption patterns based on increases in cell density, which are minimal after infection. It is known, however, that cells increase in size after infection; therefore, the driving hypothesis of this thesis was that biovolume, or the total volume enclosed by the membrane of viable cells, which accounts for both cell density and cell size, could be used to characterize nutrient consumption patterns both before and after infection.

The relationships between nutrient consumption and change in cell density and biovolume were examined by statistical correlation analysis. It was found that in uninfected cultures, no significant correlation differences, using either cell density or biovolume, were observed since cell size remained relatively constant; however, in infected cultures, more than half of the nutrients were found to be better correlated with biovolume than with cell density.

When examining the nutrient and metabolite concentration data on a biovolume basis, nutrient consumption remained relatively constant. It is hypothesized that since it has been reported that the rate of cell respiration increases after infection, a more complete oxidation of nutrients occurs to satisfy increased energy needs during infection.

By having a basis to base nutrient consumption, we can better assess the needs of the culture. This will allow the development of feeding strategies based on cellular requirements instead of supplying the cultures with generic nutrient cocktails. It is

expected that different nutrient mixtures can be used to target different goals such as 1) enhancing cell growth (before infection) and 2) improving the production of recombinant products (after infection). This will not only increase the efficiency of AAV vector production, but will also reduce the cost of production and make the process more economical by eliminating the addition of unnecessary nutrients.

Although promising, some limitations of using biovolume still exist. A first limitation is the biovolume measure itself. This measure requires a device that measures cell size, such as a Coulter Counter Multisizer (Beckman-Coulter, Miami, FL, USA), which can be expensive. Capacitance probes can be a more cost effective tool to estimate biovolume; however, the availability of capacitance probes is still not common. A second limitation is the interpretation of the biovolume profiles, which can depend strongly on the fraction of cells in culture that are infected. If the culture is infected asynchronously, then there will be many different cell populations in the culture. Future work may require separating the cell size distribution into populations of viable and non-viable cells to get a better biovolume measure as opposed to assuming that viability is well distributed over the entire range of cell sizes. In infected cultures where the viability may be low, it is likely that the cell size distribution of non-viable cells will be concentrated at the lower end of the distribution (smaller diameter) rather than being well distributed over the whole range. If this is the case, for the infected cultures with low viability, the mean cell diameter calculated will be underestimated, which will lead to an overestimation of nutrient consumption for cultures with low viability. This will certainly affect the accuracy of the nutrient consumption profiles. By separating cell size distribution data into different cell populations of viable and nonviable, the accuracy can be improved.

Acknowledgements

I would like to thank:

My supervisor, Marc Aucoin, for taking me as his student and giving me the opportunity to participate in this research. I would also like to thank him for all the helpful discussions and constructive criticism that he has given me along the way for making the completion of this degree possible. I would also like to thank my previous supervisor, Pu Chen, for giving me the opportunity to learn techniques in cell culture.

The Biotechnology Research Institute of the National Research Council Canada for providing the experimental data used in this thesis (Aucoin, et al. 2007).

Prof. Hector Budman for all his help in making the transition of supervisor possible. His constant care and warm conversations and hellos in the hallways were much appreciated. If it wasn't for Prof. Budman, I might not have continued my study at the University of Waterloo.

Prof. Eric Jervis and Prof. Thomas Duever for not only teaching me valuable knowledge in Biochemical Engineering and Statistics, respectively; but also willing to spend extra personal time with me to discuss and help me with aspects of my research.

Lillian, the instructor of the lab course that I TA-ed. She is always so helpful and considerate and I enjoyed all the conversations we had and all the thoughts and advices she shared with me.

All the secretaries in the Department of Chemical Engineering, Liz, Pat, Rose, and Ingrid for all their secretarial help no matter how busy they were, and their warm smiles and hellos in the hallways. I really enjoyed chatting with all of them.

Prof. Yu-chen Hu, a dedicated and well-known researcher in the field of BEVS, for giving me the opportunity to visit his lab and spending so much time talking to me, touring me around his lab, and introducing to me people working in his lab.

All my friends for all the supports they had given me during my study at Waterloo. All the people in Prof. Chen's lab, especially Maggie and May for training me on all the techniques, Tony, Francis, Michelle, and most importantly Leanne for all their

encouragements, helps, supports, and all the funs we had together; all the people who shared the same office with me for all the experience we shared together; and everybody in Prof. Feng's lab for all the chats and funs we had; and all my UBC friends who also came to Waterloo, especially Tina, for the unique 2 years experience we went through together. Thank you all for constantly listening to everything I have to say, and making my life at Waterloo more enjoyable!

My parents, my sister and my brother. They are always there for me no matter what. They reminded me of who I am in times when I lost myself. I love you all so much, and I am so glad that I was born in this happy family.

Last but not least, my dearest boyfriend, Jordan. Thank you for coming to Waterloo to take care of me during my study at Waterloo. Thank you for cheering my up whenever I am depressed or sad. Thank you for coping with my weird working schedules regardless of if you had to work or study the next day; and thank you for enduring all my negative emotions during the frustrating moments of my life. I don't know why I am so lucky to have you by my side and I thank God for having you in my life. I love you more than I can express by words and I wish we'll always be supportive in each other's life and love each other always and forever.

Table of Contents

List of Figures

List of Tables

List of Abbreviation

1. 2-OG: 2-oxoglutarate
2. %CV: % coefficient of variation
3. AAV: adeno-associated virus
4. AcMNPV: *Autographa californica* multinucleopolyhedrovirus
5. ATP: adenosine triphosphate
6. BacCap: recombinant baculovirus containing the structural (capsid) gene for AAV vectors
7. BacITRGFP: recombinant baculovirus containing the green fluorescent protein gene
8. BacRep: recombinant baculovirus containing the replication gene for AAV vectors
9. BEVS: baculovirus expression vector system
10. BioV: biovolume
11. BV: budded virus
12. Caco-2: human epithelial colorectal adenocarcinoma cell line
13. C_i: corrected Coulter count for i^{th} cell diameter
14. c_i: original Coulter count for i^{th} cell diameter
15. CM: conditioned media
16. CMV: cytomegalovirus
17. CPP: cell-penetrating peptides
18. CTS: cytoplasmic translocation signal
19. D: aperture diameter
20. D_0: the average diameter of uninfected, healthy cells
21. D_{dt}: diameter at doubling time
22. D_{inf}: the average maximum diameters in the infected cultures
23. d_i: is the i^{th} cell diameter
24. DO: dissolved oxygen
25. DNA: deoxyribonucleic acid
26. dsRNA: double-stranded RNA

27. ECM: extracellular matrix
28. EPR: enhanced permeability and retention effect
29. FDA: Food and Drug Administration
30. G_1: first gap phase in cell cycle; between the end of mitosis (M) and the start of synthesis (S)
31. G_2: second gap phase in cell cycle; between the end of synthesis (S) and the start of mitosis (M)
32. GFP: green fluorescent protein
33. GV: granulovirus
34. HepG2: human hepatocellular liver carcinoma cell line
35. HIV: human immunodeficiency virus
36. HPLC: high performance liquid chromatography
37. HPV: human papillomavirus
38. Huh7: human hepatoma cell line
39. ICD: initial cell density
40. LNA: locked nucleic acids
41. MCV: mean cell volume
42. MOI: multiplicity of infection
43. M phase: mitosis phase
44. mRNA: messenger RNA
45. NPV: nucleopolyhedrovirus
46. OA: oxaloacetate
47. ODV: occlusion-derived virus
48. *p:* coincident factor
49. PEC: polyelectrolyte complex
50. PEG: polyethylene glycol
51. PEI: polyethyleneimine
52. PLL: polylysine
53. PS: phosphorothioate
54. PTD: protein transduction domains
55. R^2: coefficient of determination
56. RES: reticuloendothelial system

57. rF: ribo-difluorotoluyl
58. RISC: RNA-induced silencing complex
59. ROS: reactive oxygen species
60. RNA: ribonucleic acid
61. RNAi: RNA interference
62. Saos2: human epithelial-like osteosarcoma cell line
63. SARS-CoV: severe acute respiratory syndrome coronavirus
64. Sf-9: *Spodoptera frugiperda* cell line
65. Sf900-II: protein-free insect cell culture medium optimized for Sf-9 growth
66. shRNA: short-hairpin ribonucleic acid
67. siRNA: small interfering RNA
68. S phase: synthesis phase
69. TC: total count
70. TCA cycle: tricarboxylic acid cycle
71. TNF-β: tumor necrosis factor-β
72. TOI: time of infection
73. VCD: viable cell density
74. VLP: virus-like particle

Glossary of Terms

1. Apoptosis: programmed cell death
2. Complexation: the binding of two substances through electrostatic linkage
3. Conjugation: the binding of two substances through covalent bonding
4. Cytotoxicity: the measure of toxicity in cell
5. Hydrophilicity: a measure describing solubility of a substance in water
6. Transfection: the process of introducing nucleic acids or proteins into the cells through non-viral methods, such as electroporation or mixing with cationic lipids.

Forward

This thesis is the culmination of two years of work in two separate areas. The first area I was involved with was siRNA delivery in Prof. Pu Chen's lab. The second area was the baculovirus-insect cell expression system in Prof. Marc Aucoin's lab. The two areas might at first glance seem to be quite different; however, there are definite connections between the two. The baculovirus system in this thesis was used to generate AAV vectors that are heavily used to deliver genes for therapy, among which include genes to produce siRNA.

To reflect both these areas, this thesis first describes siRNA and the use of various delivery systems for effective use of this gene silencing mechanism, followed by the analysis of the production of AAV vectors in insect cells. The experimental data used in this thesis were part of an experimentation aimed at improving AAV vector yields at high temperature in high density cultures. It has been speculated that the reason why productivity decreases in high density cultures is due to nutrient limitation. This thesis aims to characterize nutrient consumption profiles of insect cell cultures, which are the platform used for production of AAV vectors, before and after baculovirus infection, based on the cumulative size of cells (also known as biovolume).

Chapter 1 Introduction

From finding the relationship between a molecule (e.g. RNA) and the biological effect associated with that molecule (e.g. gene silencing), to the widespread use of the molecule as a treatment, a huge number of obstacles need to be overcome. For viral delivery methods, one of these obstacles is often to produce significant amounts of the therapeutic material (i.e. viral vector, which in the case of this thesis is based on the adeno-associated virus (AAV)). AAV vectors have shown potential for the treatment of diseases using RNA interference (RNAi) by serving as the delivery agent. AAV production has mainly been accomplished by transient transfection or through the use of stable mammalian cell lines; however, recently, researchers have shown the ability to produce these vectors using the baculovirus expression vector/insect cell system (Aucoin, et al. 2008). Baculoviruses are very efficient at transferring genes to insect cells, which are amenable to producing human-like proteins and being cultivated in suspension to relatively high cell densities, making the baculovirus/insect cell system an interesting production platform for human therapeutics.

In fact, the production of AAV vectors in insect cells has emerged as a competitive process to traditional mammalian cell systems, especially with the potential of achieving significantly higher cell densities in serum-free suspension cultures and the ability to avoid using genes of pathogenic helper organisms (i.e. adenovirus or herpes virus). A major limitation of high cell density cultures, however, is the drop in specific production at high cell densities. Significant improvements in the yield have been achieved in the BEVS system due to medium replacement and cocktail additions; but, further improvements will rely on the ability to truly identify nutritional needs. It seems from our review of the literature that the reason why nutritional needs after infection have not yet been fully characterized is probably due to the difficulty in describing nutrient consumption patterns after infection when cells cease to double. If the cells cease to grow, the traditional characterization basis (cell density) is thus unavailable. We know, however, that nutrient consumption is as much present after infection as before. This is mainly to support viral replication and product synthesis.

One phenotypic change of the cells after infection is their sizes, which could be used as a basis for characterizing nutrient consumptions.

This thesis aims to establish nutrient consumption patterns in insect cell cultures, especially after cells have been infected. Better understanding of nutrient consumption could lead to the development of efficient and effective feeding strategies to maximize the production of AAV vectors at high cell densities.

1.1 Hypothesis and Objectives

The driving hypothesis of this research is that biovolume can be utilized as a parameter to characterize nutrient consumptions.

The objective of this work is to:

1. Determine the validity of using data from high temperature production of AAV vectors to assess nutrient consumption after infection;
2. Compare the relationship between nutrient consumption, metabolite production, cell density and biovolume;
3. Establish if biovolume can be used to monitor nutrient consumption and metabolite production; and,
4. Investigate, using biovolume as a new basis, differences in nutrient consumption and metabolite production before and after infection.

Chapter 2 Literature Review – siRNA Delivery

2.1 RNA Interference

RNA interference (RNAi), discovered by Andrew Fire and Craig Mello (1998), is a gene silencing phenomenon that is conserved in most eukaryotic organisms including fungi, plants and animals. This is an ancient ubiquitously-conserved mechanism used by organisms to guard against viral infection and to regulate cellular gene expression, which ensures the integrity of their genomes (Sharp 2001).

Naturally, the RNAi phenomenon is initiated by the cleavage of long dsRNAs by the RNase III endonuclease called Dicer, to form short interfering RNAs (siRNAs), which are the effector molecules of the RNA interference mechanism. These shorter segments of dsRNA range from 21 to 23 bps and are characterized by 2-nucleotide overhangs at the 3' hydroxyl end, and phosphate groups at the 5' end. The antisense strand of the siRNA is incorporated into a protein complex called the RNA-induced silencing complex (RISC) where it is able to base-pair with a gene specific mRNA (Martinez, et al. 2002). The sequence, structure, and thermodynamic stability of the siRNA determine which strand is the guide strand to be incorporated into the RISC (Tomari and Zamore 2005). After ATP-dependent unwinding and incorporation of the guide strand (Nykanen, et al. 2001), the RISC will cleave the mRNA at a site that is perfectly complementary to the siRNA sequence, committing the mRNA to being degraded.

RNAi has been found to be very useful. For example, it has been used in the study of functional genomics (Ganesan, et al. 2008). It has been studied for use in gene therapy for the treatment of cancer (Chen and Huang 2008) and also as a treatment for HIV infections (Weber, et al. 2008).

Although siRNA, can be delivered to cells as a "naked" molecule, the negative charge and the hydrophilicity of nucleic acids make the entry into cells difficult because cell membranes are also negatively charged and hydrophobic (Schiffelers, et al. 2004). Other difficulties associated with siRNA delivery include the lack of cell target selectivity, the low stability, the potential for off-target effects and the fact that it is prone to nuclease degradation in human plasma. Therefore, like most drugs and

therapeutics, either the siRNA molecule needs to be modified or a delivery agent needs to be used, or a combination of the two needs to be applied in order to successfully transport the molecule to its destination site, especially for systemic applications.

2.1.1 Chemical Modification of siRNA

Short interfering RNAs differ from traditional drugs in that they are relatively big molecules, negatively charged and have a molecular weight of approximately 7000 Da, while traditional small-molecule drugs are apolar and a have molecular weight less than 700 Da (Corey 2007). The large size and charged characteristic of siRNA make it hard to cross the cell membrane, which is also negatively charged.

RNA is a short lived molecule prone to degradation. Degradation is a serious concern in the delivery of most therapeutic molecules *in vivo*. RNA is susceptible to hydrolysis in acidic or basic environments due to its hydroxyl groups at the 2' end. It is also prone to nuclease degradation in human plasma; therefore, methods to increase the stability of the molecule have been sought. The stability of the siRNA molecule, enhanced cellular uptake and potency can be manipulated through chemical modifications; however, modifications can also complicate the incorporation of siRNA into the RISC, the unwinding of the siRNA duplex, the rate of target cleavage and the rate of product release from the RISC (Dorsett and Tuschl 2004).

The chemical modifications of siRNA fall into three categories including 1) backbone modification, 2) sugar modification, and 3) base modification.

Backbone modifications include phosphorothioate linkages and boranophosphate linkages. Both are the replacement of one or more of the non-bridging oxygen atoms on the phosphate backbone with sulfur and boron atoms, respectively (Eckstein 2002; Hall, et al. 2004). Phosphorothioate (PS) backbones can increase the resistance of siRNA to serum nucleases and increase the half-life of siRNA, while retaining its silencing ability (Corey 2007); however, cytotoxic effects have been observed when too many PS linkages were placed on the backbone (Harborth, et al. 2003). Boranophosphate linkages can improve the siRNA's silencing ability and enhance resistance to nucleases as well (Hall, et al. 2004).

Modifications to ribose have resulted in locked nucleic acids (LNA), 2'-O-methyl RNA, 2'-O-methoxyethyl (2'-MOE) RNA, 2'-fluoro RNA and 4'-thio RNA. The LNAs use a methylene bridge to link the 2' and 4' carbons on the ribose ring. LNAs improve the potency and stability of siRNA duplexes (Braasch, et al. 2003; Frieden and Orum 2006). The rest of the 2'-modified RNAs enhance the affinity of the siRNA and increase their nuclease resistance. Alternating 2'-modifications (2'-O-methyl and 2'-fluoro) have been shown to have a 500 fold increase in potency when compared to unmodified siRNA, while retaining the siRNA's silencing ability (Allerson, et al. 2005). In addition, placing the 2'-O-methyl modifications near the termini of the siRNA strand can reduce off-target effects, which are the mal-expressions of non-targeted genes (Corey 2007). The 4'-thio modification increases siRNA's resistance to nuclease digestion (Corey 2007).

Base modification is the substitution of bases using the ribo-difluorotoluyl (rF) nucleotide (Xia, et al. 2006). This modification has been shown to enhance resistance to nuclease degradation. This modification is interesting in that although the rF nucleotides cannot form normal Watson-Crick base-pairs, the silencing ability of siRNA is still retained.

None of these modifications however, allow for efficient uptake of the siRNA in the cell; therefore, the use of therapeutic delivery systems is required.

2.2 Therapeutic Delivery Systems

A successful gene delivery system should at least have one or more of the following attributes: 1) to provide targeted (cellular/ tissue) delivery; 2) to improve oral bioavailibity, 3) to sustain drug/ gene effect in target tissue, 4) to solubilize drugs for intravascular delivery, and 5) to improve the stability of therapeutic agents against enzymatic degradation (nuclease and proteases), especially for protein, peptide, and nucleic acid drugs (Panyam and Labhasetwar 2003). There are two major areas of work in gene therapy: 1) to find an effective therapeutic gene that can be expressed at the target site; and 2) to efficiently deliver that gene to the specific tissue or organ (Park, et al. 2006). In RNAi therapeutics, siRNA is used as the effective gene to be expressed

at the target site. This section will focus on the second aspect, which is the successful design of a gene-delivery vehicle. The delivery systems can be divided into two major categories, which are 1) non-viral delivery, and 2) viral delivery.

2.2.1 Non-viral Delivery

Non-viral delivery methods include conjugation and complexation of siRNA with other molecules, such as peptides, to form nano-particles. The resulting nano-particles allow improvements in cellular uptake, increased half-life and potency, and increased cell targeting specificity.

Because of their sub-micron size, nano-particles can easily penetrate deep into tissues through fine capillaries and be efficiently taken up by cells (Panyam and Labhasetwar 2003; Pinto Reis, et al. 2006). It has been proven that 100 nm size nano-particles show 2.5 folds greater uptake compared to 1 um, and 6 folds greater uptake compared to 10 um micro-particles in the Caco-2 cell line (Panyam and Labhasetwar 2003); thereby showing that size does make a difference. The size of nano-particles also allows them to be easily accumulated around tumor sites because tumor sites usually have defective vascular architectures, and an increased production of permeability factors (Yang, et al. 2006). Due to the leakiness of the tumor vessels, small particles can pass through the blood stream and accumulate at the disease site more easily. This passive accumulation phenomenon is called the enhanced permeability and retention (EPR) effect. The size of the small particles usually needs to be less than 150 nm for EPR to take effect (Li and Szoka 2007). In addition to the size, the surface properties are also important for delivery. It has been reported that particles with hydrophilic surfaces are more desirable because particles with hydrophobic surfaces are more susceptible to uptake by mononuclear phagocytes, macrophages and reticuloendothelial systems (RES) in the blood and organs (Yang, et al. 2006).

In siRNA delivery, nano-particles are usually formed by conjugation and complexation. Conjugates of siRNA are chemically modified or unmodified siRNA linked covalently to another molecule that can improve other *in vivo* properties.

Complexation involves the mixing of charged peptides/molecules with siRNA and establishing electrostatic linkages. Although compared to viral delivery systems, nano-particles are relatively safe, the delivery efficiency is usually not as high as for viral systems. An example of a nano-particle used for this purpose involves the conjugation of a chemically modified siRNA, having phosphorothioate backbone and 2'-O-methyl modification, with cholesterol, which increases the biodistribution of siRNA delivered to the liver, heart, kidneys, adipose tissue, and lungs (Soutschek, et al. 2004). A more detailed review of different types of formulations (conjugations and complexations) is presented in the following sections.

2.2.1.1 Cationic Lipids and Polymers

Cationic lipids and polymers can condense nucleic acids, which are anionic particles, through charge-charge interactions to form nano-particles. Cationic lipids enhance the uptake of the nano-particles by binding to the negatively-charged cell membranes. This advantage makes cationic lipids the most popular choice as transfection reagents *in vitro* (Li and Szoka 2007). However, this advantage becomes a disadvantage when delivered *in vivo* in that the positively charged lipids will bind to anionic serum proteins such as serum albumin causing aggregation of proteins and immune responses. To solve this problem, the siRNA can be condensed with a cationic polymer such as polyethyleneimine (PEI), protamine sulfate or polylysine (PLL) first to form the interior of the nano-particle; then, an anionic lipid can be added as the outside coat to form a neutral nano-particle (Li and Szoka 2007).

Another way to avoid the problem of positively charged lipids is to pre-condense siRNA with the cationic lipid and coat the surface with polyethylene glycol (PEG) (Park, et al. 2006; Yang, et al. 2006). PEG is a biocompatible inert polymer, which is known to increase particle stability in the presence of serum proteins and alleviate *in vivo* cytotoxicity of the particles (Chitkara, et al. 2006; Park, et al. 2006; Yang, et al. 2006). PEG-stabilized particles, however, suffer from low uptake rates because of minimized particle interaction with the cell membrane (Wheeler, et al. 1999). Polyelectrolyte complexes (PECs) are based on the principle of polynucleotide condensation followed by surface modification and are promising candidates for

siRNA delivery. Most commonly, siRNA PECs are formed by interacting siRNA with a polycation first and then conjugating PEG onto the surface of the particle. Studies have shown that PECs are able to be successfully delivered to human hepatoma cells (HuH-7) resulting in considerable RNAi activity being observed (Park, et al. 2006).

2.2.1.2 Peptide Delivery System – Cell-Penetrating Peptides

Peptides are also a promising category of gene delivery system because of their biocompatibility and programmability (Chitkara, et al. 2006; Ramachandran and Yu 2006; Yang, et al. 2006). Polycationic peptides can neutralize the negative charges present on the surface of the siRNA molecule, thus condensing it into a hydrophobic core. Synthetic peptides can furthermore be designed to incorporate a cytoplasmic translocation signal (CTS) (Brokx, et al. 2002; Simeoni, et al. 2003). The CTS enhances the translocation of the peptide-based delivery vehicle through cellular membranes (Brokx, et al. 2002; Simeoni, et al. 2003).

There is a class of short peptides, made of less than 30 amino acids, such as TAT and oligoarginine, that have been used to internalize different bioactive compounds into cells (Fischer, et al. 2004; Mae and Langel 2006; Morishita and Peppas 2006; Noguchi and Matsumoto 2006; Sato, et al. 2006; Zatsepin, et al. 2005). These peptides are termed cell-penetrating peptides (CPP) or protein transduction domains (PTD) and are able to deliver bioactive materials into tissues and cells by chemically hybridizing with and perturbing the lipid bilayer structure of the cell membrane without the need for a receptor. Table 1 below lists some of the common CPPs and their sequences (Pujals, et al. 2006; Sato, et al. 2006).

By linking these CPPs with peptides containing other desired properties, the previously non-CPP can become a CPP (Noguchi and Matsumoto 2006). Once the peptides cross the cell membrane and enter the interior of the cell, they will be rapidly degraded, thus releasing the genetic material (Jarver and Langel 2004).

Table 1: Effective CPPs for the Delivery of Molecules to Cells

CPP	Sequence	Length
Protein-derived peptides		
Tat	GRKKRRQRRRPPQ	11
Penetratin (Antp)	RQIKIWFQNRRMKWKK	16
VP22	DAATATRGRSAASRPTERPRAPARSASRPRRVD	33
Amphipathic peptides		
MAP	KLALKLALKALKAALKLA	18
Transportan	GWTLNSAGYLLGKINLKALAALAKKIL	27
Transportan-10	AGYLLGKINLKALAALAKKIL	21
KALA	WEAKLAKALAKALAKHLAKALAKALKACEA	30
Pep-1	KETWWETWWTEWSQPKKKRKV	21
MPG	GALFLGFLGAAGSTMGAWSQPKSKRKV	27

A common feature existing in all CPPs is that they have a high degree of positive charges due to their high content of the basic amino acids, lysine and arginine. The presence of the cationic amino acids is important for internalization of the CPP-binding cargo. At physiological pH, both lysine (pKa = 10.5), and arginine (pKa = 12) are protonated; therefore, they will interact with the negatively charged sulphate and phosphate groups of the extracellular cell matrix (ECM) (Pujals, et al. 2006). The number of arginines needed for optimal cell-penetration is between 7 and 15 depending on the techniques and the cell line used (Pujals, et al. 2006). Studies have shown that attaching a small hydrophobic molecule like biotin to a CCP like the Tat peptide can cause a 6-fold increase in cellular uptake of the peptide (Pujals, et al. 2006).

2.2.2 Viral Delivery System

The benefit of using viral vectors to deliver genes coding for the production of siRNA *in vivo* and *in vitro* is that viruses have evolved to successfully transduce cells efficiently. Once cells are transduced, the recombinant genes can be expressed in the host cell for knockdown of the target genes. To produce siRNAs in the cells, usually a

segment of DNA coding for short hairpin RNA (shRNAs) is inserted into the expression vector driven by RNA polymerase III-dependent promoters such as pU6 and pH1-RNA (Shen, et al. 2003) or pRNA polymerase II CMV (Xia, et al. 2002). As the recombinant gene enters the cell, siRNA will be synthesized from the shRNA as was previously described for RNA interference (Section 2.1). Another way to produce siRNA in cells is to use two separate vectors: one coding for the sense and one coding for the antisense strand of a small RNA with 19 nucleotides matching the targeted mRNA gene sequence. Small interfering RNA usually has 21 nucleotides with 2 nucleotides overhanging at the 3' end; therefore, only 19 nucleotides are needed to match to the gene sequence. The two strands will form a duplex *in vivo* (Elbashir, et al. 2001). Of the two methods, the method that utilizes the shRNA appears to inhibit gene expression more efficiently than the duplex-forming method (Yu, et al. 2002). Viruses that have been used to deliver recombinant genes for siRNA synthesis include retrovirus, lentivirus, adenovirus, adeno-associated virus and more recently even baculovirus (Dorsett and Tuschl 2004; Ong, et al. 2005).

2.2.2.1 Retroviruses

Retroviruses were the first viral vectors to be used for RNAi (Li, et al. 2006). Although successful applications in many cell lines have been achieved *in vitro*, there are two major drawbacks of using retroviruses *in vivo*. The first disadvantage is that retroviruses work by integrating its genome into the host cell's chromosome, thus raising safety concerns. The risk with chromosome integration is that it has great potential to cause insertional mutagenesis and thus causing potential carcinogenesis (Li, et al. 2006). The second major disadvantage is that retroviruses are only able to infect actively dividing cells. Most mammalian cells are not actively dividing; therefore, its use in human therapeutic applications is limited (Li, et al. 2006). Nevertheless, Brummelkamp et al. (2002) and Rubinson et al. (2003) have used retroviruses for RNAi in mammalian cells.

2.2.2.2 Lentiviruses

Lentiviruses are a subclass of retroviruses, which include the human immunodeficiency virus (HIV). There are several advantages of using lentivirus as a delivery agent. The first is that lentiviruses are able to infect a wide range of cell lines *in vitro* including primary cells such as stem cells, fertilized oocytes, and blastocysts, and various cellular targets *in vivo* such as brain and liver cells (Wiznerowicz and Trono 2003). Secondly, lentiviruses, unlike retroviruses, are able to infect non-cycling and post-mitotic cells. Thirdly, transgenes delivered by lentiviruses are not silenced during cell development; thus, transgenic animals can be generated by infecting embryonic stem cells or embryos using lentiviral vectors (Rubinson, et al. 2003). Lastly, lentiviruses are able to accommodate large inserts into its genome and are less immunogenic than adenoviruses (Li, et al. 2006). Lentiviruses have been used to deliver vectors containing shRNA for the synthesis of siRNA into primary mammalian cells, stem cells and transgenic mice (Rubinson, et al. 2003). In addition, Wiznerowicz and Trono (2003) have used lentivirus-mediated expression of siRNA to trigger RNAi in a drug-inducible fashion.

2.2.2.3 Adenoviruses

Adenoviruses are a popular choice of virus especially in the area of cancer gene therapy. About 25% of current clinical gene therapy trials use adenoviruses (Relph, et al. 2005). The genome delivered by adenovirus cannot be efficiently integrated into the host cell's genome; thus, the probability of having insertional mutagenesis with the use of this viral vector is relatively low (Calos 1996). At the same time, the genetic expression is relatively transient because the information can be lost in the process of cell replication (Li, et al. 2006). In cancer-therapy, transient expression of a toxic gene is sufficient (Li, et al. 2006). Advantages of using adenovirus include the availability of high virus titers, and the ability to infect a wide spectrum of cell types including primary cell lines (Arts, et al. 2003; Shen, et al. 2003) . Disadvantages of using adenovirus include the lack of cell specificity and the significant cytotoxicity to liver cells (Li, et al. 2006). Examples of adenoviral applications include the delivery of siRNA to both brain and liver *in vitro* and *in vivo*. Xia et al. (2002) have also used

adenovirus-mediated expression of siRNA to successfully reduce the expression of polyglutamine in neurons, which is a major cause of at least nine inherited neurodegenerative diseases.

2.2.2.4 Adeno-associated Viruses

The advantages of using adeno-associated viruses (AAVs) as gene therapy vectors include: 1) the ability to infect a broad spectrum of both dividing and non-dividing cells; 2) wild-type AAV has never been found to be associated with any disease and it cannot replicate inside infected cells without the aid of a helper virus; and 3) it usually does not stimulate a cell-mediated immune response (Stilwell and Samulski 2003). AAVs have been used to deliver shRNA to generate disease models (Hommel, et al. 2003) that target tyrosine hydroxylase mRNA within the neurons of the midbrain. Tyrosine hydroxylase is an important enzyme for the production of dopamine, a neurotransmitter responsible for a range of actions including food intake, addiction, and control of movements (Hommel, et al. 2003). In addition, the degeneration of dopamine-generating neurons is the primary cause of Parkinson disease (Gibb 1997).

2.2.2.5 Baculoviruses

Baculoviruses are insect cell viruses (see Section 3.1) that have recently found themselves as gene delivery vehicles for mammalian cells. More commonly known in this setting as BacMam vectors, these vectors have gained attentions because: 1) they have a high capacity for large inserts of recombinant genes, and 2) they are not known to replicate or express viral proteins inside mammalian cells because their natural hosts are insects. Nicholson et al. (2005) have recently used baculoviruses for siRNA delivery into Saos2, HepG2, Huh7, and primary human hepatic stellate cells and have successfully knocked down a recombinant GFP gene in each. In addition, Ong et al. (2005) used baculovirus in the delivery of siRNA to reduce recombinant luciferase being expressed in rat brain.

Chapter 3 Literature Review – Baculovirus–Insect Cell System

3.1 Baculoviruses

Baculoviruses are rod-shaped, circular double-stranded DNA viruses. They are about 40 – 50 nm in diameter and 200 – 400 nm in length (Kelly, et al. 2007). The circular double-stranded DNA consists of approximately 80 – 200 kbps (Kelly, et al. 2007). Baculoviruses are characterized by their ability to form occlusion bodies around virions. There are two genera in the Baculoviridae family, the granuloviruses (GVs) and the nucleopolyhedroviruses (NPVs). The GVs form small granular occlusion matrices called granulin, which usually only encapsulate one virion. The NPVs form large occlusion matrices called polyhedrin, which usually encapsulate many virions. There are also two forms of baculovirus progeny, the budded virus (BV) and the occlusion-derived virus (ODV), which will be explained in more details in Section 3.1.1.

More than 500 types of baculoviruses have been identified (Hu 2005). The most studied baculovirus is the *Autographa californica* multinucleopolyhedrovirus (AcMNPV). This virus was originally isolated from alfalfa looper (a lepidopteran). The baculoviruses used in this thesis are AcMNPV.

Baculovirus' host ranges are restricted to invertebrates. The most common hosts are members of the order Lepidoptera (moth). Other orders that are also infected by baculoviruses include Diptera (flies), Hymenoptera (sawflies), and Trichoptera (caddis flies) (Hu 2005; Kelly, et al. 2007). In cell culture, the two most commonly used insect cell lines are from *Spodoptera frugiperda* and *Trichoplusia ni.*

3.1.1 Structure of Baculoviruses

Budded viruses (BV) and occlusion-derived viruses (ODV) are genetically identical, but they differ in morphology, time and cellular site of maturation, structural proteins, and infectivity (Figure 1) (Kelly, et al. 2007). The rod-shaped, circular double-stranded

DNA is condensed in the nucleocapsid of both forms of the virus (Blissard 1996). The BVs have spike-like structures on one end of the virion known as a peplomer that is composed of the glycoprotein gp64 (Volkman, et al. 1984). The glycoprotein, gp64, is an important protein for budded virus infection. The ODV does not have gp64, instead it has the envelope protein P74, which is important for ODV attachment to midgut cells (Kelly, et al. 2007). The occlusion matrices envelop protein is called polyhedrin. Polyhedrin protein protects the ODVs against proteolysis at the late stage of infection as well as against physical and biochemical decay while outside of the host (Hu, et al. 1999).

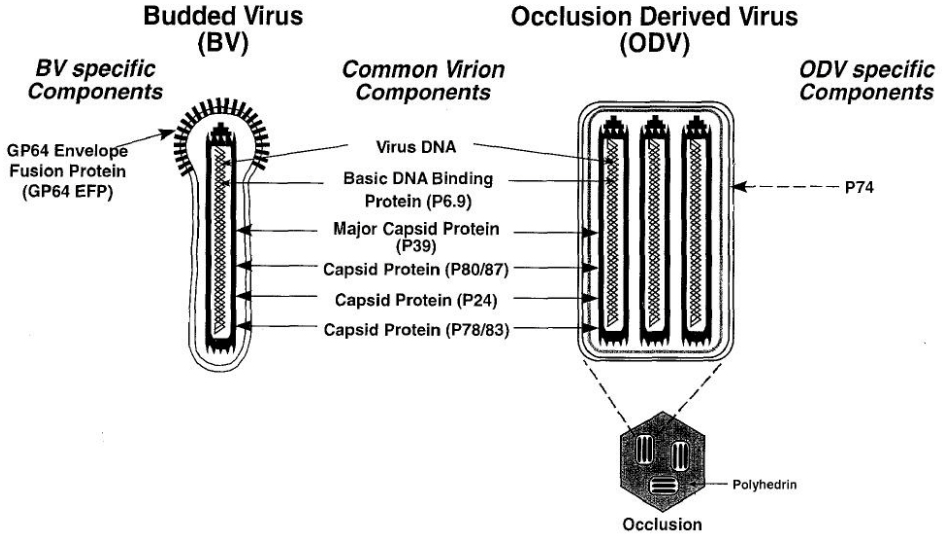

Figure 1: Budded and Occluded Form of Baculoviruses (Blissard 1996)

3.2 Baculovirus and the Baculovirus Expression Vector System

The baculovirus expression vector system is an attractive system for recombinant protein production because:

1. The host cell for this virus is eukaryotic. Insect cells can perform higher order post-translational modification of proteins compared to bacterial and yeast cells.

The recombinant proteins made in insect cells will more closely resemble the human proteins made for therapeutic purposes.

2. Baculoviruses have a high capacity for inserts of multiple or large recombinant genes.
3. Baculoviruses are considered safe because they are unable to replicate in mammalian cells.
4. The two very late baculoviral genes, p10 and polyherin, are highly expressed and they are not essential in culture for the production of recombinant proteins. Thus, the two genes can be removed and replaced by a transgene of choice.
5. Insect cells can be cultured to very high cell densities. The reported cell density achieved in culture is > 1 x 10^7 cells/ml (Elias, et al. 2000). Therefore, coupling the high cell density with the strong promoters inside insect cells, can greatly amplified protein production.
6. It is relatively easy to culture insect cells (Sander and Harrysson 2007) compared to the culture of mammalian cells.

3.2.1 Recombinant Proteins Production

One of the major applications of BEVS is the production of recombinant proteins. Smith et al. (1983) were the first ones to use AcMNPV as an expression vector to produce human β-interferon in insect cells. Since then, many foreign genes have been expressed using the baculovirus expression system. Examples of recombinant proteins produced by BEVS include monoclonal antibodies and tumor necrosis factor-β (TNF-β) (Sandhu, et al. 2007).

Virus-like particles (VLPs) can also be produced through baculovirus infection of insect cells. Virus-like particles are generally composed of viral structural proteins that self-assemble to form “viruses” that do not contain viral nucleic acid (Palomares, et al. 2006). VLPs are made by the simultaneous assembly of major viral structural proteins. Virus-like particles are not infectious but they are able to cause immunogenic responses due to the epitopes present on the viral proteins; therefore, they can be used as vaccines (Palomares, et al. 2006).

The production of VLPs usually requires the production of more than one viral protein. There are two ways of producing VLPs. One way is by employing more than one baculovirus, each carrying a gene that is responsible for one viral structural protein. After co-infection of cells with multiple vectors, simultaneous production of the viral proteins will allow them to self-assemble into viral particles (Aucoin, et al. 2007; Mena, et al. 2007). The other method is to use a single baculovirus containing multiple genes coding for multiple viral structural proteins (Mena, et al. 2007). The first method is more popular because it allows for the manipulation of different multiplicities of infection (MOI) for each recombinant baculovirus, which can lead to the production of VLPs with varying protein composition (Mena, et al. 2007).

Virus-like particles expressed using the baculovirus expression vector system include HIV, herpes simplex virus, polyomavirus, parvovirus, infectious bursal disease virus, hepatitis C virus, enterovirus 71, and very recently the severe acute respiratory syndrome coronavirus (SARS-CoV) (Hu 2005). To date, there is still no approved human therapeutic based on the BEVS in North America (Sandhu, et al. 2007). However, there are several products in their advanced clinical trials. These include PROVENGE®, from Dendreon Corporation, which is a therapeutic for prostate cancer in the late stage phase III of clinical trial, and it has received fast track review from the FDA; Cervarix®, made by GlaxoSmithKline, which is approved in Australia and Europe, is a prophylactic vaccine against human papillomavirus (HPV); and FLUBLOK™, from Protein Sciences Corporation, which is a therapeutic for influenza that is in phase III of clinical trials (Cox 2004).

3.3 Nutrient Requirements

There are many factors that can influence recombinant protein expression levels in insect cells using the baculovirus vector expression system. These factors include: the ratio of the number of virus particles to the number of, also known as the multiplicity of infection (MOI); the density of the cells when the infection is carried out, often referred to as the time of infection (TOI); the type of recombinant protein expressed; the type of the cell line used; the type of nutrient supplemented; and the way of nutrient supplementation. This section of the review will focus on of the nutrient requirements

of insect cells, specifically for Sf-9 cells. It is important to understand the nutrient requirements of insect cells because nutrient levels affect cell metabolism, which will have impacts on the production of recombinant proteins. It is known that the nutritional requirements of insect cells before and after infection are different (Palomares, et al. 2004; Radford, et al. 1997; Wang, et al. 1993; Wang, et al. 1993). Although, it is known that metabolic differences exists before and after infection, the exact differences in terms of nutrient uptake have not yet been thoroughly investigated. The following section is meant to report on the state of the art of insect cell metabolism.

3.3.1 Sf-9 Cells

This cell line was derived from the pupal ovarian tissue of the fall armyworm, *Spodoptera frugiperda*. This cell line is highly susceptible to AcMNPV baculovirus infection. Therefore, it is often used to produce recombinant baculoviral stocks and to produce recombinant proteins. The nutrient review that follows in this section focuses on Sf-9 cells.

3.3.2 Essential Nutrients and Supplements

3.3.2.1 Carbohydrates

Glucose is considered to be the most important source of carbon for biomass production (Ferrance, et al. 1993). It is the most consumed nutrient (Rhiel and Murhammer 1995) and the main energy source (Drews, et al. 2000). The flux through glycolysis is three times higher than the flux from glutamine for energy generation (Drews, et al. 2000). The high levels of glucose consumption are an indication of an active glycolytic pathway in insect cells (Benslimane, et al. 2005). Glucose is also metabolized through the pentose phosphate pathway generating reducing power and nucleic acid precursors (Benslimane, et al. 2005). Benslimane et al (2005) reported about 4 times more glucose being metabolized through the pentose phosphate pathway than through the glycolytic pathway (TCA cycle) for Sf-9 cells.

When glucose is in excess, the rate of consumption will increase. Since cells only require certain amounts of cellular energy and precursors, when glucose supply is exceeding the requirements, overflow metabolism through the TCA cycle will occur, generating metabolic byproducts including alanine, lactate and ammonia (Doverskog, et al. 1997). Glucose-derived pyruvate is the major carbon source for alanine production (Doverskog, et al. 1997); thus, alanine formation is regulated by glucose concentration. Although, alanine itself is nontoxic to cells at high-levels, the production of alanine will result in loss of carbon source and reducing power (Ohman, et al. 1995) since alanine will only yield 7% of energy compared to complete oxidation of glucose (Mendonca, et al. 1999).

Very little overflow metabolism is observed when both glucose and glutamine are limiting as seen when operating in fed-batch mode (Doverskog, et al. 1997). It is best to maintain the glucose level just above its critical value to avoid unnecessary substrate consumption – something not often done in batch cultures. The critical concentration of glucose may differ from culture to culture due to different culture conditions, e.g. age of the cell-line, type of cells, and the type of media. When glucose is exhausted, the main energy supplier is likely to be switched to glutamine, alanine formation will stop and ammonia will start to form (Bedard, et al. 1993) causing increases in pH of the culture (Rhiel and Murhammer 1995). Following glucose exhaustion, the growth of the cells will usually stop (Bedard, et al. 1993) and apoptosis can be triggered (Meneses-Acosta, et al. 2001). Although glucose and glutamine have been identified as the main energy sources, feeding strategies using only glucose and glutamine have not allowed significant increases in cell concentration and protein productivity. This failure indicates that other nutrients might be the limiting factors in achieving the two objectives (Mendonca, et al. 1999).

Other carbon sources that can also be utilized by insect cells include fructose, maltose and sucrose. Fructose is only consumed after glucose depletion. Maltose, a dimer of glucose, is also found to be completely consumed at the end of cultures containing also glucose and fructose (Bedard, et al. 1993; Rhiel and Murhammer 1995). Cultures containing serum, such as the one used in the aforementioned studies, may be responsible for the depletion of maltose due to the presence of maltase in

serum. Sucrose, a dimer consisting of glucose and fructose, is normally not consumed in insect cell lines; however, some reports have indicated sucrose consumption after baculovirus infection (Benslimane, et al. 2005; Wang, et al. 1993). Sucrose can be broken down to release glucose by α-glucosidase, which is the same enzyme that breaks down maltose (Wang, et al. 1993). Sucrose metabolism will add to the energy burden for the cells because the cells will need to synthesize α-glucosidase to break down sucrose (Wang, et al. 1993). The maximum specific growth rate in glucose-deficient culture is 25% lower than in glucose-supplied cultures. This indicates that other carbon sources are not as effective as glucose in providing energy to the cells (Mendonca, et al. 1999). This ineffectiveness might be due to the loss of energy in producing the enzymes needed for the metabolism of other carbon sources as in the case of sucrose metabolism (Mendonca, et al. 1999; Wang, et al. 1993).

3.3.2.2 Amino Acids

3.3.2.2.1 Glutamine

Glutamine is the most consumed amino acid in insect cell culture. It is also the only amino acid known to undergo significant degradation in culture media (Ozturk and Palsson 1990). The half-life of glutamine is about 600 hrs at 27 °C (Ferrance, et al. 1993). Ozturk and Palsson (1990) have reported a glutamine half-life to be about 500 h at 37 °C. It is used by the cells as an energy source, as well as for biomass and nucleic acid synthesis (Lehninger 1975; Rhiel and Murhammer 1995). It is also a major source of nitrogen (Drews, et al. 2000). It can be metabolized via the TCA cycle as 2-oxoglutarate (2-OG) to generate energy and liberate ammonia ions as shown in Figure 2 (Benslimane, et al. 2005; Drews, et al. 2000). About 4.6% of the glutamine consumed in the culture enters the TCA cycle (Benslimane, et al. 2005) in the presence of glucose. In glucose-deprived cultures, the glutaminase/glutamate dehydrogenase pathway will be up-regulated to generate energy using glutamine via the TCA cycle (Drews, et al. 2000).

Glutamine is the major source of ammonia (Ohman, et al. 1995). Ammonia can be liberated from glutamine via the glutaminase/glutamate dehydrogenase pathway as

shown in Figure 2. Since alanine formation requires the incorporation of ammonia, glutamine metabolism will also affect alanine production (Ohman, et al. 1995). As a result in glutamine-limiting conditions, alanine formation will be decreased as well (Doverskog, et al. 1997). Consumption of other amino acids increase when glutamine becomes limiting in the culture. Of these other amino acids, the consumption of glutamate, aspartate, and asparagine increase the most because they can act as precursors for oxaloacetate (OA) as shown in Figure 2 (Bedard, et al. 1993).

Ohman et al. (1996) have shown that insect cells can be sustained in cultures without glutamine, glutamate and aspartate if ammonium ions are supplied to culture medium. This indicates that insect cells are able to synthesize glutamine. Although synthesis of glutamine is possible, the maximum specific growth rate of the cells grown is reduced by 63% in glutamine-limiting cultures, indicating exogenous glutamine is more efficiently used by the cells (Mendonca, et al. 1999).

Similar to mammalian cells, it is found that glutamine consumption rate is not affected by glucose concentration in insect cells (Rhiel and Murhammer 1995). However, glucose and glutamine metabolic routes are co-regulated; therefore, as mentioned previously, appropriate amounts of glucose and glutamine are important to avoid the accumulation of potentially toxic byproducts and metabolic wastes (Palomares, et al. 2004). The optimum glucose/glutamine ratio found for hybridoma cells is 2 – 7 (Savinell and Palsson 1992). In insect cell cultures, the glucose/glutamine ratios are often maintained around 2 – 7 as well, with reported values of 5 (Bruggert, et al. 2003; Ohman, et al. 1995), and 2.5 (Bedard, et al. 1993; Ferrance, et al. 1993; Weiss, et al. 1981). Just like glucose, the initial concentration of glutamine will affect its consumption rate. Increased initial concentration will result in increased uptake rate (Mendonca, et al. 1999).

Cells need to achieve certain sizes before they can progress through the cell cycle (Bussolati, et al. 1996). The increase in cell size is associated with the increase in cell volume, which is related to the cell water content (Bussolati, et al. 1996). Therefore, cell volume is regulated by the transport rates of osmolytes across the cell membrane (Bussolati, et al. 1996). A significant portion of intracellular amino acids do not have metabolic function; instead, those amino acids act as osmolytes (Bussolati, et al. 1996).

Glutamine and glutamate, which can be converted interchangeably, make up more than 70% of amino acid contents intracellularly. As a result, glutamine is important in cell cycle regulation and increase in cell volume (Bussolati, et al. 1996). It is desirable to maintain a high extracellular concentration of glutamine to be used as osmolytes for optimal cellular growth (Bussolati, et al. 1996).

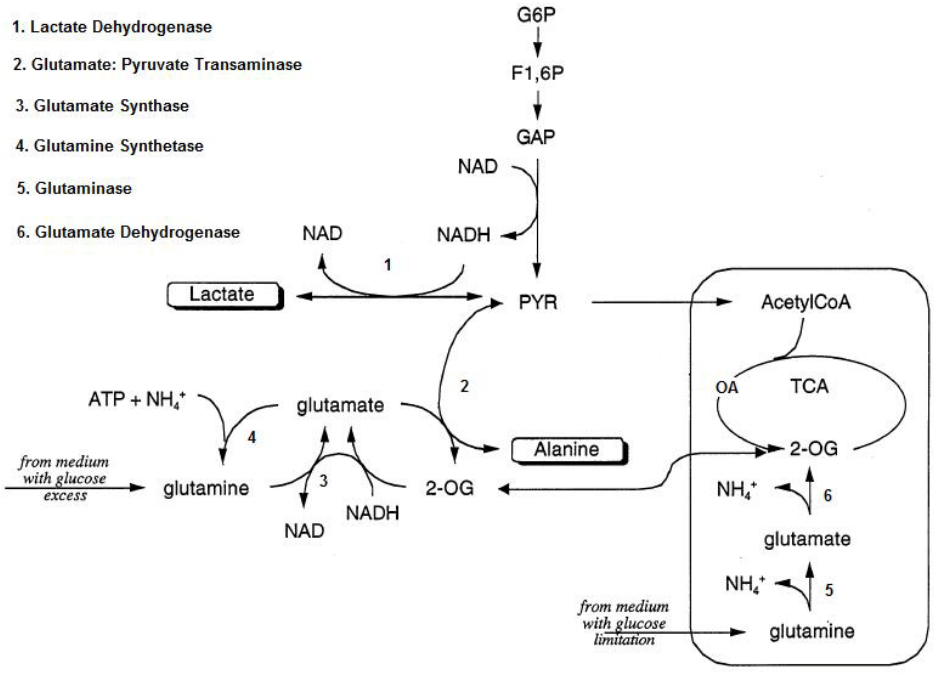

Figure 2: Sf-9 Cell Metabolism (modified from Drews, et al. 2000)

3.3.2.2.2 Glutamate

Glutamate is a non-essential amino acid because it can be synthesized in insect cells. Glutamate can be made from aspartate, glutamine, alanine and proline (Bruggert, et al. 2003; Mitsuhashi 1982). Although non-essential, glutamate is often contained in yeastolates (about 2 mM) and serums, thus found in insect cell cultures (Bruggert, et al. 2003; Drews, et al. 2000; Mitsuhashi 1982). It is used for energy production in addition to biomass generation (Ferrance, et al. 1993). It is one of the most rapidly consumed nutrients (Bedard, et al. 1993) and is one of the major sources of nitrogen

(Drews, et al. 2000). When glucose is abundant, decreased amount of glutamate will account for increased amount of alanine production (Bedard, et al. 1993) by glutamate-pyruvate transaminase:

$$\text{Glutamate (providing } NH_4^+\text{) + pyruvate} \rightarrow \text{alanine + 2-oxoglutarate.}$$

Glutamate accumulates when 2-oxoglutarate is in abundance (Bedard, et al. 1993). When both glucose and glutamine become scarce, glutamate can be converted to 2-oxoglutarate and ammonia by glutamate dehydrogenase (Ohman, et al. 1995). The TCA cycle can then metabolize 2-oxoglutarate to generate energy for the cell. The liberated ammonium ions will accumulate in culture. Glutamate is used to synthesize nucleic acids indirectly because it can be converted to glutamine at the cost of ATP molecules. Glutamate conversion to glutamine will be limited when glucose is limiting because glutamate is preferentially used as an energy source (Mendonca, et al. 1999).

3.3.2.2.3 Asparagine

Asparagine is a non-essential amino acid (Bruggert, et al. 2003). It is often found in culture media because of supplementation by yeastolates and serums (Bruggert, et al. 2003; Drews, et al. 2000; Mitsuhashi 1982). Asparagine is used for energy production (Drews, et al. 2000) and biomass generation (Ferrance, et al. 1993). Glutamine is preferred over asparagine in energy generation. Only when glutamine is depleted will asparagine consumption increase (Ohman, et al. 1995); thus, it is often found to accumulate in culture (Benslimane, et al. 2005). Asparagine can act as a precursor for oxaloacetate and enter the TCA cycle to generate energy when glutamine is depleted in the culture (Bedard, et al. 1993). Asparagine metabolism usually begins with conversion to aspartate (Rhiel, et al. 1997; Rhiel and Murhammer 1995).

3.3.2.2.4 Aspartate

Aspartate is a non-essential amino acid (Bruggert, et al. 2003). It is used for energy production and nucleic acid formation in addition to biomass generation (Ferrance, et al. 1993). It is also one of the most consumed nutrients (Bedard, et al. 1993). Aspartate can be catabolized from asparagine with the release of ammonium ion.

3.3.2.2.5 Alanine

Alanine is a non-essential amino acid for insect cells (Bruggert, et al. 2003). Alanine is the only major byproduct formed under excess glucose and glutamine conditions (Doverskog, et al. 1997). Glutamine metabolism will release ammonium ions, part of these ammonium ions will be incorporated in the anabolism of alanine. Alanine production will stop once glucose is depleted in the culture; this indicates that glucose is the carbon source for alanine formation (Bedard, et al. 1993). Alanine is often produced early in the culture due to excess carbon sources (Mendonca, et al. 1999). Alanine is consumed once glucose is depleted and can serve as an energy source for the cells by releasing pyruvate, which can enter the TCA cycle to generate energy, as shown below. The glutamate released can also enter the TCA cycle as 2-oxoglutarate by releasing an ammonium ion. Therefore, as a result of alanine catabolism, ammonia will start to accumulate in culture (Bedard, et al. 1993; Ohman, et al. 1995; Rhiel and Murhammer 1995).

Alanine + 2-oxoglutarate → Glutamate (providing NH_4^+) + Pyruvate.

Although alanine accumulation does not inhibit growth (Drews, et al. 1995; Drews, et al. 2000), excess alanine formation will drain the cells of reducing powers (Ohman, et al. 1995) since most biosynthetic processes will require energy.

3.3.2.2.6 Serine

Serine is used for the production of energy and generation of biomass (Ferrance, et al. 1993). It is one of the most rapidly consumed nutrients (Bedard, et al. 1993). Serine can be used to synthesize nucleic acids (Drews, et al. 1995; Tremblay, et al. 1992). It is also used in cysteine biosynthesis (Doverskog, et al. 1998). Cell division will stop once serine in the media is depleted (Bruggert, et al. 2003).

3.3.2.2.7 Glycine

Glycine is important in threonine metabolism (Ferrance, et al. 1993). Glycine can be made from serine in some organisms, but it cannot be formed in Sf-9 cells because the cells lack mitochondrial serine hydroxymethyltransferase (Tremblay, et al. 1992). Glycine is an absolute requirement for Sf-9 cells (Tremblay, et al. 1992), although the consumption is usually negligible and is usually not within the detection limit of the protocols generally used (Bedard, et al. 1993; Drews, et al. 1995). Glycine is used for biomass generation (Drews, et al. 1995) and nucleic acid production (Doverskog, et al. 1997). Insufficient amounts of glycine will lead to about 50 – 60% reductions in protein synthesis (Bruggert, et al. 2003).

3.3.2.2.8 Threonine

Threonine is used for energy production and biomass generation (Ferrance, et al. 1993). Consumption of threonine increases as glutamine becomes limiting, suggesting that threonine is also used as an energy source (Ohman, et al. 1995).

3.3.2.2.9 Cysteine

Cysteine is a non-essential amino acid for insect cells (Bruggert, et al. 2003). It can be synthesized from methionine. However, the synthesizing ability depends on the proliferation state of the cells. Only cells in the early exponential phase can synthesize cysteine and grow well in cysteine-free media (Doverskog, et al. 1997). Cysteine is consumed more than 25% over the period of culture for Sf-9 cells (Palomares and

Ramirez 1996), though the consumption is not related to biomass generation (Doverskog, et al. 1998). Cysteine is used to synthesize proteins and produce glutathione, an antioxidant protecting cells from free radicals (Doverskog, et al. 1998). Cysteine also plays a role in the cysteine transport system (Doverskog, et al. 1998). The transport system exchanges cysteine with glutamate and is operated by concentration gradients across the cell membrane. When cysteine concentration increases, there will be an increase in the export of glutamate (Bannai 1986). When intracellular glutamate concentration is low, the cell will restore the concentration by use of other transport systems (Doverskog, et al. 1998). All these transport systems require energy. Increased cysteine concentration will result in increased cysteine uptake rate. As a result, increased uptake rate will increase the cellular maintenance energy and will have a negative effect on cell growth (Doverskog, et al. 1998). In addition, increased intracellular concentration of cysteine will lead to the production of H_2S, which is inhibitory to cells (Mehler 1986). Nonetheless, insufficient amount of cysteine will affect the transport of leucine, valine, and tryptophan to cells, which depends on the export of cysteine and methionine (Doverskog, et al. 1998). In Sf900-II medium, the amount of cysteine is sufficient for cells and not limiting (Rhiel, et al. 1997).

3.3.2.2.10 Methionine

Methionine is an essential amino acid for insect cell growth (Mitsuhashi 1982). It is used as an energy source for cells (Drews, et al. 1995) and can be used to synthesize cysteine (Doverskog, et al. 1997). It is also used as an exchange substrate for leucine, isoleucine, valine and tryptophan (Doverskog, et al. 1998). Therefore, decreases in methionine will affect the transport of all these amino acids (Doverskog, et al. 1997). Methionine uptake rate is inversely related to cysteine concentration (Doverskog, et al. 1998). Methionine feeding has been shown to slow down cell death (Mendonca, et al. 1999).

3.3.2.2.11 Leucine

Sf-9 cells do not consume much leucine (Ferrance, et al. 1993; Palomares and Ramirez 1996). Leucine can be used for protein synthesis and biomass generation (Doverskog, et al. 1998; Drews, et al. 1995), but is not used for energy generation (Ferrance, et al. 1993). Uptake of leucine will increase when the concentration of cysteine in the culture increases (Doverskog, et al. 1998).

3.3.2.2.12 Isoleucine

Sf-9 cells do not consume much isoleucine (Ferrance, et al. 1993; Palomares and Ramirez 1996). Cultures usually have a net accumulation of isoleucine at the end of the culture (Benslimane, et al. 2005). Isoleucine can be incorporated into cell mass (Drews, et al. 1995) and is not used for energy generation (Ferrance, et al. 1993). Uptake of isoleucine will increase when the concentration of cysteine in the culture increases (Doverskog, et al. 1998).

3.3.2.2.13 Valine

Sf-9 cells do not consume much valine (Ferrance, et al. 1993). It can be used for protein synthesis and biomass generation (Doverskog, et al. 1998; Drews, et al. 1995), but is not used for energy generation (Ferrance, et al. 1993). Uptake of valine will increase when the concentration of cysteine in the culture increases (Doverskog, et al. 1998).

3.3.2.2.14 Histidine

Sf-9 cells do not consume much histidine (Ferrance, et al. 1993; Palomares and Ramirez 1996). Histidine can be incorporated into cell mass (Drews, et al. 1995).

3.3.2.2.15 Arginine

Arginine is used for energy production and biomass generation (Drews, et al. 1995; Ferrance, et al. 1993). Consumption of arginine increases as glutamine becomes

limiting, suggesting that arginine can be used as an energy source (Ohman, et al. 1995). Without sufficient amounts of arginine, the cells will stop to divide (Bruggert, et al. 2003).

3.3.2.2.16 Proline

Sf-9 cells do not consume much proline (Ferrance, et al. 1993; Palomares and Ramirez 1996). Proline can be used to produce glutamate in culture (Ferrance, et al. 1993).

3.3.2.2.17 Tyrosine

Tyrosine is important for insect cell growth (Mitsuhashi 1982) and it is an essential amino acid for Sf-9 cells (Gibbs, et al. 1993). It can be used to make ring-containing components in biosynthesis (Ferrance, et al. 1993) and can be incorporated into cell mass (Drews, et al. 1995). Feeding the cells with tyrosine will slow down cell death (Mendonca, et al. 1999). Cell division will stop if tyrosine is not supplied in sufficient amounts (Bruggert, et al. 2003). However, too much tyrosine in the media can cause the precipitation of other medium components that might be essential for cell growth (Marteijn, et al. 2003).

3.3.2.2.18 Lysine

Sf-9 cells do not consume much lysine (Ferrance, et al. 1993; Palomares and Ramirez 1996). The consumption of lysine increases as glutamine becomes limiting, suggesting that this amino acid can be used as an energy source (Ohman, et al. 1995). Lysine can also be incorporated into cell mass (Drews, et al. 1995). Insufficient amount of lysine can reduce protein production by 50 – 60% (Bruggert, et al. 2003).

3.3.2.2.19 Phenylalanine

Sf-9 cells do not consume much phenylalanine (Ferrance, et al. 1993; Palomares and Ramirez 1996). It can be used to make ring-containing components in biosynthesis (Ferrance, et al. 1993) and can be incorporated into cell mass (Drews, et al. 1995).

3.3.2.3 Metabolic By-products

3.3.2.3.1 Lactate

Lactate production is not as common in insect cells as it is in mammalian cells (Ohman, et al. 1995) and the production never reaches inhibitory levels (Reuveny, et al. 1993a). Lactate usually only accumulates in oxygen-limiting cultures (Reuveny, et al. 1993b); however, lactate has also been found to accumulate in cultures with high initial glucose concentration (around 50 mM) (Rhiel and Murhammer 1995). Lactate production is generally a signal of low protein yield and off-balance metabolism (Wang, et al. 1996). The major source of lactate production comes from glucose (Wang, et al. 1996). Lactate production below 2 mM indicates a stress-free culture and shows that most glucose is completely oxidized (Garnier, et al. 1996). Lactate consumption will start once glucose is exhausted; however, cell growth cannot be presumed even if lactate can act as a carbon source (Bedard, et al. 1993). Lactate accumulation might also have an effect on culture pH as Rheil and Murhammer (1995) observed decreases in pH values coinciding with the accumulation of lactate in their cultures.

3.3.2.3.2 Ammonia

Ammonia production is a result of amino acid metabolism (Ferrance, et al. 1993). Ammonia is produced by the catabolism of glutamine by glutaminase in the mitochondria (Ohman, et al. 1995). Ammonia can also be formed by the spontaneous decomposition of glutamine in the culture media (Ohman, et al. 1995). Insect cells generally are less sensitive to ammonia accumulation than mammalian cells. Sf-9 cells can support ammonia concentrations up to 180 mg/ml without having an inhibitory

effect on cell growth (Bedard, et al. 1993). For Sf-9 cells, minimal ammonia accumulation occurs (Ohman, et al. 1995) and the level of production does not inhibit cell growth (Bedard, et al. 1993). Glutamine and glutamate are the two major sources of ammonia (Ohman, et al. 1995). When both glucose and glutamine are present in the culture, ammonia is not produced; instead, alanine is produced (Mendonca, et al. 1999). When glucose is exhausted, alanine is metabolized to glutamate to enter the TCA cycle and produce more energy for the cells. As glutamate is metabolized, ammonia is released and starts to accumulate in culture (Bedard, et al. 1993; Ohman, et al. 1995).

3.3.3 Medium

Originally, insect cells were cultured using Grace's basal medium supplemented with 5 – 10% fetal bovine serum. Grace's basal medium was originally developed to support the growth of Australian emperor gum moth, *Antherea eucalypti*. It has been used to culture insect cells of the order Lepidopterans and Dipterans (Grace 1962; Grace 1966; Grace 1967). Serum is used to provide essential growth factors for cells and can promote recombinant protein production up to day 1 post-infection (Yamaji, et al. 2006). There are several disadvantages associated with the use of serum: 1) serum complicates downstream processing of proteins; 2) the quality of serum can vary lot-to-lot; 3) serum can contain potential infectious contaminants; and 4) serum is costly (Mendonca, et al. 2007; Shen, et al. 2007). To avoid potential problems that can be caused by serum, yeastolate and several different types of hydrolysates have been used as substitutes for serum. Today, SF-900 II (Gibco/Invitrogen) and Excell 405 (Sigma-Aldrich) media are the two most commonly used serum-free media.

3.3.3.1 Serum-free Medium Supplements

Hydrolysates and peptones are produced by enzymatic or chemical digestion of casein, albumin, yeast cells, plant and animal tissues (Batista, et al. 2005). They are undefined and complex mixtures of amino acids, polypeptides, polysaccharides, vitamins, nucleic acids and minerals (Ikonomou, et al. 2003). Examples of hydrolysates include soy hydrolysates, meat hydrolysates, yeast hydrolysates, wheat

hydrolysates, and rice hydrolysates (Mendonca, et al. 2007). Of these hydrolysates, yeastolate, which is an aqueous extract of autolysed baker's or brewer's yeast, has been found to be the most efficient hydrolysate for promoting insect cell growth and enhancing recombinant protein production (Batista, et al. 2006; Ikonomou, et al. 2003; Shen, et al. 2007).

3.3.3.2 Conditioned Medium

Conditioned media (CM) are media that have previously been used to culture cells, so they usually contain growth factors secreted by the cells. Doverskog et al. (2000) have shown that CM can stimulate the proliferation of Sf-9 cells in serum-free medium. In addition, CM from Sf-9 cells has been found to contain antimicrobial activity (Svensson, et al. 2005): it exhibits strong antibacterial activity against the Gram-positive bacteria, *B. megaterium*, and weaker activity against the Gram-negative bacteria, *E. coli* (Svensson, et al. 2005). It has been proposed that the antibacterial peptides might be synthesized and secreted by the Sf-9 cells as a defense mechanism against bacterial infection (Svensson, et al. 2005). However, the exact protein responsible for the antimicrobial activity has not been identified, yet.

3.3.4 Dissolved Oxygen

Dissolved oxygen (DO) is an important parameter to cell metabolism because oxygen is the final electron acceptor. DO content can also affect nutrient utilization and waste metabolite accumulation (Rhiel and Murhammer 1995). There should always be enough oxygen in the culture to avoid oxygen deprivation; but at the same time, too much oxygen can also form free radicals (Rhiel and Murhammer 1995) which will damage the cells. The optimum level of DO is affected by the type of media used (Rhiel and Murhammer 1995). Sf-9 cell cultures are found to be rather insensitive to the level of dissolved oxygen (Bedard, et al. 1993; Hensler, et al. 1994; Rhiel and Murhammer 1995), which is evidenced by the lack of lactate formation. In general, the oxygen demand of insect cells is higher than that of mammalian cells (Shuler and Wood 1995).

3.4 Baculovirus Infection

3.4.1 Baculovirus Infection Life Cycle and Gene Expression

The two progeny phenotypes of baculovirus have different roles in the virus' life cycle. The ODV is usually contained in a protein matrix called polyhedron in the case of AcMNPV and is responsible for infecting the gut epithelial cells of the insect that ingested the virus. Once the infection is established within the host insect, the BV is responsible for infecting the other cells inside the insect's body.

The BV is the type of virus used to infect cells in culture. The ODV does not participate in the propagation of the viruses in culture. Thus, the p10 and polyhedrin genes, which are the genes responsible for making the occlusion bodies, can be replaced by the recombinant gene of interest to express recombinant proteins in culture.

There are four stages of gene expression in the baculovirus infection life cycle in culture: the immediate-early, the delayed-early, the late and the very late. The immediate-early genes are expressed before viral DNA replication (Blissard and Rohrmann 1990). They can be expressed by healthy insect cells and do not require expression of other viral genes (Blissard and Rohrmann 1990). The baculovirus infection cycle starts when baculoviruses are internalized by insect cells through adsorptive endocytosis (Matilainen, et al. 2005), as shown in Figure 3. The virus' outer membrane fuses with the endosomal membrane of the cell following the acidification of the endosome. Once inside the cell, the nucleocapsids are released and transported to the cell's nucleus by the induction of actin filaments in the cytoplasm (Matilainen, et al. 2005). The nucleocapsids enter the nucleus through nuclear pores. Inside the nucleus, the nucleocapsids uncoat to release their viral DNA. The process of viral penetration and uncoating will take place between 0 and 4 hpi. After viral penetration and uncoating, the delayed-early genes will start to be expressed (Matilainen, et al. 2005). An example of a delayed-early gene is the anti-apoptotic p35 gene, which is transcribed within 2 hrs of infection (Kelly, et al. 2007). The function of the anti-apoptotic p35 gene is to prevent the host cell from undergoing apoptosis (programmed cell death), which is a natural cell defense mechanism against viral infection. The delayed-early expression will last approximately until 6 hpi (Matilainen, et al. 2005).

At 6 hpi, the expression of late genes will occur, which is also the start of viral DNA replication. Viral DNA replication and nucleocapsid formation will take place inside the cell's nucleus (Dobos and Cochran 1980). At this stage, a host-modified or viral RNA polymerase (Blissard and Rohrmann 1990) is expressed to transcribe the viral DNA to mRNA for viral protein synthesis. At around 10 to 12 hpi, progeny viruses will start to bud out of the cell, and obtain a lipid envelop through the process of budding (Carstens, et al. 1979). At 12 hpi, inactivation of the host RNA polymerase occurs, causing the degradation and destabilization of the host RNA (Ooi and Miller 1988). It is found that all the identified viral RNAs contain an ATAAG sequence, which could allow the viral enzyme to distinguish between viral and host RNA for degradation (Ooi and Miller 1988). Most of the host RNA destroyed is nuclear RNA while the host mitochondria RNA can escape degradation to continue providing energy for the cell (Ooi and Miller 1988). The decrease in host RNA levels leads to the decrease in host protein production at 12 hpi, and eventually the termination of host protein production at 24 hpi (Ooi and Miller 1988). The process of virus replication and budding can last up to 24 hpi (Ooi and Miller 1988). The maximum wild-type baculovirus replication rate is found to occur between 14 and 22 hpi; and the maximum virus yield is found to occur at 24 hpi (Tjia, et al. 1979). The estimated viral particle production rate in Sf900-II media is 9.8 ± 1.5 PFU/cell.hr (Carstens, et al. 1979). In the very late stage of the infection (about 24 hpi), the number of virus budding from the cell decreases, and the cell starts to produce proteins under the control of the p10 and polyhedron promoters. This last stage of the infection cycle can last till approximately 60-72 hpi, at which time the insect cells will start to lyse and release the occluded form of the virus (Kelly, et al. 2007).

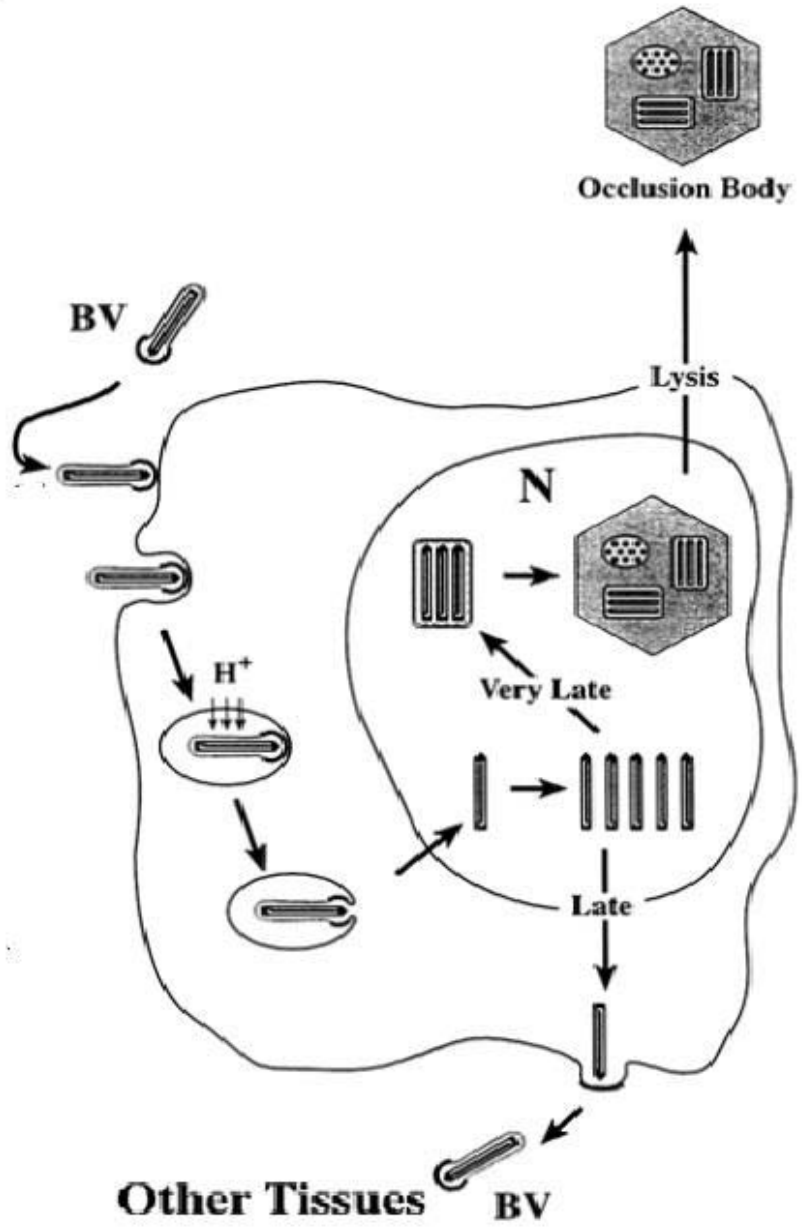

Figure 3: Baculovirus Infection Cycle (Modified from Blissard 1996)

3.4.2 Infection in Culture

3.4.2.1 State of Healthy Insect Cells

The diameter of healthy cells falls in the range of 12.2 – 15 µm (Kamen, et al. 1996; Schopf, et al. 1990), however some have reported the cell diameter as being upwards of 18.5 ± 1.5 µm (Gotoh, et al. 2008). Since osmolarity will have an effect on cell size, the discrepancies between the reported values might have been caused by different sizing solution or by the media used for the measurement. Cell size has been reported to stay approximately the same during exponential growth (Zeiser, et al. 1999).

3.4.2.2 State of Infected Insect Cells

Infection implies that at least one virus has entered the cell and has successfully started its replication cycle. In cell culture, the ratio of the total the number of viruses added to the total number of cells is referred to as the multiplicity of infection (MOI) (Licari and Bailey 1991). The concept of MOI assumes that the viral inoculums do not contain a significant amount of defective viruses, which can lead to cytopathic effects but no productive infection (Janakiraman, et al. 2006). MOI is found to be closely coupled to the time of infection (TOI), which is also referred to as the cell density at infection. It is recommended to infect cells in the exponential phase of growth. Infection in the stationary phase will reduce the cell's production capacity (Licari and Bailey 1992) and product yield (King, et al. 1992).

High MOIs will result in synchronous infections; whereas low MOIs will lead to asynchronous infections. In synchronously infected cultures, the volumetric and specific productivity of cells will increase with increasing cell density to a critical density of 5 to 7 x 10^6 cells/ml in serum-free medium (Elias, et al. 2000). Above the critical density, the productivity starts to decline, which might be limited by nutrient availability at high density cultures (Elias, et al. 2000; Hensler, et al. 1994; Ohman, et al. 1995). This problem may be overcome by supplementing fresh nutrients that would be required more intensively after infection (Hensler, et al. 1994; Ohman, et al. 1995). However, the addition of nutrient cocktails should be carefully designed as nutrient addition will increase the osmolarity of the culture and might have detrimental effects

to the cells (Elias, et al. 2000). Asynchronous infections are characterized by multiple cell populations (infected and healthy cells). The healthy cell population will compete for nutrients with the infected cells resulting in reduced product yield by the infected cells (King, et al. 1992). Although MOI is an important parameter in infection, there are some problems associated with the accuracy of MOI. First, different recombinant virus will affect the cell differently even at the same MOI. Second, it is hard to accurately determine viral titers (Licari and Bailey 1992). As a result, the actual MOI can be less or more than the calculated MOI (King, et al. 1992).

Another important parameter of infection is the cell cycle phase that the insect cells are in when infection occurs. Upon infection, the cells will stop progressing through the cell cycle (Volkman and Keddi 1990). Sf-9 cells are usually arrested in the G2/M phase following infection (Braunagel, et al. 1998). Culture infected at G1 or mid and late S phase have higher percentage of cells infected than cultures infected at the G2 phase (Lynn and Hink 1978). Therefore, cultures infected at G1/S phase will usually have higher productivities (Kioukia, et al. 1995; Saito, et al. 2002).

Although cells will usually be arrested following infection, wild-type baculovirus infected cells can keep growing until 24 hpi (Schopf, et al. 1990). A proposed explanation for this phenomenon is that the introduction of recombinant genes can increase virus infectivity by changing the degree of supercoil in the viral DNA. It was found that when the degree of supercoil of DNA is more relaxed, viral infectivity can be increased (Kelly and Wang 1981).

In addition to the phase, passage number will also affect insect cell's physiology, thus affecting productivity. Low passage numbered cells will have smaller cell sizes and express ~20 fold more proteins in total than high passage numbered cells; however, the glycosylation pattern is more complex in higher passage numbered cells (Joosten and Shuler 2003). The maximum passage number is recommended to be no more than 40 to 50 passages (Calles, et al. 2006).

Energy demand in the infected cells is found to be greater than the energy demand in the healthy cells because there are increased events of protein and DNA synthesis happening in the infected cells (Kamen, et al. 1996; Lehninger 1975). Energy consumption will be greater in the first 15 to 20 hpi due to increased protein synthesis,

viral DNA replication, and release of budded virus. After 15 to 20 hpi, the demand for energy will decline because there will be less viral progeny formation (Kamen, et al. 1996). Evidence of increased energy demand can be observed from the increase in per cell respiration rates after infection, which can increase as much as 100% (Kamen, et al. 1996; Schopf, et al. 1990). Because of the increase in oxygen uptake rate, the occurrence of oxidative stress also increases for infected cells. Oxidative stress is caused by reactive oxygen species (ROS), which can induce cell death. Nonetheless, the anti-apoptotic protein, p35, expressed from the virus provides an antioxidant-like mechanism that prevents insect cell death induced by blocking the permeabilization of the mitochondrial membrane caused by the ROS (Vieira, et al. 2006).

Differences in nutrient consumption patterns before and after infection have also been observed. Both Kamen et al. (1996) and Rheil and Murhammer (1995) reported that glucose consumption rate after infection did not increase on a per cell density bases, in contrast to what would be normally expected due to the increased energy demand in the cells after infection. However, the extra demands of energy might be met by the increase in the utilization of other energy-yielding substrates. In fact, Wong et al. (1994) have reported an increase in the specific consumption rates of aspartate, asparagines, glycine, and threonine after infection. All of these amino acids can enter TCA cycle to generate energy for the cells.

Infected cells usually have bigger cell sizes (cell volume) than healthy cells because of the extra protein production inside the infected cells (Hensler, et al. 1994; Kamen, et al. 1996; Schopf, et al. 1990). The DNA content within the cell also increases following infection (Schopf, et al. 1990); therefore, infected cells' nuclei will also be enlarged (Sandhu, et al. 2007). The mean cell diameter will increase by 20 to 40% or 3 to 4 μm following infection (Ansorge, et al. 2007; Janakiraman, et al. 2006). Palomares et al. (2001) found that the level of protein expression can be related to diameter change of infected cells.

The cell viability in the first 36 hpi is usually greater than 95% (Kamen, et al. 1996). The viability of the cell will start to decline after 36 hpi and there will be an increased accumulation of cell debris leading to the difficulty of obtaining accurate cell viability measurements (Kamen, et al. 1996).

Chapter 4 Materials and Methods

The experimental data used in this thesis were part of experimentation aimed at improving high temperature (30ºC) and high density insect cell culture production of adeno-associated viral (AAV) vectors conducted at the Biotechnology Research Institute of the National Research Council Canada (Aucoin 2007). The Sf-9 cells were maintained at 28ºC during routine passages. A single stock culture seeded at 0.5 x 10^6 cells/ml and grew to a cell density of 2 x 10^6 cells/ml at 28ºC was used for the experiments. Once at 2 x 10^6 cells/ml, the cells were centrifuged, separated from the waste media, and resuspended in fresh media or fresh media containing baculovirus (MOI=23) to densities of 1, 2, 4, 8, or 10 x 10^6 cells/ml. The cells were then incubated at 30ºC for optimal AAV productions (Aucoin, et al. 2007). A total of 20 cultures (10 uninfected cultures and 10 infected cultures) were observed, which included duplicate cultures. Details on the origins of the data are provided in this chapter.

4.1 Cells and Media

The cells used in the experiments were *Spodoptera frugiperda* (Sf9) cells. They were maintained in suspension in SF-900 II medium (Gibco BRL, Burlington, Ont., Canada) at 28ºC. Cell densities were assessed by both hemocytometer and Coulter Counter Multisizer (Beckman-Coulter, Miami, FL, USA). Cell viabilities were determined using the trypan blue dye exclusion method (Aucoin, et al. 2007). Cell size distribution profiles were obtained using the Coulter Counter Multisizer.

4.2 Baculovirus Stock

Three recombinant baculoviruses, BacITRGFP, BacRep, and BacCap, needed for the production of AAV vectors were used (kindly provided by Dr. R.M. Kotin from the National Institutes of Health (Bethesda, MD, USA)). Prior to use, baculoviral titers were verified using an EPICS XL-MCL flow cytometer (Beckman-Coulter, Miami, FL, USA) (Shen, et al. 2002) and by plaque assay.

4.3 Experimental Cultures

Four cultures, for the set of experiments described herewith, were initiated by inoculating cells in the exponential phase at 0.5 x 10^6 cells/ml in 2L flasks. These cells were allowed to grow to 2 x 10^6 cells/ml at 28ºC. Once at 2 x 10^6 cells/ml, the four cultures were combined and centrifuged at 600 *g* for 15 min at room temperature. The spent medium was removed and the cells were resuspended in fresh media or in fresh media containing baculoviruses (40 ml total) and distributed into 250 ml shake flasks to various cell densities (1, 2, 4, 8, and 10 x10^6 cells/ml). Cultures (uninfected and infected) were then maintained at 30ºC for 72 hrs. A total of 10 different culture conditions were done in duplicate: 5 different cell densities for uninfected cultures and 5 different cell densities for infected cultures. A MOI of 23 viruses/cell was used for all infected cultures ($MOI_{BacITRGFP}$=3, MOI_{BacRep}=10, and MOI_{BacCap}=10). One ml samples were taken at 0, 6, 12, 24, 48 and 72 hrs and analyzed for cell density, cell size distribution, and cell viability. For certain time points (0, 12, 24, and 48 hrs), media compositions were analyzed as well.

4.3.1 Cell Density Calculation

Cell densities, for the cultures mentioned above, were determined using both a hemocytometer and a Coulter Counter Multisizer. The number of counts recorded by the Coulter Counter Multisizer was corrected for coincidence. There are two ways coincidence can occur: 1) when two or more particles having sizes normally detectable by the Coulter pass through the measuring zone simultaneously and are counted as one big particle (primary coincidence); or, 2) when two or more particles having sizes below the detectable limit of the Coulter cluster together and are detected and counted as one large particle (secondary coincidence). Primary coincidence results in a diminished cell count with no change in overall volume measured, which in turn increases the observed mean diameter. Secondary coincidence results in both increased cell count and overall cell volume. The possibility of having secondary coincidence may be increased in cultures of low viability because the majority of the cells may have very small cell sizes due to cell shrinkage, lysis, and death in cultures with low

viability. However, the effect of secondary coincidences is usually minimal and therefore, is typically neglected (Wynn and Hounslow 1997). To correct for primary coincidence, the following empirical formula has been suggested (Allen 1990):

$$C_i = c_i + pc_i^2 \qquad \text{Equation 1}$$

where C_i is the corrected Coulter count, c_i is the original observed count recorded by the Coulter and p is the coincidence factor, which can be calculated from (Allen 1990):

$$p = 2.5\left(\frac{D}{100}\right)^3\left(\frac{500}{v}\right)x10^{-6} \qquad \text{Equation 2}$$

where D is the aperture diameter (μm) and v is the volume of suspension used for the count (μl).

Given the two independent measures (hemocytometer and Coulter), the average of the two methods was used as the cell density for each sample. The viabilities of the cultures were determined by using the trypan blue dye exclusion method. The viable cell densities (VCD) were then determined by multiplying cell viability with cell density.

4.3.2 Biovolume Calculation

Biovolume has been defined as the volume enclosed by the plasma membrane of viable cells (Zeiser, et al. 2000). Dead cells are not considered to contribute to biovolume because dead cells usually have leaky membrane or no structural membranes left. Assuming cells are spherical, biovolume can be calculated from the cell size distributions obtained by the Coulter Counter Multisizer. Particles in the range of 9.63 – 26.5 μm were used for the calculation of biovolume (*BioV*) using the following equation:

$$BioV = VCD\ x\ MCV \qquad \text{Equation 3}$$

where *VCD* is the viable cell density and *MCV* is the mean cell volume. Equation 3 assumes that viable cells have a size distribution between 9.63 – 26.5 µm. *MCV* is calculated using Equation 4:

$$MCV = \frac{\sum_{i=1}^{n} \frac{1}{6}\pi {d_i}^3 C_i}{TC} \qquad \text{Equation 4}$$

where d_i is the ith cell diameter (µm), C_i is the corrected Coulter count having the ith diameter, and *TC* is the total number of particles counted having diameters in between 9.63 – 26.5 µm.

4.3.3 Growth Rate Calculation

Growth is a result of changes in both cell density and cell size (Shuler and Kargi, 2002). The relationship between nutrient utilization and cell mass increase is described as:

$$Substrate + cells \rightarrow extracellular\ products + more\ cells$$

$$\sum S + X \rightarrow \sum P + nX \qquad \text{Equation 5}$$

X is the cell mass concentration (g/ml). X can also be substituted with N, which is the cell number concentration, in other words, the cell density concentration (cells/ml). The latter is the parameter that is often used to characterize nutrient utilizations in insect cell cultures in literature, although it does not take into account the changes in cell size. In this experiment, cell density and cell size distribution data were both recorded. Since growth is a result of changes in both cell density and cell size, combining the two data, biovolume (um^3/ml) profiles can be generated to characterize

growth in a more complete sense than just cell density data alone. If one assumes that changes in cell volume is proportional to changes in cell mass, then this notion of biovolume can actually be equated to cell mass concentration. Equation 5 can then be changed to:

$$\sum S + BioV \rightarrow \sum P + nBioV \qquad \text{Equation 6.}$$

The net specific growth rate can then be defined to be,

$$\mu_{net} \equiv \frac{1}{BioV}\frac{dBioV}{dt} \qquad \text{Equation 7}$$

with BioV = $BioV_1$ at t = t_1, and BioV = $BioV_2$ at t = t_2, integration of Equation 7 gives,

$$ln\frac{BioV_2}{BioV_1} = \mu_{net}(t_2 - t_1) \qquad \text{Equation 8}$$

μ_{net} is the slope of a plot of $ln\frac{BioV_2}{BioV_1}$ $vs.\Delta t$.

4.4 Nutrient/ Metabolite Quantification

Samples were centrifuged (Heraeus Pico microcentrifuge, Waltham, MA, USA) at 2000 rpm for 10 min. The resulting supernatant from the centrifugation (about 500 µL) were then put in an Ultrafree-MC 30000 NMWL Filter Unit (Millipore) and centrifuged at 8000 rpm for at least 20 min. The permeates from the filter unit were frozen at -80 °C until used for nutrient/ metabolite analyses. Amino acid analyses were performed for all cultures by analytical HPLC following the methods reported by Kamen et al. (1991). Both internal and external standards were used to normalize

results. Glucose, lactate and ammonia analyses were performed using a Kodak Biolyzer (Kodak, New Haven, Connecticut, USA).

4.4.1 Accounting for the Errors in Nutrient/ Metabolite Quantification

To account for measurement variability, multiple samples of Sf-900 II taken from the same source were analyzed. The error associated with each nutrient in the media was calculated as a % coefficient of variation (%CV) by dividing the standard deviation of all the measurements of the original media by the average of all the measurements. The error (%CV) of each nutrient/metabolite was then compared to the % changes recorded for each nutrient/metabolite. If the % changes recorded were smaller than the error; then the % changes were adjusted to 0, as having no changes, because the % changes recorded needed to be more significant than the error in order to be justified as a true consumption or production.

4.4.2 Yield Coefficients and Consumption Rates Calculations

In order to characterize growth kinetics, yield coefficients and nutrient consumption rates were calculated. The yield coefficient was defined as the amount of substrate used in order to generate a unit of biomass (Shuler and Kargi, 2002):

$$Y_{S/BioV} = \frac{\Delta S}{\Delta BioV} \qquad \text{Equation 9.}$$

Nutrient consumption rate were then defined as,

$$q_s = \frac{1}{X}\frac{dS}{dt} = \mu_{net} Y_{S/BioV} \qquad \text{Equation 10.}$$

4.4.3 Average Nutrient Consumption Rates Calculations

Nutrient/metabolite analysis was done for samples taken at 0, 12, 24, and 48 hrs.. Since there were four time points, there were three time segments, namely 0 – 12, 12 – 24, and 24 – 48 hrs/hpi. For each nutrient/metabolite, three yield coefficients were calculated (one for each segment). There were also three μ_{net} calculated for each corresponding time segment. As a result, there were three consumption/production rates calculated for each nutrient/metabolite utilization profile. Since the length of each time segment, i.e. the total number of hours, was not the same, the average consumption rate, q_{avg}, was calculated as a weighted average. The length of first and second time segments were the same (12 hrs), but the length of the last time segment was twice the length of the first and the second time segments (24 hrs). Therefore, the last time segment with double the length was given double the weight in calculating the average:

$$q_{avg} = \frac{(q_1 + q_2 + 2q_3)}{4} \qquad \text{Equation 11.}$$

Chapter 5 Results and Discussion

5.1 Analysis of Culture Profiles

5.1.1 Justification of Using Viable Cell Density

Viable cell densities were used in this thesis instead of using total cell densities because it is assumed that only viable cells will consume nutrients. Using either viable cell density or total cell density does not have a significant impact in uninfected cultures as shown in Figure 4 because the viability of the uninfected cultures are high (greater than 95%) throughout the culture period; however, the choice becomes important when dealing with the infected cultures as shown in Figure 5 because the viability of the infected cultures is continuously decreasing. The total cell density in the infected culture stayed relatively constant, which is to be expected because infected cells will be arrested and will not continue to divide. From the beginning of the culture to the end of the culture, the density profile of an infected culture is almost a perfect horizontal line. The viability profile as shown in Figure 5, however, constantly decreased as the culture proceeded. This decrease in viability is reflected in the viable cell density but not in the total cell density. If the total cell density was used in any of the nutrient consumption rate calculations, both the cell density and biovolume profiles would be overestimated. For example, when calculating nutrient consumption rates, the rates would be underestimated due to the inflated profiles. Due to the reasons stated above, viable cell density profiles were used in this thesis.

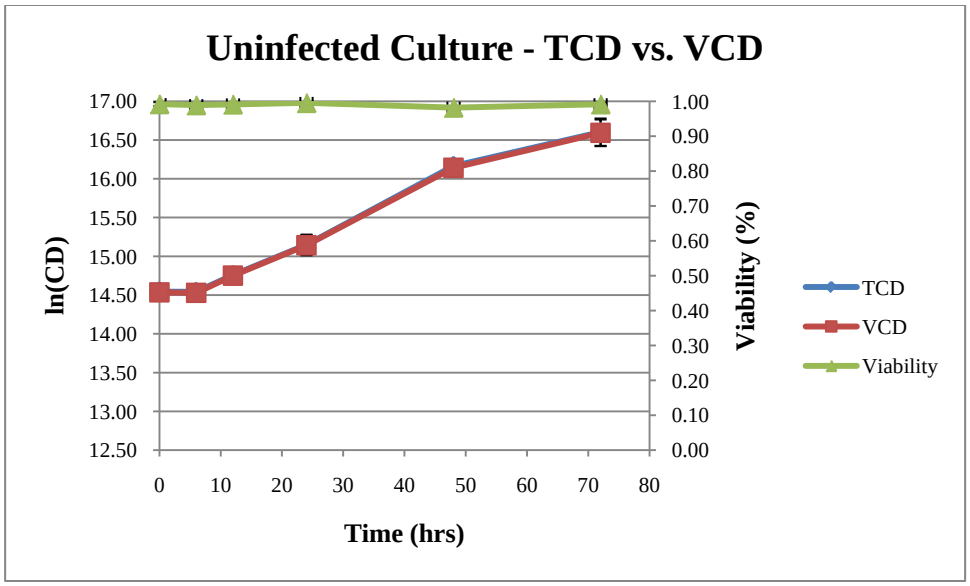

Figure 4: TCD vs. VCD for Uninfected Culture (2 x 10^6 cells/ml)

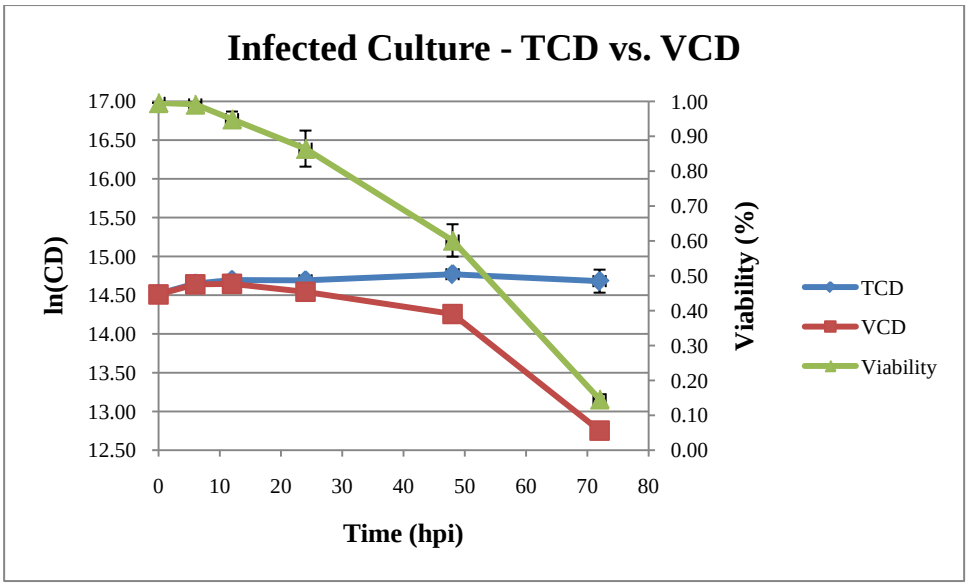

Figure 5: TCD vs. VCD for Infected Culture (2 x 10^6 cells/ml)

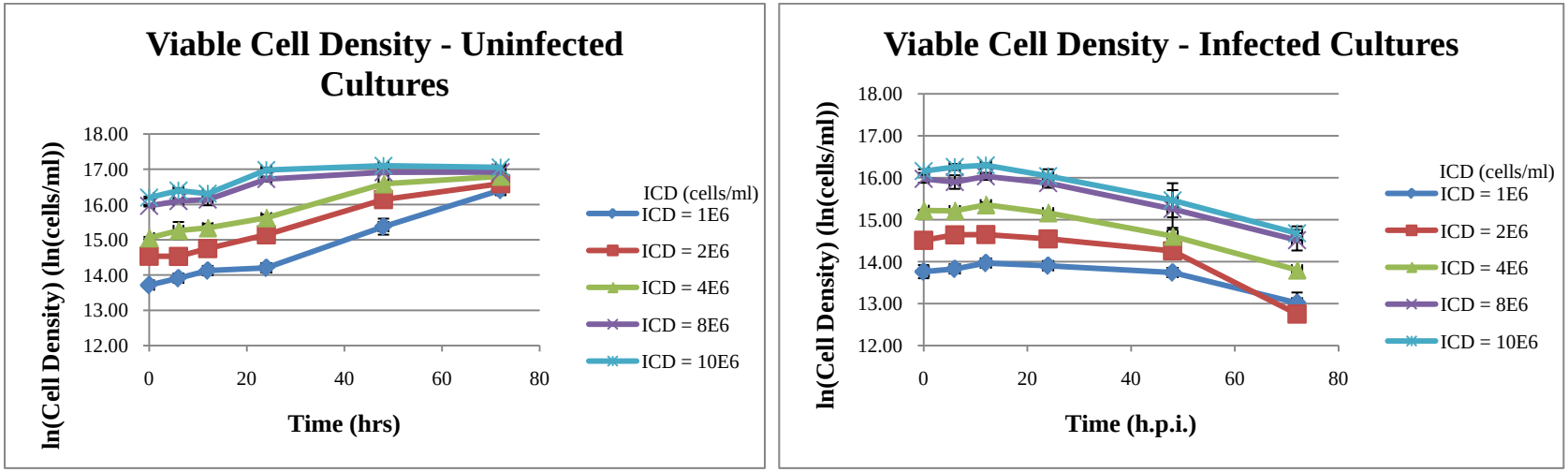

Figure 6: Viable Cell Density Profiles for Uninfected (Left) and Infected (Right) Cultures

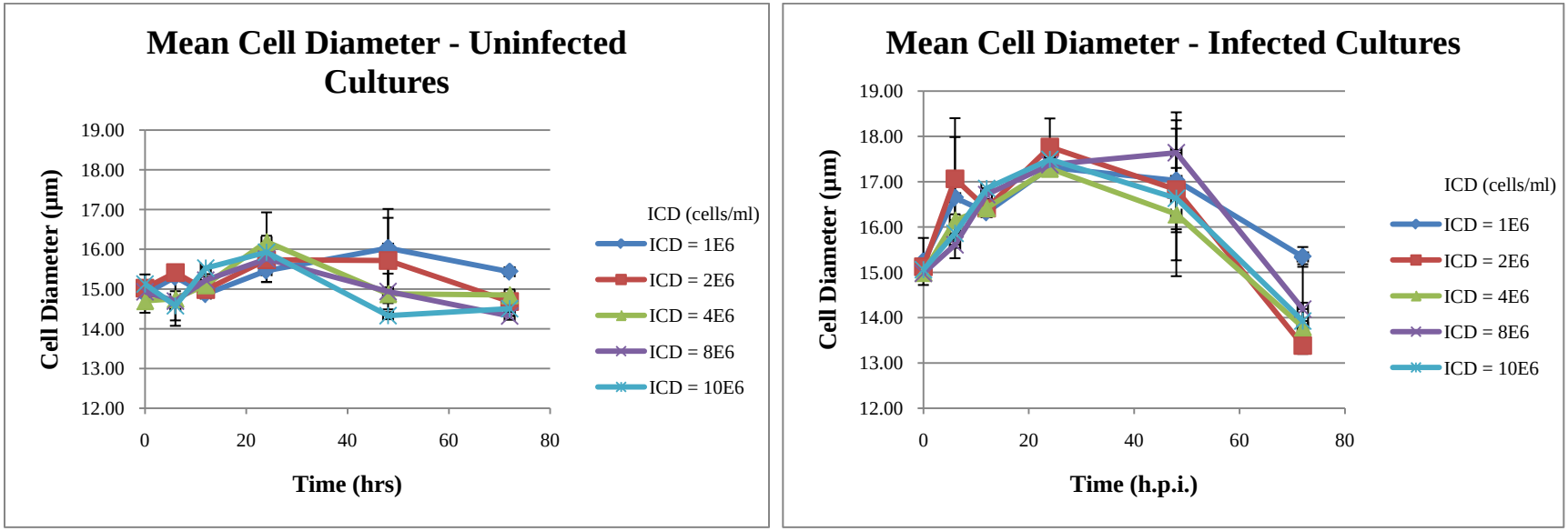

Figure 7: Mean Cell Diameters for Uninfected (Left) and Infected (Right) Cultures

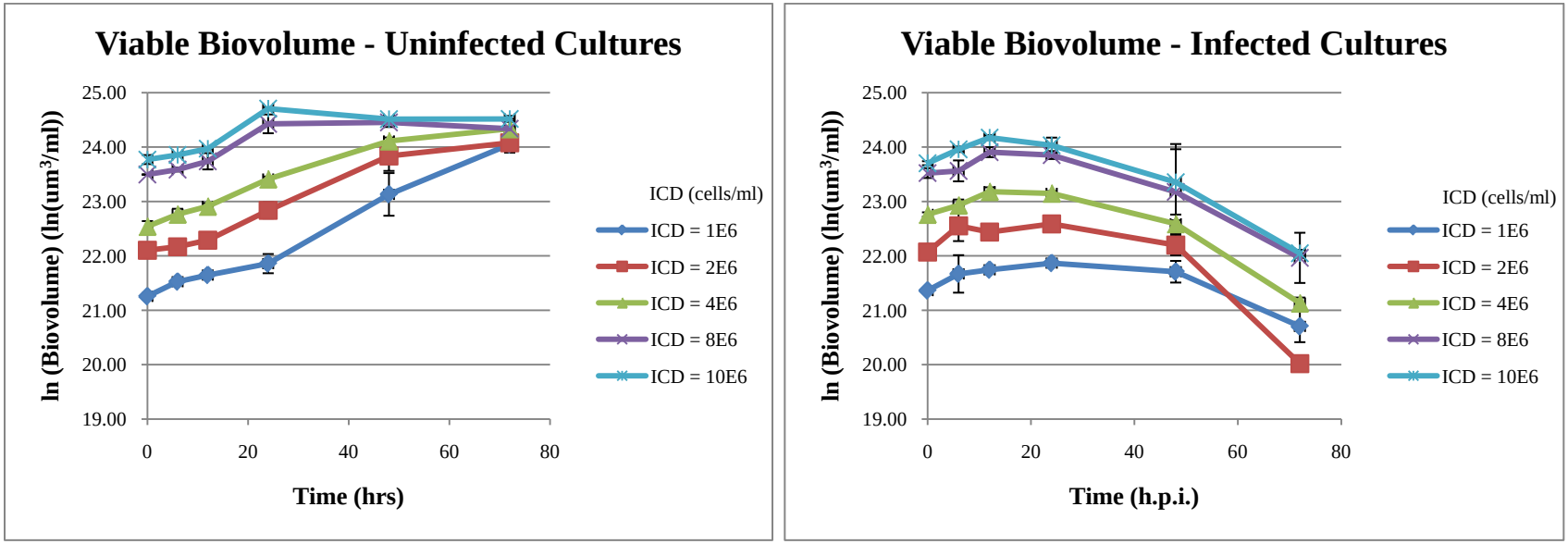

Figure 8: Viable Biovolume Profile for Uninfected (Left) and Infected (Right) Cultures

5.1.2 Uninfected and Infected Culture

The left graphs of Figure 6, Figure 7, and Figure 8 show the average profiles of viable cell density, mean cell diameter, and biovolume, respectively, for the uninfected cultures; and the right graphs of Figure 6, Figure 7, and Figure 8 show the average profiles of viable cell density, mean cell diameter, and biovolume, respectively, for the infected cultures. The error bars represent the standard deviations of the sample measurements (n = 2).

5.1.2.1 Analysis for the Uninfected Cultures

There are five phases that can be observed in a batch culture: lag, exponential growth, deceleration, stationary, and death phases. The lag phase is defined as the period of time in which the cells adjust to a new environment before entering exponential growth phase. In the experiments, the cells were pre-cultured at 28 ºC; at the start of the experiment, the cells at early to mid-exponential phase were moved and incubated at 30 ºC. Although there was a difference in the pre-incubation temperature and the experimental temperature, a lag phase was not observed. As will be discussed in Section 5.2, optimal growth of insect cells occurs in the range of 27 – 30 ºC (Shuler, et al. 1990); therefore, the shift in temperature was within the acceptable physiological temperature ranges for insect cells. Temperature changes within the acceptable range do not induce a lag phase (Ingraham and Marr 1996; NG, et al. 1962; Shaw 1967). Depending on the initial cell densities of the cultures, at the end of the culture, the cells either remained in exponential growth, entered the deceleration phase or were seen to be in the stationary phase.

The stationary phase is often caused by the exhaustion of certain nutrients (Nystrom 2004). For cells in the stationary phase, although the net specific growth rate is zero, cells are still metabolically active and will still consume nutrients, albeit most likely at a slower rate. In our experiment, it was found that serine depletion coincided with the start of stationary phase. The stationary phases were only observed in the high density cultures (8, and 10 x 10^6 cells/ml), and they occurred beyond 48 hrs of culture time.

Bruggert et al. (2003) have also found that the exhaustion of serine causes Sf-9 cells to stop proliferating. Cells consume serine for the synthesis of nucleic acids (Drews, et al. 1995; Tremblay, et al. 1992). When serine is depleted, nucleic acid synthesis may be hindered, thus hindering cell growth. When more and more essential nutrients are depleted, the cells will start to self-digest to generate energy needed for survival (Nystrom 2004). The endogenous materials consumed include cell membrane, free amino acid pools inside the cells, RNAs, ribosomes and cellular proteins (Campbell, et al. 1963; Gronlund and Campbell 1961; Gronlund and Campbell 1963; Maaloe and Kjelgaard 1966; Nystrom 2004). The number of ribosomes and RNAs within a cell is proportional to the cell growth rate and the rate of protein synthesis within the cell (Maaloe and Kjelgaard 1966; Saint-Ruf, et al. 2007). Since protein synthesis and DNA replication are kept to a minimum during stationary phase, the excess number of ribosomes and RNAs can be metabolized by the cells to generate energy (Maaloe and Kjelgaard 1966). Due to self-digestion, cells will continually shrink in size (Givskov, et al. 1994; Nystrom 2004; Siegele and Kolter 1992). When too much of cellular material is degraded, cell death will occur. In the experiments, the death phase was not observed in the cultures because cell viabilities remained high (> 95%) throughout the culture period.

From Figure 7 (right), it was observed that there were small fluctuations in the mean cell diameters during culture time probably due to cells cycling through different cell cycle phases. There are four phases of a cell cycle, the mitotic phase (M), the first gap phase (G1) between the completion of mitosis and the entrance into DNA synthesis, the DNA synthesis phase (S), and the second gap phase between the completion of DNA synthesis and the entrance into mitosis (G2). Cells will increase in size before division (M phase); therefore, cell sizes are larger in the S/G2 phase and smaller in the G1 phase (Al-Rubeai, et al. 1991; Al-Rubeai, et al. 1995). The mean cell diameter distribution that is represented in Figure 7 shows the average movement of the cell population in the cultures over time. The increase in the mean cell diameter distribution can be viewed as more cells being synchronized in the S/G2 phase; and the decrease trend can show that more and more cells were synchronized toward the G1 phase. By observing the mean cell diameter distributions in Figure 7 (right), one can tell 1) the cell cycle

phase that the majority of the cells are synchronized to in at a specific time (can be estimated by determining if the mean cell diameter lies on an increasing or decreasing trend) and 2) the length of time for the majority of the cells to complete one cell cycle, which is determined by the completion of one increasing and one decreasing trend. Figure 7 (right) shows that the majority of cells in cultures having ICD = 1 and 2 x 10^6 cells/ml completed one cell cycle faster than the other cultures; and the length of time for cell cycle completion increased as ICD increased. This correlated well with the growth rates of the cultures: cells grew fastest at the lowest ICD, and the growth rate decreased with increasing ICD as shown in Table 2. These observations were to be expected since the concentrations of the nutrients in the media were fixed; therefore, there were more nutrients available for fast growth of low initial cell density cultures. In addition, culture heterogeneity will increase when cell density increases because every single cell can behave differently. In fact, it has been reported for CHO cells, individual cell cycling time can range from 20 to 35 hrs, a difference of 15 hrs with the same conditions (Lloyd, et al. 1999). The majority of the variation in cell cycle time occurs in the G1 phase (Darzynkiewicz, et al. 1982; Zetterberg 1996). Cell populations in the G1 phase are the most heterogeneous and this is the result of unequal divisions of the parent cells that generate unequal-sized daughter cells (Darzynkiewicz, et al. 1982). The inequality in the sizes of the daughter cells will cause variability in the metabolism of the two daughter cells (Darzynkiewicz, et al. 1982), thus affecting the time the cells require preparing themselves for the entrance into the S phase. When there are more cells present in the culture, the variability can increase resulting in a longer average time for the majority of the cells in the batch culture to complete one cell cycle, which can also explain why the average growth rate decreases as ICD increases. The fluctuations in the mean diameters of the cells throughout the culture period were within 3.73%. Since there were still small fluctuations in cell sizes, the net specific growth rates from biovolume and cell density will be slightly different as expected.

Table 2. Initial Cell Density and Average Growth Rate of Uninfected Cultures

ICD (x106 cells/ml)	Avg Growth Rates(/hr)
1	0.0374
2	0.0286
4	0.0243
8	0.0133
10	0.0119

5.1.2.2 Analysis for the Infected Cultures

The viable cell densities of the infected culture stayed relatively constant until 24 hours post-infection (hpi), and they decreased thereafter until the end of the culture. Cell sizes fluctuate widely at different stages of infection as illustrated in Figure 7 (left). Increases in cell sizes have been used as indications of successful infection (Palomares, et al. 2001). The biovolumes of the cultures increased up to 12hpi. From 12 hpi to 24 hpi, biovolumes remained relatively constant. Ansorge et al. (2007) have also observed a plateau region of permittivity measurements, which is linearly related to biovolume, at 12 to 20 hpi. This plateau region has been associated with the maximum CO_2 evolution rate of infected insect cell culture (Zeiser, et al. 2000), the maximum oxygen consumption rate (Kamen, et al. 1996; Schmid 1996), the release of budded virus and the start of secondary infection (Ooi and Miller 1988 ; Wong, et al. 1994). Biovolume started to decrease continuously after 24 hpi due to the continuous decreases in cell viability and the budding of progeny viruses (Kelly, et al. 2007). The late promoters, p10 and polyhedrin, start to drive recombinant protein production at the very late stage of infection (after 24 hpi), and can last up to 72 hpi (Kelly, et al. 2007).

5.1.3 Justification of Using Mean Cell Diameters

Mean cell diameters were used to compare the uninfected and infected cultures in this thesis. It is acknowledged that at each culture time, there were always more than one cell population present in the culture due to cells in different cell cycle phase, growth phase, and infection stage. The % of cells present in different phases and stages would all have impacts on the diameter distribution, which were reflected in the mean

cell diameter since mean cell diameters are calculated by dividing the sum of cells of different diameters by the total number of cells as shown in Equation 12,

$$MCD = \frac{\sum_{i=1}^{n} d_i C_i}{TC} \qquad \text{Equation 12}$$

Where d_i is the ith cell diameter (μm), C_i is the corrected number of particles counted having the ith diameter, and TC is the total number of particles counted having diameters in between 9.63 – 26.5 μm, which is the viable cell diameter range. The mean diameter profiles in Figure 7 were calculated from this range.

5.2 Cell Size

5.2.1 Cell Size Range

In this work, viable cells were assumed to be equally distributed in a diameter range between 9.63 – 26.5 μm. Previous work (Zeiser, et al. 2000), a diameter range of 5 – 20.11 μm was assumed for viable cell distribution. The difference in the diameter range observed could be explained by the different culture conditions used in Zeiser's experiments. Although both used Sf-9 cells with Sf900-II media, Zeiser's paper described cells cultured at a lower temperature (27 ºC) compared to the temperature used for this study (30 ºC). In addition, the product produced in Zeiser's experiments was β-galactosidase, which only required one type of recombinant baculovirus; whereas, in our experiment, adeno-associated viral vectors were produced, which required triple-infection with three types of recombinant baculoviruses. All these differences in culturing conditions are expected to have contributed to the difference in the distribution ranges observed.

Three factors can affect cell size: 1) protein and DNA content in a cell (Nurse 1975; Stocker and Hafen 2000); 2) nutritional conditions surrounding the cell (Nurse 1975), and 3) lastly, temperature around the cell (Stocker and Hafen 2000). Both Zeiser's and our work used the same media, therefore, the effect of nutritional conditions on the

variability of cell size observed was ruled out. The successful production of AAV vectors requires Sf-9 cells to be infected by three types of recombinant baculoviruses that carry the AAV ITR sequences, and the AAV Rep and Cap genes. Since the number of recombinant genes transduced into a Sf-9 cell for the production of AAV vectors are higher than the number of recombinant gene transduced for β-galactosidase production, the amount DNA and protein content in a Sf-9 cell targeted to produce AAV vectors is thought to be higher than in a Sf-9 cell targeted to produce β-galactosidase. The higher contents of DNA and proteins could result in increased cell sizes observed in our experiments. In addition, temperature can also affect cell size. When temperature changes occur in a non-harmful range and when nutrient resources are abundant in the environment, increases in temperature will usually lead to increases in growth rate and cell size (Atkinson and Sibly 1997). Insect cells are usually cultured at 27 or 28 ºC; nonetheless, Shuler et al. (1990) have reported that insect cells can grow optimally at the temperature range between 27 to 30 ºC. Furthermore, Huhtala et al. (2005) have found no heat shock protein production in Sf-9 cells cultured below 37 ºC. All these indicate that culturing the cells at 30 ºC was non-harmful to the cells. Since the nutrients were abundant and the temperature was not harmful, the increase in temperature in our experiments could also lead to the increases in cell sizes observed.

5.2.2 Cell Size Distribution of Uninfected and Infected Cultures

The cell size distributions of healthy and uninfected insect cells remained more or less constant as the cells proliferated and increased in cell density. Baculovirus-infected insect cells, however, cease to divide once arrested in the S and G_2/M phase of their cell cycle, which occurs due to the expression of early viral genes. The cell population increases in size due to the additional production of viral nucleic acids and proteins (Hensler, et al. 1994; Kamen, et al. 1996; Schopf, et al. 1990), until their viability decreases due to infection-induced cell death.

To better illustrate the differences between the cell profiles of healthy and infected cells, the diameter distribution profiles of both healthy and infected cells inoculated at

an initial cell density (ICD) of 2 x 10^6 cells/ml are shown in Figure 9 and Figure 10, respectively.

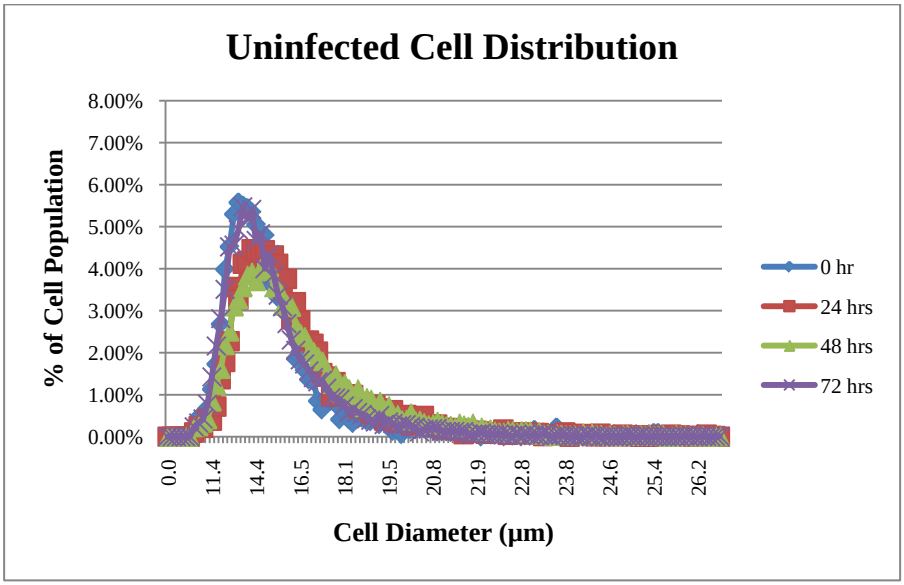

Figure 9: Diameter Distribution at ICD = 2 x 10^6 cells/ml for Uninfected Cells

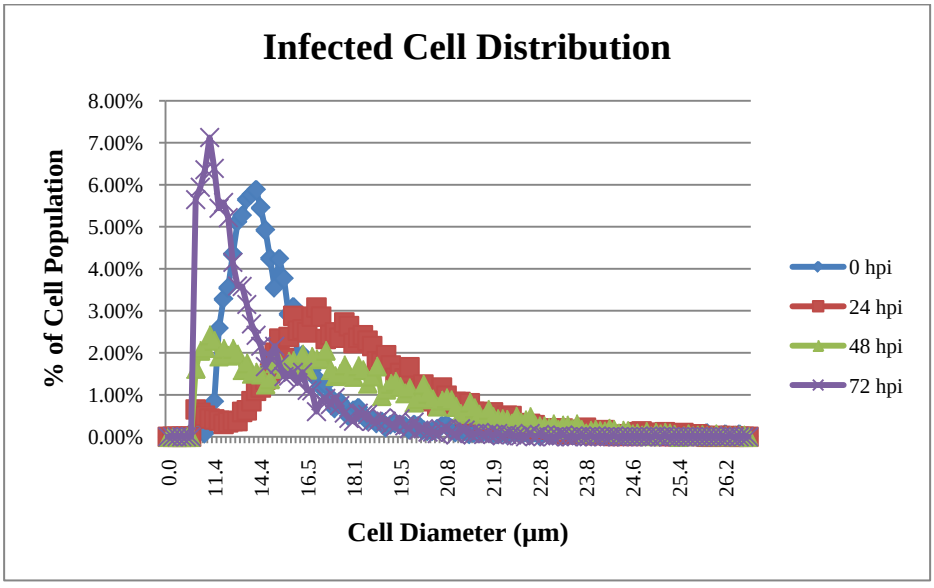

Figure 10: Diameter Distribution at ICD = 2 x 10^6 cells/ml for Infected Cells

In both figures, the cell populations at 0 hr had similar cell diameter distribution profiles. The mean cell diameter at 0 hr in Figure 9 was 15.00 ± 0.13 μm, while in Figure 10, the mean cell diameter was 15.02 ± 0.05 μm. Eighteen other cultures were performed, and the % coefficient of variation (% CV) of the mean cell diameters at 0 hr for all cultures was 1.30%.

As time proceeded, differences started to emerge as can be seen from the cultures at 24 hrs. At 24 hrs, in Figure 9 (Uninfected Cells), the mean cell diameter was 15.74 ± 0.06 μm. This increase was most likely due to the fact that cells were switched to a 30ºC environment from a 28ºC environment. Still, the increase in diameter was relatively small and the diameter distribution remained approximately constant.

At 24 hpi, the mean cell diameter increased to 17.74 ± 0.62 μm for the infected culture shown in Figure 10. The mean cell diameter in the infected culture increased by 2.74 ± 0.75 μm or by 18.26 ± 5.00 %, which was close to the 3 – 4 μm or 20 % increases observed by others (Ansorge, et al. 2007; Janakiraman, et al. 2006). The slight differences in the observed increases in diameters might be due to the differences in culturing conditions such as temperature, media compositions, and the isotonic solutions used when running measurements on the cells. The latter two differences could cause differences in osmolarity, which would ultimately affect cell sizes, in addition to the effect of temperature discussed in the previous section. Although cultures with varying ICD were used, the % CV of the increases in mean cell diameters was within 9.31%.

At 48 and 72 hrs, the distribution profiles of the uninfected cells remained approximately the same. The mean cell diameter at 48 hrs was 15.72 ± 1.07 μm, and the mean cell diameter at 72 hrs was 14.69 ± 0.05 μm. However, there was an apparent shift in the distribution to the left (decreased cell diameters) for the infected cell cultures, most likely due to decreased protein production, and cell shrinkage and death at 48 and 72 hpi. The mean cell diameter at 48 hpi was 16.77 ± 0.82 μm, and the mean cell diameter at 72 hpi was 13.38 ± 0.07 μm.

5.3 Cell Viability

To undertake a comprehensive analysis of the uninfected and infected cultures, the viabilities of the populations were also examined. Cell viability can also affect cell size distributions especially at the end of the cultures since dying cells will shrink in size. Cell cultures at ICD = 2 x 10^6 cells/ml were used as examples to show the changes in mean cell diameters and viabilities over the entire culture periods for the uninfected and infected cells in Figure 11 and Figure 12, respectively.

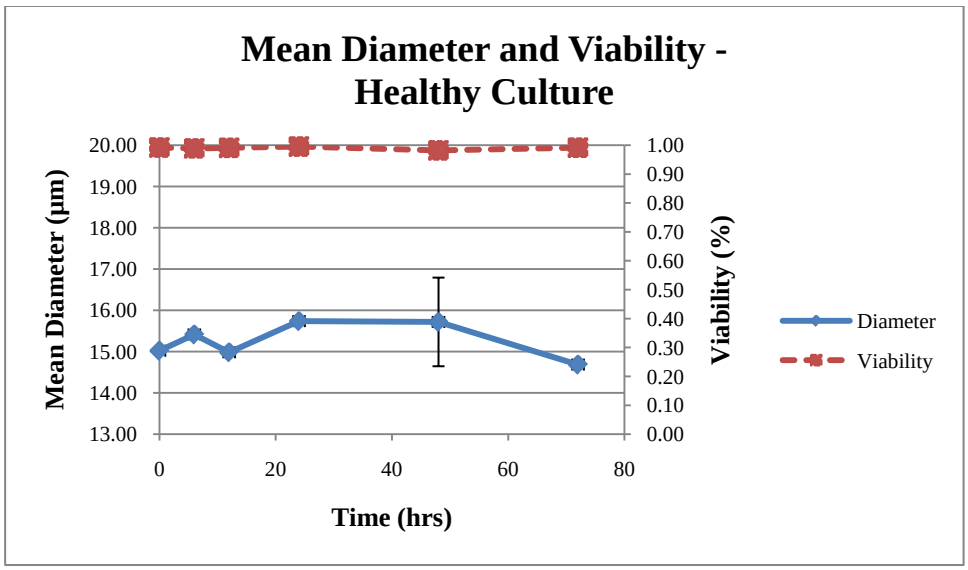

Figure 11 : Mean Cell Diameter and Viability of Uninfected Culture (ICD = 2 x 10^6 cells/ml)

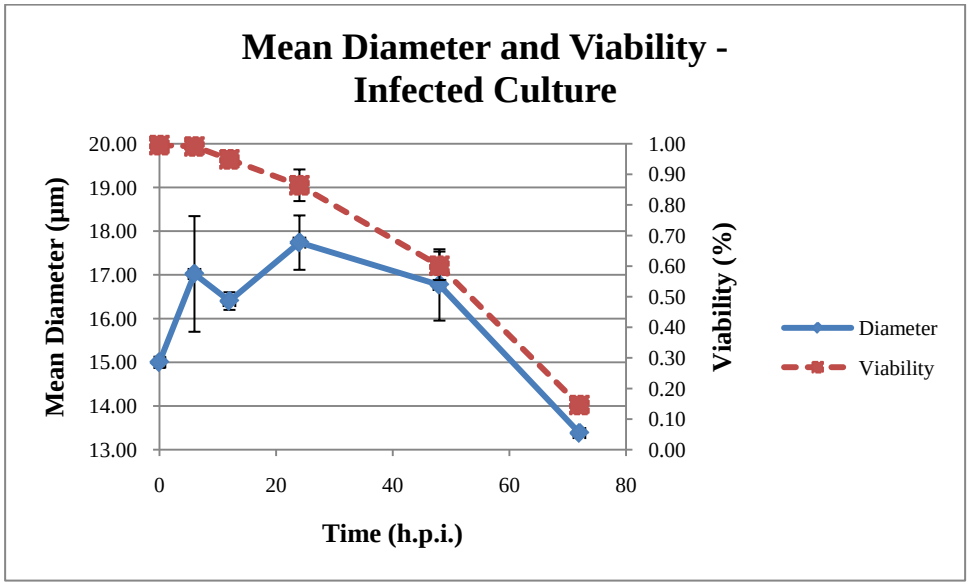

Figure 12 : Mean Cell Diameter and Viability of Infected Culture (ICD = 2 x 10^6 cells/ml)

The viability of the uninfected culture at ICD = 2 x 10^6 cells/ml stayed constant at around 100% indicating that at the end of the culture, most of the cells were still healthy, alive, and actively proliferating. The diameters of the healthy and actively proliferating cells were approximately constant. On the other hand, the viability of the infected culture remained high for the first 6 hpi, and decreased thereafter. In the first 6 hpi, while viability was still 100%, there was a sharp increase in the mean diameter of the cells, indicating infection was successful. From 6 to 24 hpi the diameter continued to increase. The time of peak viral DNA replication has been reported to occur at 24 hpi (Tjia, et al. 1979); and the maximum mean cell diameter in our experiment also occurred at 24 hpi. The mean diameter of the cell decreased a bit from 24 hpi to 48 hpi due most likely to the decreased rate of viral DNA replications and progeny virus formations. However, the mean diameter still remained large which is attributed to the accumulation of viral vectors within the cell. After 48 hpi, the mean cell diameter decreased at about the same rate as the decreases in viability as shown in Figure 12. At the end of the culture, a significant portion of the cells had loss viability. The small

mean diameter observed at the end of the culture was likely due to cells losing membrane integrity.

5.4 Synchronicity of Infection

It is known that infected cells will be arrested in the S and G2/M phase of the cell cycle and cease to divide (Braunagel, et al. 1998). The efficiency of infection could be dependent on the cell cycle phase the cells were in (Kioukia, et al. 1995; Springett, et al. 1989). Figure 13 shows the maximum increase in cell density following infection versus the initial cell densities for the 10 infected cultures at 30ºC. By removing the sole outlier, determined by the residual plot analysis and the median of absolute deviation about the median test (MAD test), the R^2 increased from 0.4956 to 0.9146. It was shown in Figure 13 that there was an average of about 17.55% increase in cell densities following infections. Palomares et al. (2001) have also observed cell density increase by as much as 5×10^5 cells/ml for a culture inoculated at 1×10^6 cells/ml (50% increase) and infected with a MOI of 5. The MOI employed in the experiments was 23, at such a high MOI, synchronous infection was expected.

To investigate the synchronicity of infection in the experiments, the fraction of cells infected instantaneously (% of infection) was calculated. Three methods were used for the investigations: the first method estimated % of infection based on viable cell densities; the second estimated % of infection based on cell sizes; and the third method investigated was based on the rates of infection via computer simulations.

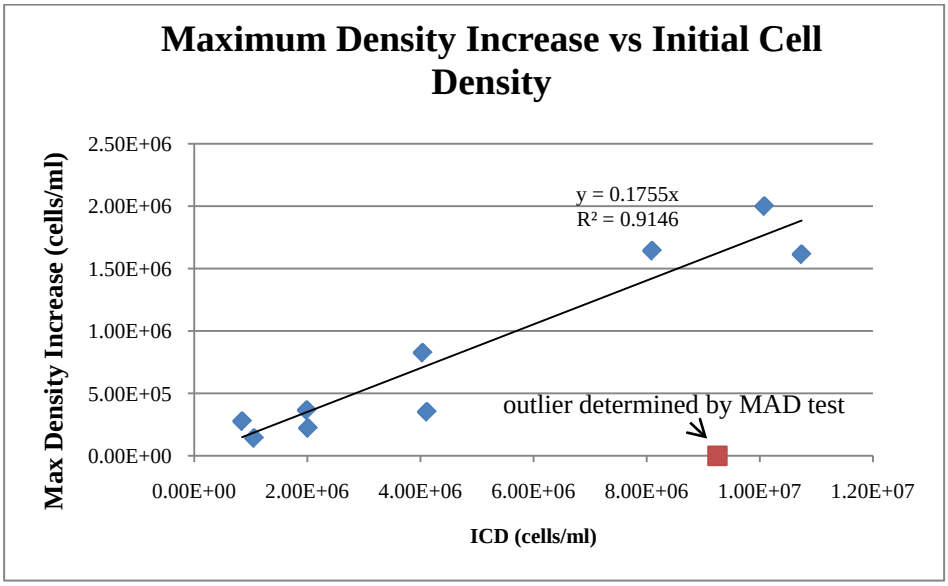

Figure 13 : Maximum Increase in Cell Density vs. Initial Cell Density for all Infected Cultures

5.4.1 Method 1 – Estimation via Viable Cell Densities

The concept behind this method was that the cell densities at doubling time would be equal to twice the uninfected cell density plus the infected cell density assuming all uninfected cells would double once within doubling time and the infected cells would cease to divide upon infection. This method also assumed that there was no significant number of progeny viruses released within the period of doubling time (no secondary infection); therefore, from 0 hr to doubling time, only primary infection occurs.

The first step was to find the doubling time of the healthy cells. The range of cell densities encompassing the infected cultures was from 8.47×10^5 to 1.24×10^7 cells/ml. The dynamics of the portion of uninfected cells in the infected cultures would be most similar to the dynamics of the healthy cells at ICD = 1×10^6 cells/ml, which had a range of 8.55×10^5 to 1.48×10^7 cells/ml. Therefore, the average doubling time of the duplicate cultures at ICD = 1×10^6 cells/ml was used, and the doubling time was found to be 18.54 ± 0.44 hrs. The doubling time of Sf-9 cells generally reported in the literature is around 24 hrs (Janakiraman, et al. 2006). The faster rate observed in our

experiments could be caused by the higher culturing temperature, 30°C, used in the experiments, which might have lead to faster cell metabolism. The cell densities at doubling time were obtained by interpolation of the logarithmic growth data.

Let I denote the initial cell density at 0 hr, and let X denote the % of cells infected at 0 hr. The number of cells generated by replication in 18.54 hrs, R, is defined to be I(1-X). Then, the cell density at 18.54 hrs, F, can be calculated by I+R. Assuming infected cells will be arrested and will not divide or die within 18.54 hours, and assuming that all the uninfected cells will double in 18.54 hrs, the equation for calculating X, the % of cells infected at 0 hr can be calculated as follows,

$$\begin{aligned} F &= I + R \\ &= I + I(1 - X) \\ &= I + I - IX \\ &= 2I - IX \end{aligned}$$ Equation 13

Rearrange and solve for X,

$$X = \frac{2I - F}{I}$$ Equation 14.

The range of X is from 0 – 100%. Any calculated value outside of the range would be set to fall within the range. For example, if X was calculated to be 106%, it would be recorded as 100%. Note that when the calculated value of X exceeded 100%, which only happened in 2 out of the 10 samples and those 2 samples were high cell density samples, this might imply that cell death occurred within 18.54 hrs, and the above calculation was based on the assumption that no cell death would occur within 18.54 hrs. The assumption alternatively implied that cell death would occur only after the whole population was infected, and it assumed that 100% infection might not happen at 0 hr, so that was why no cell death would occur within 18.54 hrs. Therefore, having an

X calculated above 100% only showed that 100% infection did happen at 0 hr. Thus, returning X back to 100% was justified.

5.4.2 Method 2 – Estimation via Cell Sizes

The second method was based on the concept that cells would increase in size following infection. The higher the % of synchronous infection in the cultures the higher the mean cell diameters because there would be less effects from the uninfected cell population, which had relatively constant smaller diameters that could reduce the calculated mean cell diameters. Assuming cells at the maximum mean cell diameter had achieved synchronous infection, then comparing the cell diameter at doubling with the maximum cell diameter, the degree of infection achieved at doubling time can be calculated. This method was a modification of a method proposed by Janakiramann et al. (2006) for the estimation of baculovirus titer.

Let P denote % of infection at doubling time, D_{dt} denote the diameter at doubling time, which was estimated by interpolation of the cell size data, D_0 denote the average diameter of uninfected, healthy cells, and D_{inf} denote the average maximum diameter in the infected cultures, which usually occurred at 24 or 48 hpi. The formula for calculating the % of infection at doubling time is as follows,

$$P = \frac{D_{dt} - D_0}{D_{inf} - D_0} \qquad \text{Equation 15.}$$

In order to calculate X, the % of infection at 0 h, a relationship between X and P needed to be developed. Let I denote the initial cell density at 0 h, then the number of infected cells could be calculated as IX. If all the uninfected cells would double in the period of doubling time, subsequently the number of cells generated in 18.54 h could be calculated as I(1-X). Then, the total cell density at doubling time could be calculated by adding the initial cell density and the replicated cells together. The % of infection at doubling time could also be expressed as,

$$P = \frac{Infected\ Cells\ at\ 18.54\ h.p.i.}{Total\ Cells\ at\ 18.54\ h.p.i.}$$

$$= \frac{IX}{I+I(1-X)} \qquad \text{Equation 16}$$

Rearranging the terms and solve for X in terms of P,

$$X = \frac{2P}{1+P} \qquad \text{Equation 17}$$

Again, the range of X is from 0 – 100%. Any results outside of this range would be set to return to this limit.

5.4.3 Method 3 - Infection Rate Simulation

The first two methods aimed to calculate the % of infection; whereas, this method aimed to investigate rates of infection. The rate of infection, k_i, was calculated by solving the set of differential equations in a Matlab simulation:

$$\frac{dX}{dt} = \mu X - k_i X \qquad \text{Equation 18}$$

$$\frac{dX_i}{dt} = k_i X \qquad \text{Equation 19}$$

and,

$$X_f = X + X_i \qquad \text{Equation 20}$$

The growth rate of the uninfected cells, μ, was set to be equal to the growth rate of the uninfected culture at ICD = 1 x 10^6 cells/ml (the same reason as stated previously). X_f is the final viable cell density at 24 hpi, X is the uninfected viable cell density at 24 hpi calculated by the simulation, and X_i is the infected viable cell density at 24 hpi calculated by the simulation.

Equation 18 describes the changes in the uninfected cell population; Equation 19 describes the increase in the infected cell population; and Equation 20 describes that the uninfected cell density and the infected cell density at 24 hpi need to add up to the real experimental cell density at 24 hpi. The simulation assumed no secondary infections occurred in the first 24 hpi. The Matlab codes can be found in Appendix A.

5.4.4 Discussions on the Methods

5.4.4.1 Cell Density Method

Figure 14 shows the relationship between % of infection and initial cell density. The outliers were determined by residual plot analysis and MAD test. The R^2 increased from 0.3989 to 0.5547 after taking out the outlier. The low R^2 could be explained by the variability between duplicate cultures, nonetheless the data points seemed to suggest a linear trend regardless of the low R^2.

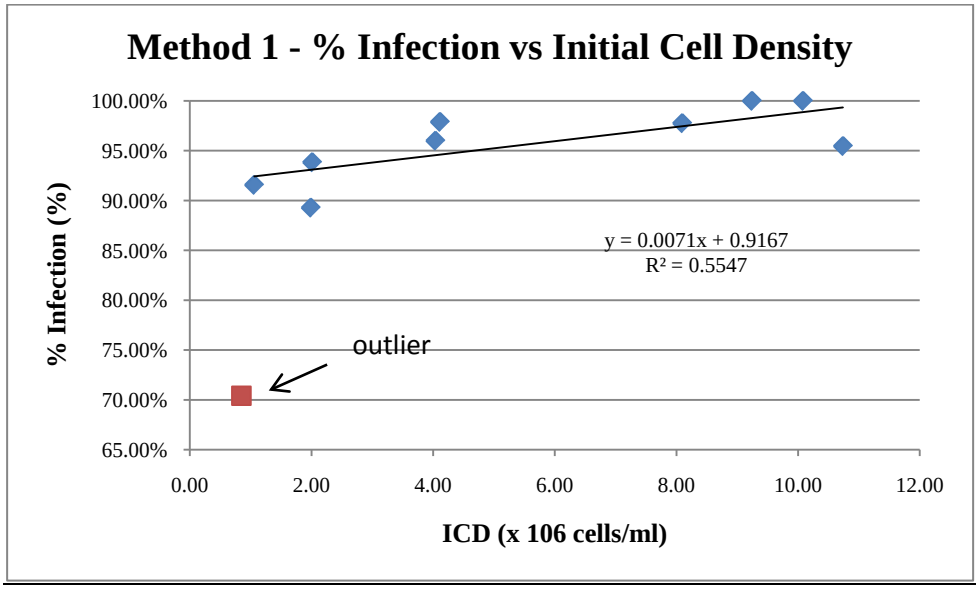

Figure 14 : Method 1's % Infection at t = 0 hr vs. Initial Cell Density

The relationship shows that the baseline of infection achieved with a MOI of 23 was 91.67% and the % of infection increased as density increased. To investigate on the accuracy of this relationship, the cell density at the doubling time, t = 18.54 hrs, were calculated with the % of infection predicted by this model. The predicted cell densities at doubling time were then plotted against the actual cell densities at doubling time and the relationship is shown in Figure 15.

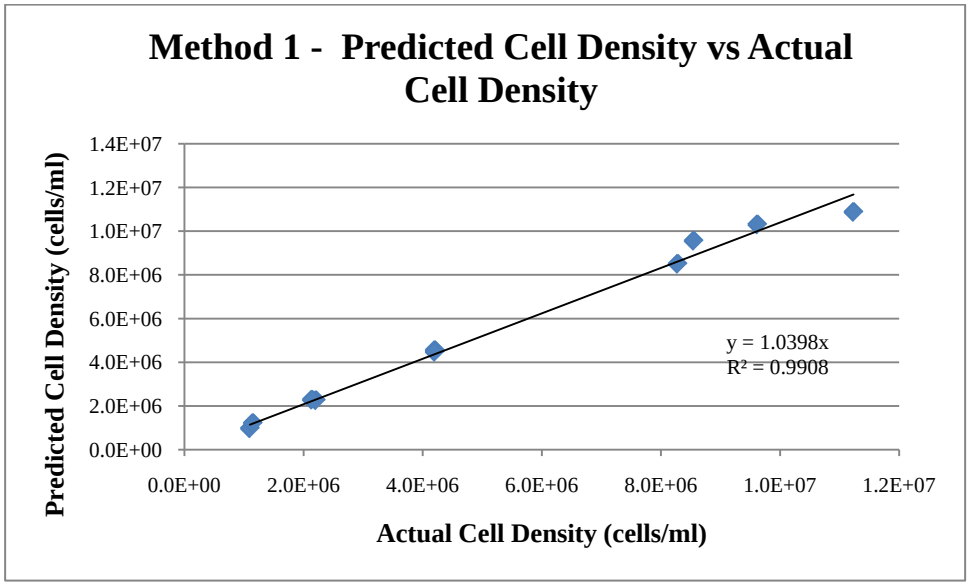

Figure 15: Predicted Cell Density vs. Actual Cell Density at Doubling Time

The relationship between the cell density predicted by the model and the actual cell density was found to be linear and close to unity, with a R^2 of 0.9908.

5.4.4.2 Cell Size

Figure 16 shows the relationship between % of infection calculated by method 2 and initial cell density. The R^2 is 0.2337. This low R^2 suggests that there was more variability in cell sizes between duplicate cultures; nonetheless the data still seemed to suggest a linear relationship.

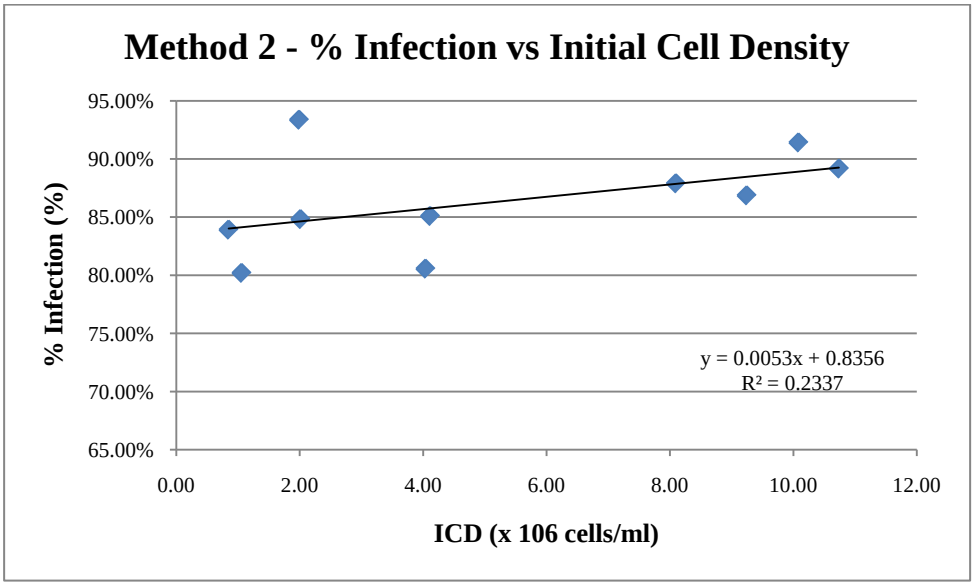

Figure 16 : Method 2's % Infection at t = 0 hr vs. Initial Cell Density

The relationship showed the baseline of infection achieved with a MOI of 23 was 83.56% and % of infection increased as density increased. To investigate on the accuracy of this relationship, again, the cell density at the doubling time, 18.54 h, was calculated with the % of infection predicted by this model. The predicted cell densities at doubling time were then plotted against the actual cell densities at doubling time and the relationship is shown in Figure 17.

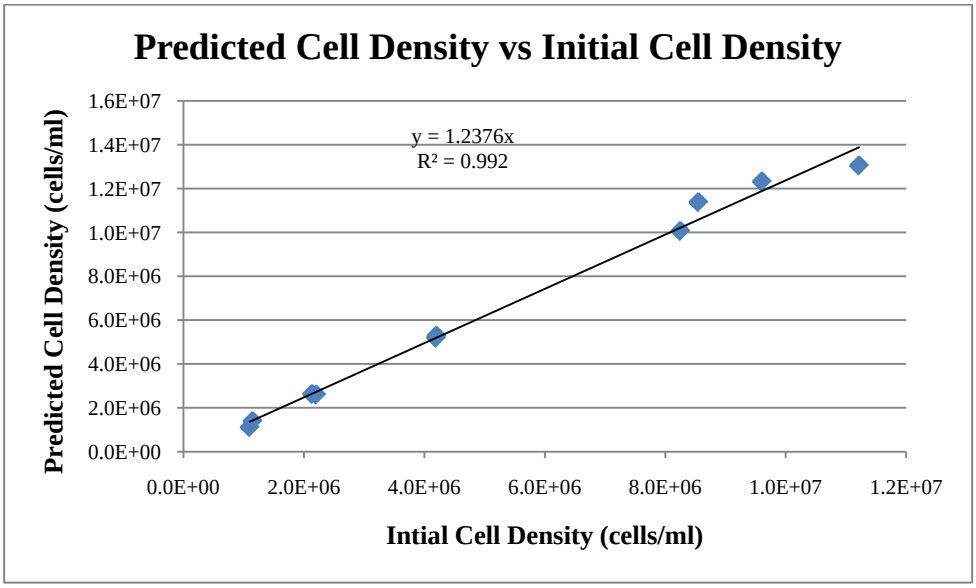

Figure 17 : Predicted Cell Density vs. Actual Cell Density at Doubling Time

The relationship between the cell density predicted by the model and the actual cell density was linear with a R^2 of 0.9920. However, the predicted cell density on average overestimated the actual cell density by 23.76%. This meant that there were actually more cells arrested than the predicted numbers, which means that the actual % of infection was higher than the predicted % of infection.

The cell size method might consistently underestimate the number of cells infected at 0 hr because it assumed that synchronous infection was only achieved at the maximum cell diameter; whereas, it was likely that synchronous infection was achieved before the cells reach maximum cell diameters. This is because maximum cell diameters usually occur when peak DNA replication and protein production takes place inside the cells. By assuming infection was achieved at the maximum cell diameter, method 2 might be prone to consistently underestimate % of infection at 0 hr.

5.4.4.3 Infection Rate

Figure 18 shows the relationship between infection rate and initial cell density for the first 24 hpi.

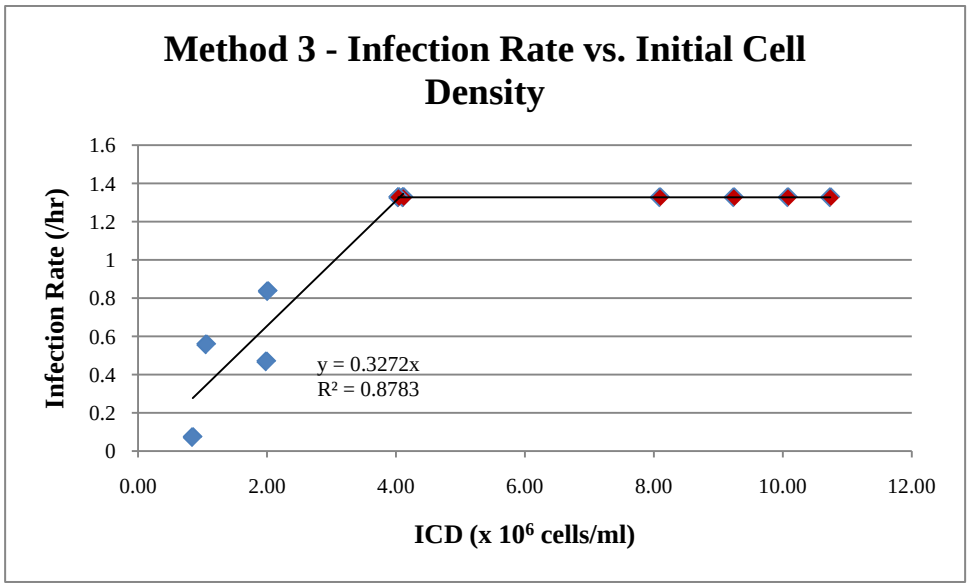

Figure 18: Infection Rate vs. ICD

Figure 18 shows that infection rates were linearly related to initial cell densities until 4 x 10^6 cells/ml was reached. After 4 x 10^6 cells/ml, the infection rate reached a maximum plateau at 1.3275 hr^{-1}. In the low density cultures, the rate of infection increased with increasing cell densities at a rate of 0.3272 cells*10^{-6}/ml·hr up to a critical cell density of 4 x 10^6 cells/ml. After the critical cell density, in the high cell density cultures, infection rates were not dependent on initial cell densities anymore; instead, high cell density cultures all reached a maximum infection rate at 1.3275 hr^{-1}.

5.4.4.4 Method Comparison

For all three methods, it was observed that both % of infection and rate of infection were linearly related to initial cell density at some points. Comparing the first two

methods, which calculated % of infection, it was observed that the estimation of % infection via cell density was more accurate than the estimation via cell size. According to the estimation via cell density, at a MOI of 23, on average, all cultures achieved at least 91.67% infection. This high % of infection was expected for the high MOI employed in the experiments.

Although some methods might provide a more clear relationship than the other methods, all three methods showed that either the % of infection or the rate of infection could be dependent on initial cell densities. In other words, it might suggest that the effectiveness of MOI, which is thought to govern the rate of infection and be independent of cell density, could be dependent on initial cell density. The same MOI at a high initial cell density might be more effective than at a low initial cell density culture because when there are more cells and viruses in the media, the probability of a cell colliding with a virus and becoming infected by the virus might increase. Based on the results, it was observed that a baseline of 91.67% infection could be achieved in cultures with high MOI, and the % of infection could increase with initial cell density by a factor of 0.0071 multiplied by the initial cell density. In addition, the rate of infection was found to linearly increase with initial cell density at a rate of 0.3272 cells*10^{-6}/ml·hr until the critical cell density of 4 x 106 cells/ml was reached; whereas, initial cell densities above the critical cell density all reached maximum rate of infection at 1.3275 hr^{-1}. Although preliminary conclusions could be drawn, still, more investigations on MOI should be carried out to validate this conclusion.

5.5 Nutrient Analysis

The cell density of an uninfected culture will continue to increase, while the cell density of an infected culture will cease to divide. The density in the infected cultures will therefore stay relatively constant before decreasing due to cell death. This can be seen in Figure 6. The cell diameters of an uninfected culture will stay relatively constant, while the diameters of an infected culture will increase (shown in Figure 19). Based on these characteristics of uninfected and infected cultures, cell density alone cannot fully characterize all the nutrient requirements of the cultures. If only cell

density was used to characterize nutrient uptake and production rates, then the amount of nutrient taken up by the cells after infection would not be properly accounted for.

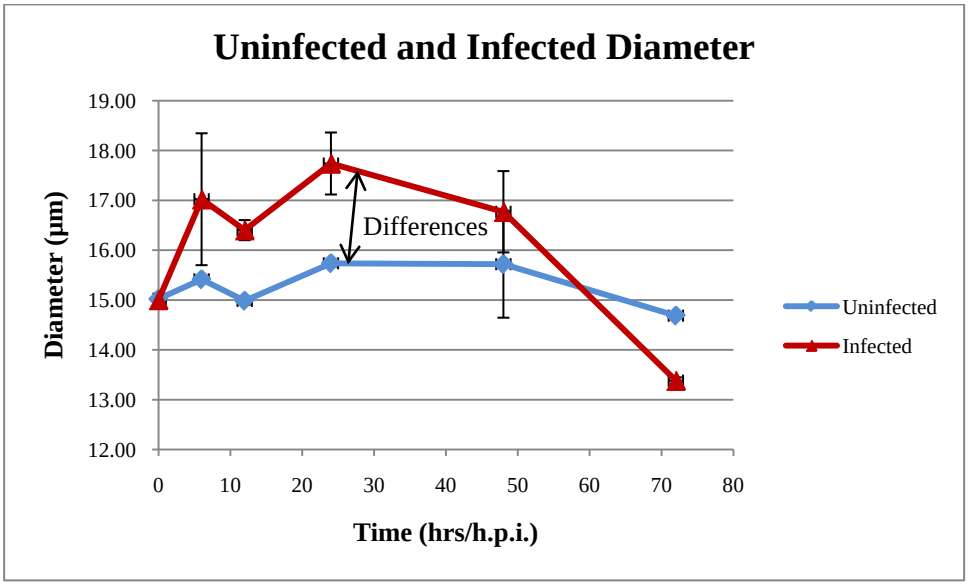

Figure 19 : Comparison of Uninfected and Infected Cell Diameter (at ICD = 2 x 10^6 cells/ml)

5.5.1 Correlation Analysis

Correlation analysis of the changes of the 22 nutrients and metabolic byproducts with changes in cell density and biovolume were done. The changes were obtained by subtracting the previous recorded nutrient concentration from the next recorded nutrient concentration. For example, the nutrient concentration at 0 hr is subtracted from the nutrient concentration at 12 hr. The errors in the data lie in the errors of the measuring instruments, which are believed to have greater than 90% accuracy. Therefore, the confidence interval is believed to be greater than 90%. The objective of running the correlation analysis was to examine which of the parameters, cell density or biovolume, correlated better with the nutrient consumption profiles. The correlation plot for the

uninfected cultures is presented in Figure 20; and, the correlation plot for the infected cultures is presented in Figure 21.

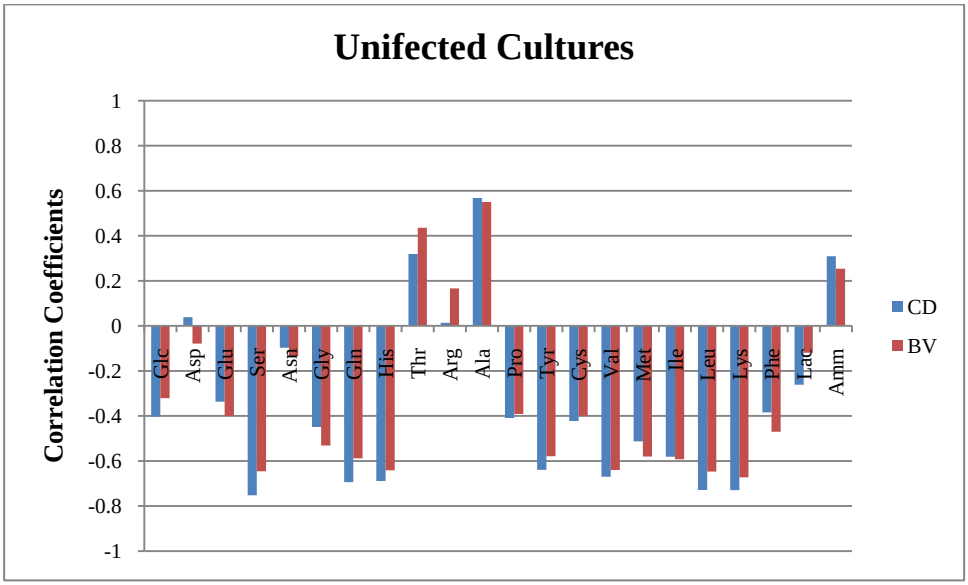

Figure 20 : Correlations of Uninfected Cultures

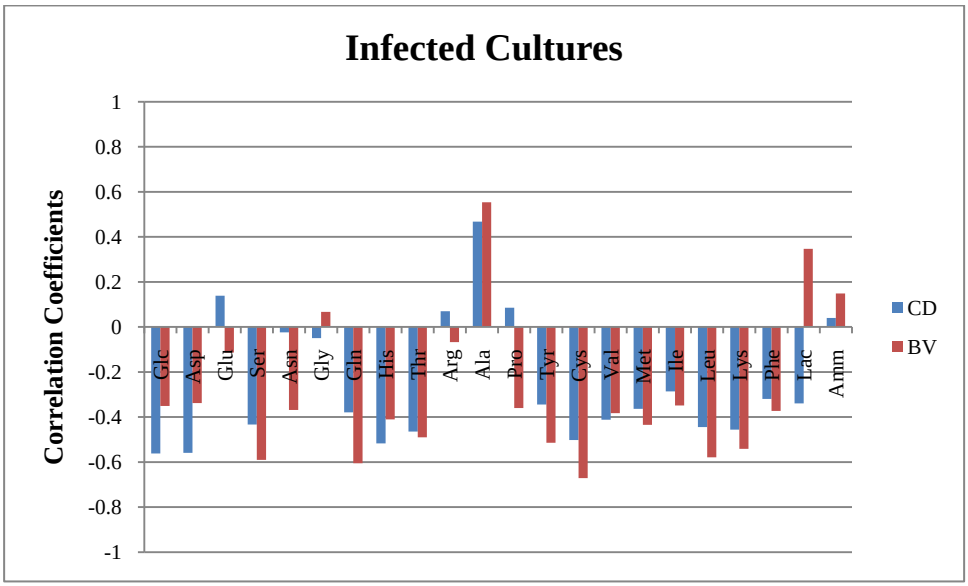

Figure 21 : Correlations of Infected Cultures

As can be seen from the uninfected cultures in Figure 20, both parameters, biovolume and cell density, did not differ much in their ability to characterize consumptions since both parameters had roughly the same correlations. The minimal difference seen in using either cell density or biovolume for the correlations was expected since cell diameters stayed relatively constant in the uninfected cultures. On the other hand, it was observed that more than half of the nutrients and byproducts correlated better with biovolume than with cell density in the infected cultures as is shown in Figure 21. More dramatic differences between the two parameters could be observed. This was again expected since infected cells would increase in size and this increase in size could not be fully characterized by using only cell density data alone. The correlation plots showed that biovolume could be a better parameter for tracking changes in nutrient consumption and byproduct production patterns than cell density, especially in the infected cultures.

5.5.2 Uninfected Cultures

The analysis of the cultures were separated into two groups, low density cultures (ICD = 1, 2, and 4 x 10^6 cells/ml) and high density cultures (ICD = 8 and 10^6 cells/ml) based on the culture profiles shown in Figure 6 (left) and Figure 8 (left). The cultures with ICD = 2 x 10^6 cells/ml were picked to represent the low density cultures and the cultures with ICD = 8 x 10^6 cells/ml were picked to represent the high density cultures in the figures.

Figure 22 shows glucose consumption and lactate production versus time. Lactate usually does not accumulate in insect cell cultures, though accumulation is possible when initial glucose concentration is high (~50 mM) (Rhiel and Murhammer 1995) and when oxygen is limiting (Reuveny, et al. 1993a). The initial glucose concentration in Sf900-II media used in the experiments was 47.75 ± 1.64 mM, which was high. Therefore, lactate accumulation was indeed observed in the cultures, although only at low levels. Maximum lactate accumulation was only 2.95 ± 0.07 mM for the high density cultures. Minimal lactate accumulation indicated that the cultures were not under stress (Garnier, et al. 1996). Lactate was also consumed in high density cultures.

Therefore, although high density cultures initially accumulated more lactate, toward the end of the culture, lactate accumulation was very minimal due to the consumption near the end of the cultures.

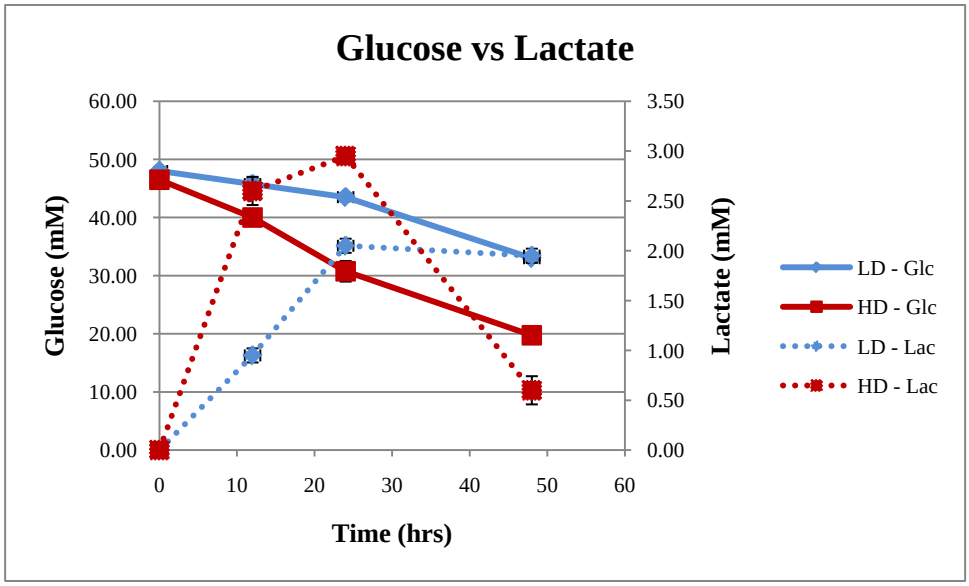

Figure 22 : Glucose Consumption vs. Lactate Production

Figure 23 shows glucose consumption and alanine production versus time. Alanine formation is common in Sf-9 cell cultures. It is a result of excess glucose and glutamine concentrations (Doverskog, et al. 1997). Glucose is known to be the main carbon source for alanine formation (Bedard, et al. 1993). As the initial concentrations of glucose and glutamine were high in Sf900-II media, formation of alanine was expected. Alanine is also known to be consumed once glucose is depleted. Since glucose never reached depletion in the experiments, alanine consumption was not expected or observed in the cultures.

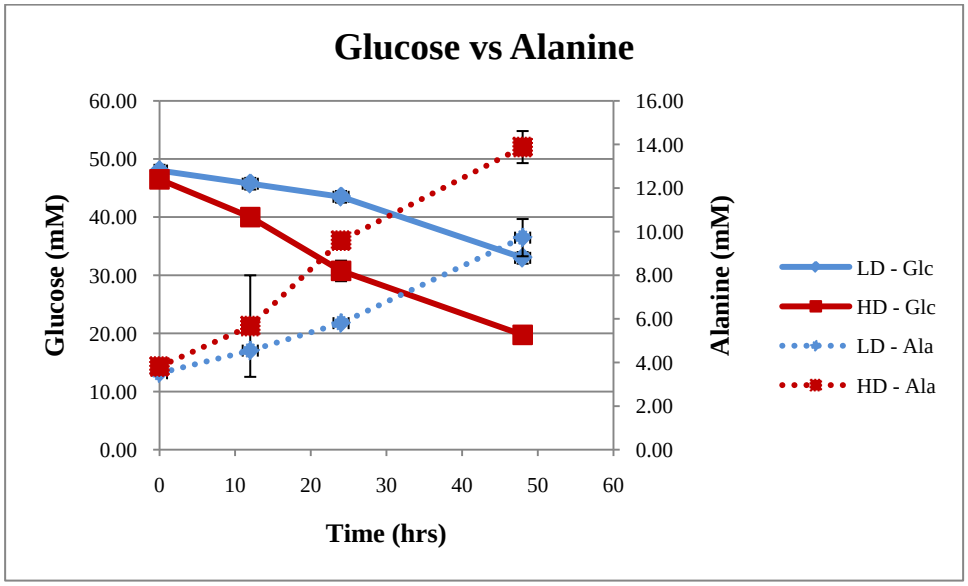

Figure 23 : Glucose Consumption vs. Alanine Production

Figure 24 shows glutamine consumption and ammonia production versus time. Amino acid metabolism and decomposition will release ammonia. Since glutamine is known to be the most consumed amino acid and the only amino acid to undergo significant decomposition, ammonia production is closely related to glutamine consumption. Ammonia accumulation was minimal in the cultures and the disappearance of ammonia from the cultures seen in high density cultures was most likely due to the incorporation of ammonia into the production of alanine.

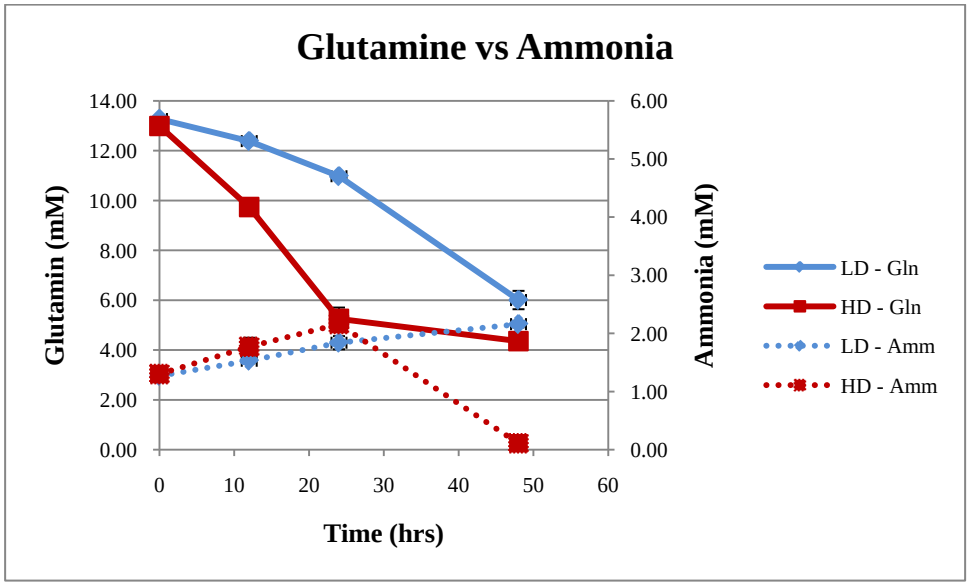

Figure 24 : Glutamine Consumption vs. Ammonia Production

The rates of consumption and production of the nutrients and byproducts related to glucose and glutamine metabolism are shown in Table 2. The rates shown were the average rates between the duplicate cultures. Glucose and glutamine are the most consumed nutrients in culture as observed by Wong et al. (1994) and Mendonca et al. (1999). The ratio of glucose vs. glutamine consumption for low density cultures was 2.17 ± 0.13, and the ratio for high density cultures was 3.32 ± 0.72. The ratios showed that a greater % of glucose as compared to glutamine was used to generate energy in the high density cultures than in the low density cultures. The increased ratio of glucose consumption to yield energy in high density cultures might suggest that more energy was needed in the high cell density cultures because glucose is able to yield more energy than glutamine.

Amino acid metabolism is the source of ammonia. Since glutamine is the major amino acid used in insect cell culture, glutamine metabolism is then the major source of ammonia generation in insect cell culture. As shown by the ratios, less glutamine was used for energy production in the high density cultures; therefore, the amount of ammonia or the rate of ammonia generation was not as high as in the low density

cultures. Therefore, most of the ammonia generated in high density cultures could be successfully removed from the media through alanine production. The rate of ammonia generation might have exceeded the rate of alanine formation in low density cultures due to the higher amount of glutamine used, thus causing small ammonia accumulation in the low density cultures. In addition, the amounts of alanine and lactate produced per mmol of glucose consumed for low density cultures were 0.52 ± 0.17 mmol and 0.27 ± 0.10 mmol, respectively; and for high density cultures were 0.32 ± 0.05 mmol and 0.09 ± 0.02 mmol, respectively.

As can be seen from Table 3, nutrient consumption rates (glucose and glutamine) decreased as culture densities increased. Furthermore, there were also greater amounts of byproducts produced per μm^3 of biovolume per hour in low density cultures than in high density cultures. Since all cultures started with the same initial concentrations of nutrients, the concentrations of nutrients were in greater excess in low density cultures. When nutrients are in excess, nutrient uptake rates increase and will lead to increased production of metabolic byproducts, this phenomenon is called overflow metabolism (Doverskog, et al. 1997; Mendonca, et al. 1999; Miller and Blanch 1991). Overflow metabolism often results in waste of energy since the increased nutrient uptake rates often lead to increased byproduct production.

Table 3: Rates Related to Glucose and Glutamine Metabolism

Nutrient	Group	ICD	Rates (10^{-9} mM/μm^3.hr)	Group Avg Rates	Group Rates Stdev
Glc	**LD**	**1**	-0.0319	-0.0313	0.0006
		2	-0.0312		
		4	-0.0308		
	HD	**8**	-0.0196	-0.0203	0.0010
		10	-0.0209		

Table 3: Rates related to Glucose and Glutamine Metabolism (Continued)

Nutrient	Group	ICD	Rates (10^{-9} mM/μm^3.hr)	Group Avg Rates	Group Rates Stdev
Gln	**LD**	**1**	-0.0155	-0.0145	0.0011
		2	-0.0146		
		4	-0.0134		
	HD	**8**	-0.0070	-0.0062	0.0011
		10	-0.0055		
Ala	**LD**	**1**	0.0227	0.0163	0.0057
		2	0.0147		
		4	0.0115		
	HD	**8**	0.0069	0.0064	0.0008
		10	0.0058		
Lac	**LD**	**1**	0.0118	0.0084	0.0032
		2	0.0080		
		4	0.0054		
	HD	**8**	0.0020	0.0019	0.0003
		10	0.0017		
Amm	**LD**	**1**	0.0022	0.0024	0.0002
		2	0.0026		
		4	0.0025		
	HD	**8**	-0.0002	-0.0002	0.0001
		10	-0.0001		

Table 4 shows the consumption and production rates of all other amino acids for the uninfected cultures. The same patterns of consumption continued for all the other amino acids: more nutrients were consumed in low density cultures than in high density cultures.

Table 4: Other Amino Acid Consumption/ Production Rates

Nutrient	Group	ICD	Rates (10^{-9} mM/μm^3.hr)	Group Avg Rates	Group Rates Stdev
Asp	**LD**	**1**	0.0014	0.0006	0.0007
		2	0.0005		
		4	0.0000		
	HD	**8**	-0.0008	-0.0009	0.0002
		10	-0.0010		
Glu	**LD**	**1**	-0.0032	-0.0028	0.0003
		2	-0.0026		
		4	-0.0026		
	HD	**8**	-0.0012	-0.0011	0.0001
		10	-0.0010		
Ser	**LD**	**1**	-0.0065	-0.0060	0.0004
		2	-0.0059		
		4	-0.0056		
	HD	**8**	-0.0033	-0.0041	0.0011
		10	-0.0049		
Asn	**LD**	**1**	-0.0086	-0.0052	0.0030
		2	-0.0041		
		4	-0.0030		
	HD	**8**	-0.0014	-0.0013	0.0001
		10	-0.0012		
Gly	**LD**	**1**	-0.0022	-0.0017	0.0005
		2	-0.0014		
		4	-0.0014		
	HD	**8**	-0.0008	-0.0007	0.0002
		10	-0.0006		

Table 4: Other Amino Acid Consumption/ Production Rates (Continued)

Nutrient	Group	ICD	Rates (10^{-9} mM/μm^3.hr)	Group Avg Rates	Group Rates Stdev
His	**LD**	**1**	0.0000	-0.0003	0.0002
		2	-0.0003		
		4	-0.0004		
	HD	**8**	-0.0003	-0.0002	0.0000
		10	-0.0002		
Thr	**LD**	**1**	-0.0005	-0.0012	0.0005
		2	-0.0014		
		4	-0.0016		
	HD	**8**	-0.0005	-0.0005	0.0001
		10	-0.0005		
Arg	**LD**	**1**	-0.0017	-0.0019	0.0003
		2	-0.0018		
		4	-0.0022		
	HD	**8**	-0.0019	-0.0017	0.0003
		10	-0.0015		
Pro	**LD**	**1**	-0.0049	-0.0035	0.0013
		2	-0.0033		
		4	-0.0023		
	HD	**8**	-0.0012	-0.0011	0.0002
		10	-0.0010		
Tyr	**LD**	**1**	-0.0016	-0.0014	0.0002
		2	-0.0015		
		4	-0.0011		
	HD	**8**	-0.0006	-0.0006	0.0001
		10	-0.0005		

Table 4: Other Amino Acid Consumption/ Production Rates (Continued)

Nutrient	Group	ICD	Rates (10^{-9} mM/μm^3.hr)	Group Avg Rates	Group Rates Stdev
Cys	**LD**	**1**	-0.0008	-0.0006	0.0002
		2	-0.0007		
		4	-0.0005		
	HD	**8**	-0.0002	-0.0002	0.0000
		10	-0.0002		
Val	**LD**	**1**	0.0000	-0.0010	0.0009
		2	-0.0012		
		4	-0.0017		
	HD	**8**	-0.0010	-0.0009	0.0001
		10	-0.0008		
Met	**LD**	**1**	0.0000	-0.0003	0.0003
		2	-0.0003		
		4	-0.0007		
	HD	**8**	-0.0004	-0.0004	0.0000
		10	-0.0005		
Ile	**LD**	**1**	0.0000	-0.0007	0.0006
		2	-0.0008		
		4	-0.0012		
	HD	**8**	-0.0007	-0.0006	0.0001
		10	-0.0006		
Leu	**LD**	**1**	-0.0027	-0.0029	0.0001
		2	-0.0029		
		4	-0.0029		
	HD	**8**	-0.0016	-0.0014	0.0002
		10	-0.0013		

Table 4: Other Amino Acid Consumption/ Production Rates (Continued)

Nutrient	Group	ICD	Rates (10^{-9} mM/μm^3.hr)	Group Avg Rates	Group Rates Stdev
Lys	**LD**	**1**	-0.0010	-0.0016	0.0005
		2	-0.0018		
		4	-0.0019		
	HD	**8**	-0.0012	-0.0011	0.0001
		10	-0.0010		
Phe	**LD**	**1**	0.0000	-0.0004	0.0004
		2	-0.0004		
		4	-0.0007		
	HD	**8**	-0.0004	-0.0004	0.0000
		10	-0.0004		

5.5.3 Infected Cultures

Figure 25 shows glucose consumption and lactate production versus time for the infected cultures. As stated in the previous section, since the initial glucose concentration in Sf900-II media was high, lactate was found to accumulate in culture, although at low levels. Since lactate accumulation was low in the cultures, the cultures were not under stress.

Maximum lactate accumulation in the high density culture was 2.45 ± 0.07 mM and occurred at 12 hpi; whereas, the uninfected high density culture had a maximum lactate concentration of 2.95 ± 0.07 mM that occurred at 24 hrs. By examining the cell populations of both cultures in the first 12 hrs, it could be observed that the cell density in the uninfected culture increased by 1.70 x 10^6 cells/ml; whereas, the cell density in the infected cell culture only increased by 0.5 x 10^6 cells/ml. On a per cell basis, the infected cells seemed to produce more lactate than the uninfected cells. However, if instead, change in biovolume was examined, a totally different conclusion might be drawn. The biovolume for the uninfected culture increased by 4.52 x 10^9 μm^3/ml; whereas, the biovolume for the infected culture increased by 7.71 x 10^9 μm^3/ml. On a

per biovolume basis, the uninfected cultures actually produced a bit more lactate than the infected cultures. This example again supports the use of an alternative basis to characterize nutrient uptake and production rates.

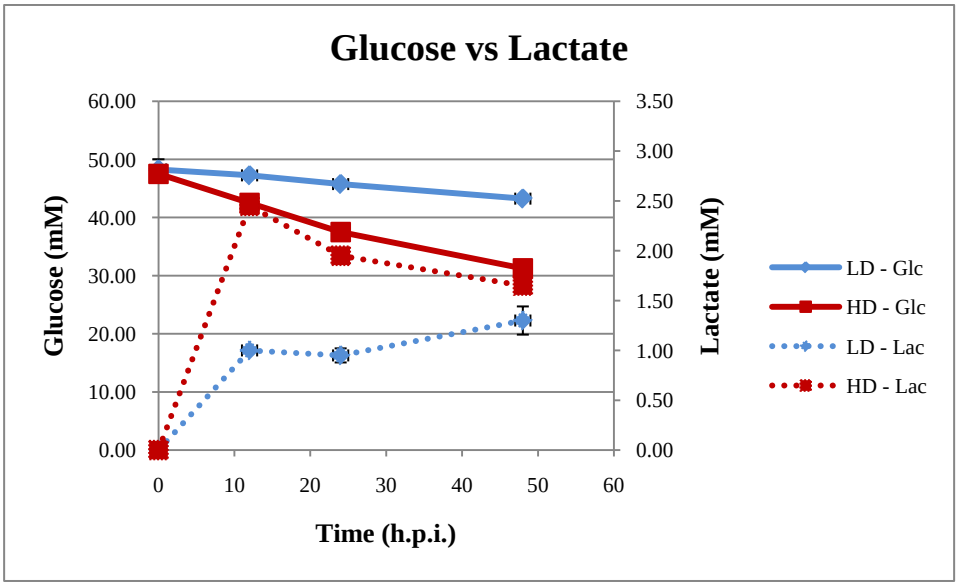

Figure 25 : Glucose Consumption vs. Lactate Production

Figure 26 shows glucose consumption and alanine production versus time. Again, alanine was formed due to excess glucose and glutamine concentrations in Sf900-II media. Since glucose was never depleted, alanine was not consumed in the cultures.

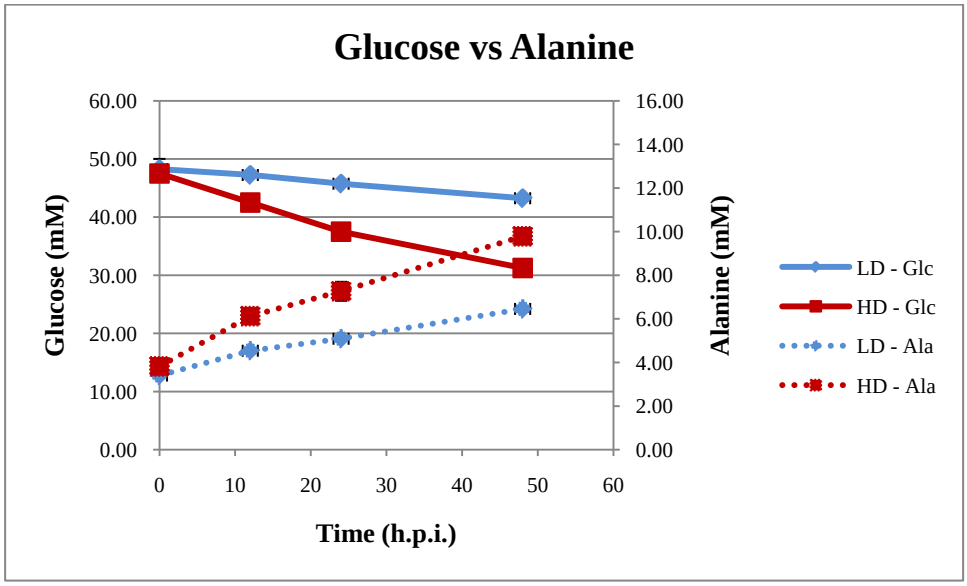

Figure 26 : Glucose Consumption vs. Alanine Production

Figure 27 shows glutamine consumption and ammonia production versus time. Glutamine metabolism is the major source of ammonia accumulation in insect cell cultures. Usually ammonia will not accumulate in cultures because it will be incorporated into the formation of alanine. However, in the infected cultures, more ammonia accumulated than in the uninfected cultures. This might be because an infected cell might be able to adjust its metabolism so that less energy would be wasted on alanine formation; therefore, leaving free ammonia accumulate in culture instead of being incorporated into alanine.

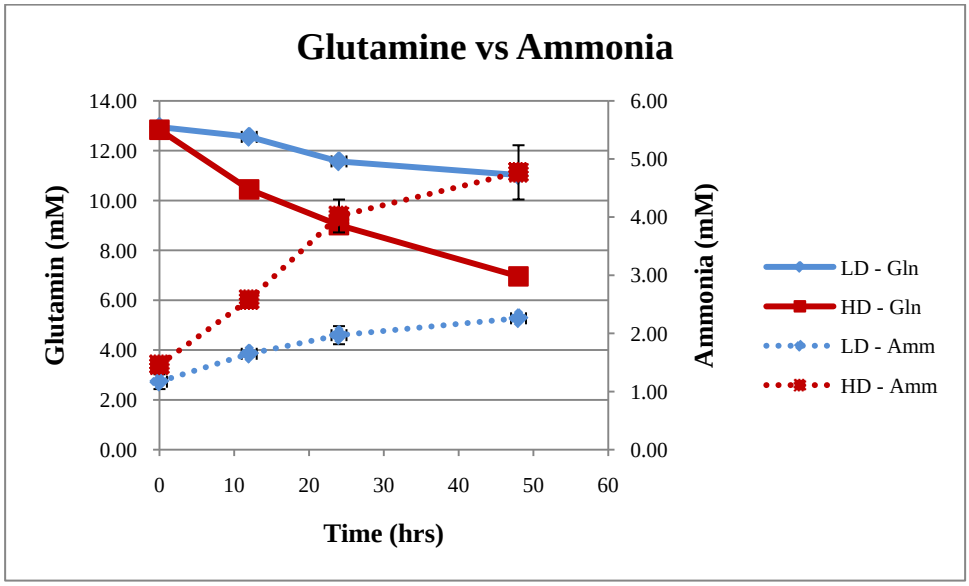

Figure 27 : Glutamine Consumption vs. Ammonia Production

The rates of consumption and production of the nutrients and byproducts related to glucose and glutamine metabolism for the infected cultures are shown in Table 5. The rates shown were the average rates between duplicate cultures. As could be observed from Table 5, nutrient consumption rates (glucose and glutamine) remained relatively constant for both low density and high density cultures. This trend is different than the trend observed in uninfected cultures. In addition, the infected nutrient consumption rates (glucose and glutamine) were similar to the uninfected nutrient consumption rates of the high density cultures. As discussed in the above section, the uninfected high density cultures might have a higher energy demand than the low density cultures due to the higher cell populations, thus the amount of glucose used in the high density cultures increased. The similar rates observed in the infected cultures could mean that the energy demand of the infected cells were similar to the energy demand of the uninfected high density cultures. In terms of byproduct formation, the trend in the uninfected culture was observed. That is more byproducts were produced per μm^3 of biovolume per hour in low density cultures than in high density cultures.

The ratio of glucose to glutamine consumption for low density cultures was 3.35 ± 1.65, and the ratio for high density cultures was 3.01 ± 0.06. The standard deviation showed that the ratios for the low density cultures were more spread out from its mean. This meant that more variability existed in the low density cultures. This could be explained by the less synchronous infection achieved in the low density cultures as discussed in Section 5.4.

Glucose is considered to be the most significant energy source for insect cells (Drews, et al. 2000). The % of glucose consumed by the infected cultures as shown by the ratios were approximately the same, with slightly higher % in the low density cultures than in the high density cultures. In addition, the amounts of glutamine used in low and high density infected cultures were also approximately the same, and the amounts of ammonia accumulated in cultures were similar, too. This supported the notion that glutamine is the major source for ammonia production. Furthermore, more alanine and lactate were produced per mmol of glucose consumed in low density cultures than in high density cultures. The amounts of alanine and lactate produced per mmol of glucose in low density cultures were 0.79 ± 0.42 mmol and 0.34 ± 0.23 mmol, respectively; and in high density cultures were 0.49 ± 0.00 mmol and 0.18 ± 0.00 mmol, respectively. Although, glucose uptake rates stayed relatively constant for both low and high density cultures, there were still more byproducts formed in the low density cultures than in the high density cultures. Fewer nutrients wasted on the production of byproducts could mean that more nutrients were metabolized more efficiently by the insect cells in the high density cultures. Comparing the infected cultures with the uninfected cultures, it was found that the infected cultures had higher glucose to glutamine usage ratios. Glucose is known to be able to yield more energy than glutamine (Mendonca, et al. 1999; Neermann and Wagner 1996). Upon complete oxidation, glucose is able to yield 32 molecules of ATP through the tricarboxylic acid cycle (TCA), and glutamine is able to yield 27 molecules of ATP (Mendonca, et al. 1999). Neerman and Wagner (1996) also determined that 14.3% of glutamine and 60% of glucose in batch cultures were completely oxidized to CO_2 in insect cell cultures by radiolabeled studies of insect cells from the early exponential growth phase cultured at 27°C. Therefore, not only is glucose able to yield more energy when completely

oxidized but insect cells also seem to use more glucose than glutamine. Since the rate of respiration has been shown to increase in infected cells (Kamen, et al. 1996), indicating increase in the demand of energy, it then makes sense for the cells to have a higher glucose/glutamine usage ratio after infection.

Comparing the uninfected and infected cultures, it might seem like less nutrients were needed to support 1 μm^3 of growth in the infected cultures than in the uninfected cultures. However, it was also found that on average the cell size increases by 17.22 ± 2.54 % after infection. Therefore, on a per cell basis comparison, multiplying the infection rate by 1.1722, the low and high density glucose infected uptake rate become -0.0206 and -0.0205 x 10^{-9} mmol/um^3.hr. Comparing this to the glucose uptake rate of the uninfected high density culture, which was -0.0203 x 10^{-9} mmol/um^3.hr, it was observed that the infected cultures had similar consumption rate as the uninfected high density culture. Palomares et al. (2004), Kamen et al. (1996), and Wong et al. (1994) have also observed that glucose uptake rate remains constant after infection. In addition, doing the same adjustment to glutamine, the infected glutamine uptake rates for low and high density became -0.0066 and -0.0068 x 10^{-9} mmol/um^3.hr. Compared to the glutamine uptake rate of the uninfected high density cultures, which was -0.0062 x 10^{-9} mmol/um^3.hr, it was observed that the glutamine uptake rates did not change much before and after infection either, as was also observed by Palomares et al. (2004) and Wong et al. (1994). The fact that nutrient uptake rates stayed relatively constant before and after infection, and that cell respiration has been shown to increase after infection, all seem to suggest that the infected cells were able to yield more energy from the nutrient molecules consumed.

Table 5: Rates related to Glucose and Glutamine Metabolism

Nutrient	Group	ICD	Rates (10^{-9} mM/μm^3.hr)	Group Avg Rates	Group Rates Stdev
Glc	**LD**	**1**	-0.0104	-0.0176	0.0066
		2	-0.0189		
		4	-0.0235		
	HD	**8**	-0.0178	-0.0175	0.0004
		10	-0.0172		
Gln	**LD**	**1**	-0.0071	-0.0057	0.0013
		2	-0.0047		
		4	-0.0052		
	HD	**8**	-0.0058	-0.0058	0.0000
		10	-0.0058		
Ala	**LD**	**1**	0.0130	0.0120	0.0014
		2	0.0126		
		4	0.0104		
	HD	**8**	0.0066	0.0065	0.0001
		10	0.0064		
Lac	**LD**	**1**	0.0061	0.0050	0.0015
		2	0.0057		
		4	0.0034		
	HD	**8**	0.0017	0.0016	0.0001
		10	0.0016		
Amm	**LD**	**1**	0.0045	0.0037	0.0010
		2	0.0039		
		4	0.0026		
	HD	**8**	0.0034	0.0029	0.0006
		10	0.0025		

Table 6 shows the consumption and production rates of all other amino acids for the infected cultures. It was observed that the nutrient uptake rates increased as density increased in the infected cultures. This trend was different from the trend observed in the uninfected cultures, which had higher nutrient uptake rates in lower density cultures. The phenomenon observed in the uninfected cultures was most likely caused by overflow metabolism as explained in the previous sections. It was suggested from the previous discussion that infected cells seemed to utilize nutrients more efficiently by having minimal overflow metabolism. Therefore, the phenomenon (increased uptake rates in lower density cultures) did not occur in the infected cultures. The trends of nutrient consumptions returned to normal: as density increased, more nutrients were needed to support growth.

Table 6: Other Amino Acid Consumption/ Production Rates

Nutrient	Group	ICD	Rates (10^{-9} mM/μm^3.hr)	Group Avg Rates	Group Rates Stdev
Asp	**LD**	**1**	0.0018	0.0019	0.0006
		2	0.0025		
		4	0.0014		
	HD	**8**	-0.0006	-0.0006	0.0000
		10	-0.0006		
Glu	**LD**	**1**	-0.0012	0.0006	0.0017
		2	0.0021		
		4	0.0011		
	HD	**8**	-0.0009	-0.0007	0.0002
		10	-0.0006		
Ser	**LD**	**1**	-0.0014	-0.0014	0.0003
		2	-0.0012		
		4	-0.0018		
	HD	**8**	-0.0023	-0.0024	0.0001
		10	-0.0025		

Table 6: Other Amino Acid Consumption/ Production Rates (Continued)

Nutrient	Group	ICD	Rates (10^{-9} mM/μm^3.hr)	Group Avg Rates	Group Rates Stdev
Asn	**LD**	**1**	-0.0058	-0.0027	0.0027
		2	-0.0011		
		4	-0.0012		
	HD	**8**	-0.0016	-0.0016	0.0000
		10	-0.0016		
Gly	**LD**	**1**	0.0010	0.0006	0.0004
		2	0.0007		
		4	0.0002		
	HD	**8**	-0.0006	-0.0006	0.0000
		10	-0.0006		
His	**LD**	**1**	0.0005	0.0004	0.0002
		2	0.0005		
		4	0.0001		
	HD	**8**	-0.0002	-0.0002	0.0000
		10	-0.0002		
Thr	**LD**	**1**	0.0009	0.0005	0.0006
		2	0.0006		
		4	-0.0002		
	HD	**8**	-0.0008	-0.0008	0.0000
		10	-0.0008		
Arg	**LD**	**1**	-0.0004	0.0000	0.0003
		2	0.0002		
		4	0.0001		
	HD	**8**	-0.0005	-0.0005	0.0000
		10	-0.0005		

Table 6: Other Amino Acid Consumption/ Production Rates (Continued)

Nutrient	Group	ICD	Rates (10^{-9} mM/μm^3.hr)	Group Avg Rates	Group Rates Stdev
Pro	**LD**	**1**	-0.0036	-0.0015	0.0018
		2	-0.0006		
		4	-0.0003		
	HD	**8**	-0.0009	-0.0008	0.0002
		10	-0.0006		
Tyr	**LD**	**1**	-0.0015	-0.0008	0.0006
		2	-0.0005		
		4	-0.0005		
	HD	**8**	-0.0006	-0.0007	0.0000
		10	-0.0007		
Cys	**LD**	**1**	-0.0006	-0.0004	0.0002
		2	-0.0003		
		4	-0.0004		
	HD	**8**	-0.0004	-0.0004	0.0000
		10	-0.0004		
Val	**LD**	**1**	0.0017	0.0012	0.0009
		2	0.0016		
		4	0.0002		
	HD	**8**	-0.0007	-0.0007	0.0000
		10	-0.0008		
Met	**LD**	**1**	0.0015	0.0011	0.0006
		2	0.0015		
		4	0.0004		
	HD	**8**	-0.0004	-0.0004	0.0001
		10	-0.0005		

Table 6: Other Amino Acid Consumption/ Production Rates (Continued)

Nutrient	Group	ICD	Rates (10^{-9} mM/μm^3.hr)	Group Avg Rates	Group Rates Stdev
Ile	**LD**	**1**	0.0016	0.0012	0.0007
		2	0.0015		
		4	0.0004		
	HD	**8**	-0.0005	-0.0005	0.0001
		10	-0.0006		
Leu	**LD**	**1**	-0.0001	-0.0003	0.0003
		2	-0.0002		
		4	-0.0007		
	HD	**8**	-0.0013	-0.0013	0.0001
		10	-0.0014		
Lys	**LD**	**1**	0.0018	0.0010	0.0009
		2	0.0013		
		4	0.0000		
	HD	**8**	-0.0007	-0.0008	0.0001
		10	-0.0008		
Phe	**LD**	**1**	0.0014	0.0010	0.0006
		2	0.0013		
		4	0.0003		
	HD	**8**	-0.0005	-0.0005	0.0000
		10	-0.0005		

Chapter 6 Conclusions and Recommendations

Biovolume has been shown to be a potential parameter for characterizing nutrient consumption profiles in this thesis. The merit of using biovolume is that this parameter allows for the comparison of nutrient consumption profiles before and after infections that the density parameter cannot. By comparing the consumption profiles, knowledge of the nutrient requirements before and after infections can be enhanced. By knowing the nutrient requirements, different nutrient cocktails can be designed to enhance cell growth (before infection) and to improve the production of recombinant proteins (after infection). This will not only increase the efficiency of achieving specific goals at different stages of the culture, but will also reduce the cost, since unnecessary nutrients will not be added and wasted, thus making the process more economical.

Although promising, this parameter still has some limitations. First of all, in order to obtain biovolume profile, a laboratory must have access to some sort of cell counter; whereas, to obtain density profile, a laboratory only needs to have a hemocytometer, which is more commonly found in cell culture laboratories. Another limitation of this method is that the accuracy of the biovolume profiles after infection depends strongly on the success of achieving synchronous infection. If the culture is too asynchronous, then there will be many different cell populations mixed in the culture. For example, at any time point, there may be an uninfected cell population, which will keep on dividing, an infected cell population, and a dead cell population. Both the uninfected cell population and the dead cell population will "dilute" the true infected biovolume exhibited by the infected cell population.

The second limitation can be resolved if different cell populations can be identified by separating the cell size distribution profiles. One possible future work is to separate the cell size distribution into viable cell size distribution and nonviable cell size distribution. In this thesis, it was assumed that viability was well distributed in the diameter range of 9.63 – 26.5 μm. This assumption might seem harmless to uninfected cultures where viability is close to 100%; however, in infected cultures where the occurrence of very low viability is possible, it is likely that the non-viable cells will be

localized at the lower end of the diameter scale of the cell size distribution rather than being well distributed over the whole range. If this is the case, for the infected cultures with low viability, the mean cell diameter calculated will be underestimated, which will lead to an overestimation of nutrient consumption for cultures with low viability. The accuracy of the nutrient consumption in terms of infected cultures without correction might then be dependent on the cell viability. This can be corrected by separating cell size distribution data into different cell populations of viable and nonviable. This analysis is currently being carried out in our group.

Once the cell size distribution data is separated into viable and nonviable populations, the % of uninfected and % of infected population of the viable cell culture can then be calculated by the % of infection method proposed in this thesis. By estimating the % of uninfected culture and knowing the average diameter of the uninfected culture, the biovolume of the uninfected culture can then be corrected. After the corrections, the "true" % of infected biovolume can then be calculated and compared with the "true" uninfected biovolume.

Four major objectives were achieved in this thesis:

1. to compare and contrast uninfected and infected culture profiles;
2. to examine synchronicity of infection;
3. to statistically compare biovolume and cell density to nutrient consumption and metabolite production;
4. to examine and discuss differences in nutrient consumption and metabolite production patterns before and after infection.

As a result, the driving hypothesis of this thesis, that biovolume can be utilized as a parameter for characterizing nutrient consumption patterns, has been validated to a certain extent. Biovolume could be used as a basis for growth and nutrient consumption characterization. In uninfected cultures, the cell density increases while the cell sizes stays relatively constant; whereas in the infected cultures, cell density stays relatively constant while cell sizes increase. Combining cell density and cell size profiles, biovolume profiles were generated and used to characterize changes in growth and nutrient consumption profiles instead of cell density data alone.

To verify that biovolume was indeed a better parameter for characterization of growth and nutrient consumption, analyses of the correlations between nutrient consumptions and changes in cell density and biovolume were performed. It was found that in the uninfected cultures, there was no significant difference in using either cell density or biovolume since cell size stayed relatively constant; however, in the infected cultures, better correlations were found using biovolume than using cell density. Since biovolume provided a better correlation, it was used to characterize the nutrient consumption profiles.

When culturing cells at 30°C, it was found that metabolites such as lactate and alanine were produced more readily in low density uninfected cultures (from 1 to 4 x 10^6 cells/ml), suggesting the use of alternative metabolic pathways in the cells, often referred to as an "overflow metabolism." Overflow metabolism occurs when the amount of nutrients present in the media are more than what the cells require because cells have a tendency to increase their nutrient uptake rate when the concentrations of nutrients increase. The increased uptake of nutrients will then result in increased generation of metabolic byproducts. The amount of alanine and lactate produced per mmol of glucose consumed for low density cultures were 0.52 ± 0.17 mmol and 0.27 ± 0.10 mmol, respectively; and the amount produced for high density cultures (> 8 x 10^6 cells/ml) were 0.32 ± 0.05 mmol and 0.09 ± 0.02 mmol, respectively.

In the production of AAV at high temperature (30°C), it was found that more glucose was consumed compared to glutamine. The ratio of glucose to glutamine consumption rates in low density and high density cultures were similar; in low density cultures, the ratio was 3.35 ± 1.65, and the ratio for high density cultures was 3.01 ± 0.06. Comparing to the uninfected cultures, which had a ratio of 2.17 ± 0.13 for low density cultures, and a ratio of 3.32 ± 0.72 for high density cultures, it was observed that the infected cultures had a higher glucose to glutamine consumption ratio than uninfected low density cultures, and the ratio of high density cultures stayed relatively constant regardless of whether the cultures were infected or not. Since glucose is able to yield more energy than glutamine, and when the cultures have more cells, more energy is needed, the increased use of glucose vs. glutamine from low density to high density

uninfected cultures was justified. It was also observed that the energy requirement of infected cultures were similar to those of the uninfected high density cultures. It is known that the uninfected cultures will increase in density, whereas the density of the infected cultures remains relatively constant. Instead, the cell sizes of the infected cultures will increase due to increased DNA replication and protein productions inside the cells. The data appeared to suggest that the amount of nutrients consumed in the infected cultures were similar to the amount of nutrient consumed in the uninfected cultures.

On the surface, it might seem that energy demand of the cells remained relatively constant in the infected and uninfected cultures because nutrient consumptions remained relatively constant. However, it has also been reported that he rate of cell respiration increases after infection. Higher reparation rates can allow a higher amounts of nutrient to be oxidized completely. As a result of a more complete oxidation, more energy can be yielded. Therefore, although the rates of consumption were similar in the infected and uninfected cultures; the energy demand in the infected cultures can still be greater due to the higher respiration rates.

Synchronicity of infection was also examined in this thesis. Three methods were used. The first two methods calculated % of infection at 0 hr; and the last method investigated on rate of infection through computer simulation. The results from all three methods seemed to suggest that synchronicity of infection could be a function of initial cell density.

Appendix A - Matlab Codes

Script File – callfile

```
clear all
close all

global u xo xf cult

u = [0.0203 0.0203 0.0203 0.0203 0.0203 0.0203 0.0203 0.0203 0.0203 0.0203];
xo = [8.47E+05 1.99E+06 4.11E+06 9.24E+06 1.07E+07 1.06E+06 2.01E+06
4.04E+06 8.09E+06 1.01E+07];
xf= [1.08E+06 2.08E+06 3.99E+06 8.47E+06 1.04E+07 1.10E+06 2.06E+06 3.72E+06
7.23E+06 8.24E+06];

ki=zeros(1,10);

for i=1:10
cult=i;
parameter=0.05;
options=optimset('TolFun',0.0001);
ki(1,i)=fminsearch(@minkierr, parameter, options);
end

ki
```

Function File – minkierr

```
function error_out=minkierr(parameter)

global xo xf cult crate

%-----------------------------------------------------------------------------------------------
% This file calculates and minimizes the error of ki

%Initial conditions
%         xo     xi
Cinit = [xo(cult), 0];
crate=parameter;

%Timespan
Tspan=[0 24];

%Differential Equation Solution
[t,x]=ode45(@balances, Tspan, Cinit);

%error calculation
j = length(t);
kierr = (x(j,2)+x(j,1) - xf(cult))^2;
error_out=kierr;
```

Function File – balances

```
function dydt=balances(t,y)

global u cult crate

%-------------------------------------------------------------------------------------
% This file calculates changes in the uninfected and infected cell populations

X=y(1);
Xi=y(2);
mu=u(cult);

%-------------------------------------------------------------------------------------
%ODEs

if X<0
  X=0;
end

dXdt=mu*X-crate*X;
dXidt=crate*X;

if dXdt<-X
  dXdt=-X;
  dXidt=X;
end

%-------------------------------------------------------------------
dydt=[dXdt; dXidt];
```

References

Allen T. 1990. Particle size measurement. London:Chapman and Hall.

Allerson CR, Sioufi N, Jarres R, Prakash TP, Naik N, Berdeja A, Wanders L, Griffey RH, Swayze EE, Bhat B. 2005. Fully 2'-modified oligonucleotide duplexes with improved in vitro potency and stability compared to unmodified small interfering RNA. J Med Chem 48:901-904.

Al-Rubeai M, Chalder S, Bird R, Emery AN. 1991. Cell cycle, cell size and mitochondrial activity of hybridoma cells during batch cultivation. Cytotechnology 7:179-186.

Al-Rubeai M, Singh RP, Emery AN, Zhang Z. 1995. Cell cycle and cell size dependence of susceptibility to hydrodynamic forces. Biotechnol Bioeng 46:88-92.

Ansorge S, Esteban G, Schmid G. 2007. On-line monitoring of infected Sf-9 insect cell cultures by scanning permittivity measurements and comparison with off-line biovolume measurements. Cytotechnology 55:115-124.

Arts GJ, Langemeijer E, Tissingh R, Ma L, Pavliska H, Dokic K, Dooijes R, Mesic E, Clasen R, Michiels F, van der Schueren J, Lambrecht M, Herman S, Brys R, Thys K, Hoffmann M, Tomme P, van Es H. 2003. Adenoviral vectors expressing siRNAs for discovery and validation of gene function. Genome Res 13:2325-2332.

Atkinson D, Sibly RM. 1997. Why are organisms usually bigger in colder environments? Making sense of a life history puzzle. Trends Ecol Evol 12:235-239.

Aucoin MG. 2007. Characterization and Optimiazation of the Production of Adeno-Associated Viral Vectors Using a Baculovirus Expression Vector/ Insect Cell System. Ecole Polytechnique de Montreal, University of Montreal

Aucoin MG, Perrier M, Kamen AA. 2008. Critical assessment of current adeno-associated viral vector production and quantification methods. Biotechnol Adv 26:73-88.

Aucoin MG, Perrier M, Kamen AA. 2007. Improving AAV vector yield in insect cells by modulating the temperature after infection. Biotechnol Bioeng 97:1501-1509.

Bannai S. 1986. Exchange of cystine and glutamate across plasma membrane of human fibroblasts. J Biol Chem 261:2256-2263.

Batista FR, Pereira CA, Mendonca RZ, Moraes AM. 2005. Enhancement of Sf9 Cells and Baculovirus Production Employing Grace's Medium Supplemented with Milk Whey Ultrafiltrate. Cytotechnology 49:1-9.

Batista FR, Pereira CA, Mendonca RZ, Moraes AM. 2006. Evaluation of concentrated milk whey as a supplement for SF9 Spodoptera frugiperda cells in culture. EJB 9:522-532.

Bedard C, Tom R, Kamen A. 1993. Growth, nutrient consumption, and end-product accumulation in Sf-9 and BTI-EAA insect cell cultures: insights into growth limitation and metabolism. Biotechnol Prog 9:615-624.

Benslimane C, Elias CB, Hawari J, Kamen A. 2005. Insights into the central metabolism of Spodoptera frugiperda (Sf-9) and Trichoplusia ni BTI-Tn-5B1-4 (Tn-5) insect cells by radiolabeling studies. Biotechnol Prog 21:78-86.

Blissard GW. 1996. Baculovirus--insect cell interactions. Cytotechnology 20:73-93.

Blissard GW, Rohrmann GF. 1990. Baculovirus diversity and molecular biology. Annu Rev Entomol 35:127-155.

Braasch DA, Jensen S, Liu Y, Kaur K, Arar K, White MA, Corey DR. 2003. RNA interference in mammalian cells by chemically-modified RNA. Biochemistry 42:7967-7975.

Braunagel SC, Parr R, Belyavskyi M, Summers MD. 1998. Autographa californica nucleopolyhedrovirus infection results in Sf9 cell cycle arrest at G2/M phase. Virology 244:195-211.

Brokx RD, Bisland SK, Gariepy J. 2002. Designing peptide-based scaffolds as drug delivery vehicles. J Control Release 78:115-123.

Bruggert M, Rehm T, Shanker S, Georgescu J, Holak TA. 2003. A novel medium for expression of proteins selectively labeled with 15N-amino acids in Spodoptera frugiperda (Sf9) insect cells. J Biomol NMR 25:335-348.

Bussolati O, Uggeri J, Belletti S, Dall'Asta V, Gazzola GC. 1996. The stimulation of Na,K,Cl cotransport and of system A for neutral amino acid transport is a mechanism for cell volume increase during the cell cycle. FASEB J 10:920-926.

Calles K, Svensson I, Lindskog E, Haggstrom L. 2006. Effects of conditioned medium factors and passage number on Sf9 cell physiology and productivity. Biotechnol Prog 22:394-400.

Calos MP. 1996. The potential of extrachromosomal replicating vectors for gene therapy. Trends Genet 12:463-466.

Campbell JJ, Duncan MG, Gronlund AF. 1963. Endogenous Metabolism of Pseudomonas. Ann N Y Acad Sci 102:669-&.

Carstens EB, Tjia ST, Doerfler W. 1979. Infection of Spodoptera frugiperda cells with Autographa californica nuclear polyhedrosis virus I. Synthesis of intracellular proteins after virus infection. Virology 99:386-398.

Chen Y, Huang L. 2008. Tumor-targeted delivery of siRNA by non-viral vector: safe and effective cancer therapy. Expert Opin Drug Deliv 5:1301-1311.

Chitkara D, Shikanov A, Kumar N, Domb AJ. 2006. Biodegradable injectable in situ depot-forming drug delivery systems. Macromol Biosci 6:977-990.

Corey DR. 2007. Chemical modification: the key to clinical application of RNA interference? J Clin Invest 117:3615-3622.

Cox MMJ. 2004. Commercial production in insect cells: one company’s perspective. Bioprocess Int Suppl

Darzynkiewicz Z, Crissman H, Traganos F, Steinkamp J. 1982. Cell Heterogeneity during the Cell-Cycle. J Cell Physiol 113:465-474.

Dobos P, Cochran MA. 1980. Protein synthesis in cells infected by Autographa californica nuclear polyhedrosis virus (Ac-NPV): the effect of cytosine arabinoside. Virology 103:446-464.

Dorsett Y, Tuschl T. 2004. siRNAs: applications in functional genomics and potential as therapeutics. Nat Rev Drug Discov 3:318-329.

Doverskog M, Han L, Haggstrom L. 1998. Cystine/cysteine metabolism in cultured Sf9 cells: influence of cell physiology on biosynthesis, amino acid uptake and growth. Cytotechnology 26:91-102.

Doverskog M, Ljunggren J, Ohman L, Haggstrom L. 1997. Physiology of cultured animal cells. J Biotechnol 59:103-115.

Drews M, Doverskog M, Ohman L, Chapman BE, Jacobsson U, Kuchel PW, Haggstrom L. 2000. Pathways of glutamine metabolism in Spodoptera frugiperda (Sf9) insect cells: evidence for the presence of the nitrogen assimilation system, and a metabolic switch by 1H/15N NMR. J Biotechnol 78:23-37.

Drews M, Paalme T, Vilu R. 1995. The Growth and Nutrient Utilization of the Insect-Cell Line Spodoptera-Frugiperda Sf9 in Batch and Continuous-Culture. J Biotechnol 40:187-198.

Eckstein F. 2002. Developments in RNA chemistry, a personal view. Biochimie 84:841-848.

Elbashir SM, Lendeckel W, Tuschl T. 2001. RNA interference is mediated by 21- and 22-nucleotide RNAs. Genes Dev 15:188-200.

Elias CB, Zeiser A, Bedard C, Kamen AA. 2000. Enhanced growth of Sf-9 cells to a maximum density of 5.2 x 10(7) cells per mL and production of beta-galactosidase at high cell density by fed batch culture. Biotechnol Bioeng 68:381-388.

Ferrance JP, Goel A, Ataai MM. 1993. Utilization of glucose and amino acids in insect cell cultures: Quantifying the metabolic flows within the primary pathways and medium development. Biotechnol Bioeng 42:697-707.

Fire A, Xu S, Montgomery MK, Kostas SA, Driver SE, Mello CC. 1998. Potent and specific genetic interference by double-stranded RNA in Caenorhabditis elegans. Nature 391:806-811.

Fischer R, Kohler K, Fotin-Mleczek M, Brock R. 2004. A stepwise dissection of the intracellular fate of cationic cell-penetrating peptides. J Biol Chem 279:12625-12635.

Frieden M, Orum H. 2006. The application of locked nucleic acids in the treatment of cancer. IDrugs 9:706-711.

Ganesan AK, Ho H, Bodemann B, Petersen S, Aruri J, Koshy S, Richardson Z, Le LQ, Krasieva T, Roth MG, Farmer P, White MA. 2008. Genome-wide siRNA-based functional genomics of pigmentation identifies novel genes and pathways that impact melanogenesis in human cells. PLoS Genet 4:e1000298.

Garnier A, Voyer R, Tom R, Perret S, Jardin B, Kamen A. 1996. Dissolved carbon dioxide accumulation in a large scale and high density production of TGF beta receptor with baculovirus infected Sf-9 cells. Cytotechnology 22:53-63.

Gibb WR. 1997. Functional neuropathology in Parkinson's disease. Eur Neurol 38 Suppl 2:21-25.

Gibbs BS, Wojchowski D, Benkovic SJ. 1993. Expression of rat liver phenylalanine hydroxylase in insect cells and site-directed mutagenesis of putative non-heme iron-binding sites. J Biol Chem 268:8046-8052.

Givskov M, Eberl L, Moller S, Poulsen LK, Molin S. 1994. Responses to nutrient starvation in Pseudomonas putida KT2442: analysis of general cross-protection, cell shape, and macromolecular content. J Bacteriol 176:7-14.

Grace TD. 1967. Establishment of a line of cells from the silkworm Bombyx mori. Nature 216:613.

Grace TD. 1966. Establishment of a line of mosquito (Aedes aegypti L.) cells grown in vitro. Nature 211:366-367.

Grace TD. 1962. Establishment of four strains of cells from insect tissues grown in vitro. Nature 195:788-789.

Gronlund AF, Campbell JJ. 1963. Nitrogenous Substrates of Endogenous Respiration in Pseudomonas Aeruginosa. J Bacteriol 86:58-66.

Gronlund AF, Campbell JJ. 1961. Nitrogenous compounds as substrates for endogenous respiration in microorganisms. J Bacteriol 81:721-724.

Hall AH, Wan J, Shaughnessy EE, Ramsay Shaw B, Alexander KA. 2004. RNA interference using boranophosphate siRNAs: structure-activity relationships. Nucleic Acids Res 32:5991-6000.

Harborth J, Elbashir SM, Vandenburgh K, Manninga H, Scaringe SA, Weber K, Tuschl T. 2003. Sequence, chemical, and structural variation of small interfering RNAs and short hairpin RNAs and the effect on mammalian gene silencing. Antisense Nucleic Acid Drug Dev 13:83-105.

Hensler W, Singh V, Agathos SN. 1994. Sf9 insect cell growth and beta-galactosidase production in serum and serum-free media. Ann N Y Acad Sci 745:149-166.

Hommel JD, Sears RM, Georgescu D, Simmons DL, DiLeone RJ. 2003. Local gene knockdown in the brain using viral-mediated RNA interference. Nat Med 9:1539-1544.

Hu YC. 2005. Baculovirus as a highly efficient expression vector in insect and mammalian cells. Acta Pharmacol Sin 26:405-416.

Hu Z, Luijckx T, van Dinten LC, van Oers MM, Hajos JP, Bianchi FJ, van Lent JW, Zuidema D, Vlak JM. 1999. Specificity of polyhedrin in the generation of baculovirus occlusion bodies. J Gen Virol 80 (Pt 4):1045-1053.

Ikonomou L, Schneider YJ, Agathos SN. 2003. Insect cell culture for industrial production of recombinant proteins. Appl Microbiol Biotechnol 62:1-20.

INGRAHAM JL, MARR AG. 1996. Effect of temperature, pressure, pH and osmotic stress on growth. In: Neidhardt F, et al., editors. Escherichia coli and Salmonella. Washington, D.C.:ASM Press. p 1570-1578.

Janakiraman V, Forrest WF, Chow B, Seshagiri S. 2006. A rapid method for estimation of baculovirus titer based on viable cell size. J Virol Methods 132:48-58.

Jarver P, Langel U. 2004. The use of cell-penetrating peptides as a tool for gene regulation. Drug Discov Today 9:395-402.

Joosten CE, Shuler ML. 2003. Effect of culture conditions on the degree of sialylation of a recombinant glycoprotein expressed in insect cells. Biotechnol Prog 19:739-749.

Kamen AA, Bedard C, Tom R, Perret S, Jardin B. 1996. On-line monitoring of respiration in recombinant-baculovirus infected and uninfected insect cell bioreactor cultures. Biotechnol Bioeng 50:36-48.

Kelly BJ, King LA, Possee RD. 2007. Introduction to baculovirus molecular biology. Methods Mol Biol 388:25-54.

Kelly DC, Wang X. 1981. The Infectivity of Nuclear Polyhedrosis-Virus Dna. Annales De Virologie 132:247-259.

King GA, Daugulis AJ, Faulkner P, Goosen MF. 1992. Recombinant beta-galactosidase production in serum-free medium by insect cells in a 14-L airlift bioreactor. Biotechnol Prog 8:567-571.

Kioukia N, Nienow AW, Emery AN, al-Rubeai M. 1995. Physiological and environmental factors affecting the growth of insect cells and infection with baculovirus. J Biotechnol 38:243-251.

Lehninger AL. 1975. Principles of Biochemistry 2nd Edition. New York:Worth Publisher. 1100 p.

Li CX, Parker A, Menocal E, Xiang S, Borodyansky L, Fruehauf JH. 2006. Delivery of RNA interference. Cell Cycle 5:2103-2109.

Li W, Szoka FC,Jr. 2007. Lipid-based nanoparticles for nucleic acid delivery. Pharm Res 24:438-449.

Licari P, Bailey JE. 1992. Modeling the population dynamics of baculovirus-infected insect cells: Optimizing infection strategies for enhanced recombinant protein yields. Biotechnol Bioeng 39:432-441.

Licari P, Bailey JE. 1991. Factors influencing recombinant protein yields in an insect cell-bacuiovirus expression system: Multiplicity of infection and intracellular protein degradation. Biotechnol Bioeng 37:238-246.

Lloyd DR, Leelavatcharamas V, Emery AN, Al-Rubeai M. 1999. The role of the cell cycle in determining gene expression and productivity in CHO cells. Cytotechnology 30:49-57.

Lynn DE, Hink WF. 1978. Infection of Synchronized Tn-368 Cell-Cultures with Alfalfa Looper Nuclear Polyhedrosis-Virus. J Invertebr Pathol 32:1-5.

Maaloe O, Kjelgaard MO. 1966. Control of Macromolecular Synthesis. New York:W. A. Benjamin.

Mae M, Langel U. 2006. Cell-penetrating peptides as vectors for peptide, protein and oligonucleotide delivery. Curr Opin Pharmacol 6:509-514.

Marteijn RC, Jurrius O, Dhont J, de Gooijer CD, Tramper J, Martens DE. 2003. Optimization of a feed medium for fed-batch culture of insect cells using a genetic algorithm. Biotechnol Bioeng 81:269-278.

Martinez J, Patkaniowska A, Urlaub H, Luhrmann R, Tuschl T. 2002. Single-stranded antisense siRNAs guide target RNA cleavage in RNAi. Cell 110:563-574.

Matilainen H, Rinne J, Gilbert L, Marjomaki V, Reunanen H, Oker-Blom C. 2005. Baculovirus entry into human hepatoma cells. J Virol 79:15452-15459.

Mehler AH. 1986. Amino Acid Metabolism II: Metabolism of the individual amino acids. In: Devlin TM, editor. Textbook of Biochemistry. New York:John Wiley and Sons. p 453-488.

Mena JA, Ramirez OT, Palomares LA. 2007. Population kinetics during simultaneous infection of insect cells with two different recombinant baculoviruses for the production of rotavirus-like particles. BMC Biotechnol 7:39.

Mendonca RZ, de Oliveira EC, Pereira CA, Lebrun I. 2007. Effect of bioactive peptides isolated from yeastolate, lactalbumin and NZCase in the insect cell growth. Bioprocess Biosyst Eng 30:157-164.

Mendonca RZ, Palomares LA, Ramirez OT. 1999. An insight into insect cell metabolism through selective nutrient manipulation. J Biotechnol 72:61-75.

Meneses-Acosta A, Mendonca R, Merchant H, Covarrubias L, Ramirez O. 2001. Comparative characterization of cell death between Sf9 insect cells and hybridoma cultures. Biotechnol Bioeng 72:441-457.

Miller WM, Blanch HW. 1991. Regulation of animal cell metabolism in bioreactors. In: Ho CS and Wang DIC, editors. Animal Cell Bioreactors. Stoneham:Butterworth-Heinemann. p 119-161.

Mitsuhashi J. 1982. Nutritional requirements of insect cells in vitro. In: Mitsuhashi J, editor. Invertebrate Cell System Applications. Boca Raton:CRC Press. p 3-20.

Morishita M, Peppas NA. 2006. Is the oral route possible for peptide and protein drug delivery? Drug Discov Today 11:905-910.

Neermann J, Wagner R. 1996. Comparative analysis of glucose and glutamine metabolism in transformed mammalian cell lines, insect and primary liver cells. J Cell Physiol 166:152-169.

NG H, INGRAHAM JL, MARR AG. 1962. Damage and derepression in Escherichia coli resulting from growth at low temperatures. J Bacteriol 84:331-339.

Noguchi H, Matsumoto S. 2006. Protein transduction technology: a novel therapeutic perspective. Acta Med Okayama 60:1-11.

Nurse P. 1975. Genetic control of cell size at cell division in yeast. Nature 256:547-551.

Nykanen A, Haley B, Zamore PD. 2001. ATP requirements and small interfering RNA structure in the RNA interference pathway. Cell 107:309-321.

Nystrom T. 2004. Stationary-phase physiology. Annu Rev Microbiol 58:161-181.

Ohman L, Ljunggren J, Haggstrom L. 1995. Induction of a metabolic switch in insect cells by substrate-limited fed batch cultures. Appl Microbiol Biotechnol 43:1006-1013.

Ong ST, Li F, Du J, Tan YW, Wang S. 2005. Hybrid cytomegalovirus enhancer-h1 promoter-based plasmid and baculovirus vectors mediate effective RNA interference. Hum Gene Ther 16:1404-1412.

Ooi BG, Miller LK. 1988. Regulation of host RNA levels during baculovirus infection. Virology 166:515-523.

Ozturk SS, Palsson BO. 1990. Chemical decomposition of glutamine in cell culture media: effect of media type, pH, and serum concentration. Biotechnol Prog 6:121-128.

Palomares LA, Estrada-Mondaca S, Ramírez OT. 2006. Principles and applications of the insect-cell-baculovirus expression vector system. In: Ozturk S, Hu WS, editor. Cell Culture Technology for Pharmaceutical and Cellular Applications. New York:Taylor and Francis. p 627-692.

Palomares LA, Lopez S, Ramirez OT. 2004. Utilization of oxygen uptake rate to assess the role of glucose and glutamine in the metabolism of infected insect cell cultures. Biochem Eng J 19:87-93.

Palomares LA, Pedroza JC, Ramirez OT. 2001. Cell size as a tool to predict the production of recombinant protein by the insect-cell baculovirus expression system. Biotechnol Lett 23:359-364.

Palomares LA, Ramirez OT. 1996. The effect of dissolved oxygen tension and the utility of oxygen uptake rate in insect cell culture. Cytotechnology 22:225-237.

Panyam J, Labhasetwar V. 2003. Biodegradable nanoparticles for drug and gene delivery to cells and tissue. Adv Drug Deliv Rev 55:329-347.

Park TG, Jeong JH, Kim SW. 2006. Current status of polymeric gene delivery systems. Adv Drug Deliv Rev 58:467-486.

Pinto Reis C, Neufeld RJ, Ribeiro AJ, Veiga F. 2006. Nanoencapsulation II. Biomedical applications and current status of peptide and protein nanoparticulate delivery systems. Nanomedicine 2:53-65.

Pujals S, Fernandez-Carneado J, Lopez-Iglesias C, Kogan MJ, Giralt E. 2006. Mechanistic aspects of CPP-mediated intracellular drug delivery: relevance of CPP self-assembly. Biochim Biophys Acta 1758:264-279.

Radford KM, Reid S, Greenfield PF. 1997. Substrate limitation in the baculovirus expression vector system. Biotechnol Bioeng 56:32-44.

Ramachandran S, Yu YB. 2006. Peptide-based viscoelastic matrices for drug delivery and tissue repair. BioDrugs 20:263-269.

Relph KL, Harrington KJ, Pandha H. 2005. Adenoviral strategies for the gene therapy of cancer. Semin Oncol 32:573-582.

Reuveny S, Kim YJ, Kemp CW, Shiloach J. 1993a. Effect of temperature and oxygen on cell growth and recombinant protein production in insect cell cultures. Appl Microbiol Biotechnol 38:619-623.

Reuveny S, Kim YJ, Kemp CW, Shiloach J. 1993b. Production of recombinant proteins in high-density insect cell cultures. Biotechnol Bioeng 42:235-239.

Rhiel M, Mitchell-Logean CM, Murhammer DW. 1997. Comparison of Trichoplusia ni BTI-Tn-5B1-4 (high fivetrade mark) and Spodoptera frugiperda Sf-9 insect cell line metabolism in suspension cultures. Biotechnol Bioeng 55:909-920.

Rhiel M, Murhammer DW. 1995. The effect of oscillating dissolved oxygen concentrations on the metabolism of a Spodoptera frugiperda IPLB-Sf21-AE clonal isolate. Biotechnol Bioeng 47:640-650.

Rubinson DA, Dillon CP, Kwiatkowski AV, Sievers C, Yang L, Kopinja J, Rooney DL, Zhang M, Ihrig MM, McManus MT, Gertler FB, Scott ML, Van Parijs L. 2003. A lentivirus-based system to functionally silence genes in primary mammalian cells, stem cells and transgenic mice by RNA interference. Nat Genet 33:401-406.

Saint-Ruf C, Pesut J, Sopta M, Matic I. 2007. Causes and consequences of DNA repair activity modulation during stationary phase in Escherichia coli. Crit Rev Biochem Mol Biol 42:259-270.

Saito T, Dojima T, Toriyama M, Park EY. 2002. The effect of cell cycle on GFPuv gene expression in the baculovirus expression system. J Biotechnol 93:121-129.

Sander L, Harrysson A. 2007. Using cell size kinetics to determine optimal harvest time for Spodoptera frugiperda and Trichoplusia ni BTI-TN-5B1-4 cells infected with a baculovirus expression vector system expressing enhanced green fluorescent protein. Cytotechnology 54:35-48.

Sandhu KS, Naciri M, Al-Rubeai M. 2007. Prediction of recombinant protein production in an insect cell-baculovirus system using a flow cytometric technique. J Immunol Methods 325:104-113.

Sato AK, Viswanathan M, Kent RB, Wood CR. 2006. Therapeutic peptides: technological advances driving peptides into development. Curr Opin Biotechnol 17:638-642.

Savinell JM, Palsson BO. 1992. Network analysis of intermediary metabolism using linear optimization. I. Development of mathematical formalism. J Theor Biol 154:421-454.

Schiffelers RM, Woodle MC, Scaria P. 2004. Pharmaceutical prospects for RNA interference. Pharm Res 21:1-7.

Schmid G. 1996. Insect cell cultivation: Growth and kinetics. Cytotechnology 20:43-56.

Schopf B, Howaldt MW, Bailey JE. 1990. DNA distribution and respiratory activity of Spodoptera frugiperda populations infected with wild-type and recombinant Autographa californica nuclear polyhedrosis virus. J Biotechnol 15:169-185.

Sharp PA. 2001. RNA interference--2001. Genes Dev 15:485-490.

Shaw MK. 1967. Effect of abrupt temperature shift on the growth of mesophilic and psychrophilic yeasts. J Bacteriol 93:1332-1336.

Shen C, Buck AK, Liu X, Winkler M, Reske SN. 2003. Gene silencing by adenovirus-delivered siRNA. FEBS Lett 539:111-114.

Shen CF, Kiyota T, Jardin B, Konishi Y, Kamen A. 2007. Characterization of yeastolate fractions that promote insect cell growth and recombinant protein production. Cytotechnology 54:25-34.

Shen CF, Meghrous J, Kamen A. 2002. Quantitation of Baculovirus Particles by Flow Cytometry. J Virol Methods 105:321-330.

Shuler ML, Cho T, Wickham T, Ogonah O, Kool M, Hammer DA, Granados RR, Wood HA. 1990. Bioreactor development for production of viral pesticides or heterologous proteins in insect cell cultures. Ann N Y Acad Sci 589:399-422.

Shuler ML, Wood HA. 1995. Baculovirus Expression Systems and Biopesticides. New York:Wiley-Liss. 259 p.

Siegele DA, Kolter R. 1992. Life After Log. J Bacteriol 174:345-348.

Simeoni F, Morris MC, Heitz F, Divita G. 2003. Insight into the mechanism of the peptide-based gene delivery system MPG: implications for delivery of siRNA into mammalian cells. Nucleic Acids Res 31:2717-2724.

Soutschek J, Akinc A, Bramlage B, Charisse K, Constien R, Donoghue M, Elbashir S, Geick A, Hadwiger P, Harborth J, John M, Kesavan V, Lavine G, Pandey RK, Racie T, Rajeev KG, Rohl I, Toudjarska I, Wang G, Wuschko S, Bumcrot D, Koteliansky V, Limmer S, Manoharan M, Vornlocher HP. 2004. Therapeutic silencing of an endogenous gene by systemic administration of modified siRNAs. Nature 432:173-178.

Springett GM, Moen RC, Anderson S, Blaese RM, Anderson WF. 1989. Infection Efficiency of Lymphocytes-T with Amphotropic Retroviral Vectors is Cell-Cycle Dependent. J Virol 63:3865-3869.

Stilwell JL, Samulski RJ. 2003. Adeno-associated virus vectors for therapeutic gene transfer. BioTechniques 34:148-50, 152, 154 passim.

Stocker H, Hafen E. 2000. Genetic control of cell size. Curr Opin Genet Dev 10:529-535.

Svensson I, Calles K, Lindskog E, Henriksson H, Eriksson U, Haggstrom L. 2005. Antimicrobial activity of conditioned medium fractions from Spodoptera frugiperda Sf9 and Trichoplusia ni Hi5 insect cells. Appl Microbiol Biotechnol 69:92-98.

Tjia ST, Carstens EB, Doerfler W. 1979. Infection of Spodoptera frugiperda cells with Autographa californica nuclear polyhedrosis virus II. The viral DNA and the kinetics of its replication. Virology 99:399-409.

Tomari Y, Zamore PD. 2005. Perspective: machines for RNAi. Genes Dev 19:517-529.

Tremblay GB, Mejia NR, Mackenzie RE. 1992. The Nadp-Dependent Methylenetetrahydrofolate Dehydrogenase-Methenyltetrahydrofolate Cyclohydrolase-Formyltetrahydrofolate Synthetase is Not Expressed in Spodoptera-Frugiperda Cells. J Biol Chem 267:8281-8285.

Vieira HL, Pereira AC, Carrondo MJ, Alves PM. 2006. Catalase effect on cell death for the improvement of recombinant protein production in baculovirus-insect cell system. Bioprocess Biosyst Eng 29:409-414.

Volkman LE, Goldsmith PA, Hess RT, Faulkner P. 1984. Neutralization of budded Autographa californica NPV by a monoclonal antibody: identification of the target antigen. Virology 133:354-362.

Volkman LE, Keddi BA. 1990. Nuclear polyhedrosis virus pathogenesis. Sem Virol 1:249-256.

Wang MY, Kwong S, Bentley WE. 1993. Effects of oxygen/glucose/glutamine feeding on insect cell baculovirus protein expression: a study on epoxide hydrolase production. Biotechnol Prog 9:355-361.

Wang MY, Pulliam TR, Valle M, Vakharia VN, Bentley WE. 1996. Kinetic analysis of alkaline protease activity, recombinant protein production and metabolites for infected insect (Sf9) cells under different DO levels. J Biotechnol 46:243-254.

Wang MY, Vakharia V, Bentley WE. 1993. Expression of epoxide hydrolase in insect cells: A focus on the infected cell. Biotechnol Bioeng 42:240-246.

Weber N, Ortega P, Clemente MI, Shcharbin D, Bryszewska M, de la Mata FJ, Gomez R, Munoz-Fernandez MA. 2008. Characterization of carbosilane dendrimers as effective carriers of siRNA to HIV-infected lymphocytes. J Control Release 132:55-64.

Weiss SA, Smith GC, Kalter SS, Vaughn JL. 1981. Improved Method for the Production of Insect Cell-Cultures in Large Volume. In Vitro-Journal of the Tissue Culture Association 17:495-502.

Wheeler JJ, Palmer L, Ossanlou M, MacLachlan I, Graham RW, Zhang YP, Hope MJ, Scherrer P, Cullis PR. 1999. Stabilized plasmid-lipid particles: construction and characterization. Gene Ther 6:271-281.

Wiznerowicz M, Trono D. 2003. Conditional suppression of cellular genes: lentivirus vector-mediated drug-inducible RNA interference. J Virol 77:8957-8961.

Wong TK, Nielsen LK, Greenfield PF, Reid S. 1994. Relationship between oxygen uptake rate and time of infection of Sf9 insect cells infected with a recombinant baculovirus. Cytotechnology 15:157-167.

Wynn EJW, Hounslow MJ. 1997. Coincidence correction for electrical-zone (Coulter-counter) particle size analysers. Powder Technol 93:163-175.

Xia H, Mao Q, Paulson HL, Davidson BL. 2002. siRNA-mediated gene silencing in vitro and in vivo. Nat Biotechnol 20:1006-1010.

Xia J, Noronha A, Toudjarska I, Li F, Akinc A, Braich R, Frank-Kamenetsky M, Rajeev KG, Egli M, Manoharan M. 2006. Gene silencing activity of siRNAs with a ribo-difluorotoluyl nucleotide. ACS Chem Biol 1:176-183.

Yamaji H, Manabe T, Kitaura A, Izumoto E, Fukuda H. 2006. Efficient production of recombinant protein in immobilized insect cell culture using serum-free basal media after baculovirus infection. Biochem Eng J 28:67-72.

Yang YY, Wang Y, Powell R, Chan P. 2006. Polymeric core-shell nanoparticles for therapeutics. Clin Exp Pharmacol Physiol 33:557-562.

Yu JY, DeRuiter SL, Turner DL. 2002. RNA interference by expression of short-interfering RNAs and hairpin RNAs in mammalian cells. Proc Natl Acad Sci U S A 99:6047-6052.

Zatsepin TS, Turner JJ, Oretskaya TS, Gait MJ. 2005. Conjugates of oligonucleotides and analogues with cell penetrating peptides as gene silencing agents. Curr Pharm Des 11:3639-3654.

Zeiser A, Bedard C, Voyer R, Jardin B, Tom R, Kamen AA. 1999. On-line monitoring of the progress of infection in Sf-9 insect cell cultures using relative permittivity measurements. Biotechnol Bioeng 63:122-126.

Zeiser A, Elias CB, Voyer R, Jardin B, Kamen AA. 2000. On-line monitoring of physiological parameters of insect cell cultures during the growth and infection process. Biotechnol Prog 16:803-808.

Zetterberg R. 1996. Cell growth and cell cycle progression in mammalian cells. In: Thomas N.S.B., editor. Oxford:Bios Scientific Publishers. p 17-26.